2012

Regulation of Mitosis by Nuclear Speckle Proteins

Keshia Nicole Torres-Munoz
Wright State University

REGULATION OF MITOSIS BY NUCLEAR SPECKLE PROTEINS

A thesis submitted in partial fulfillment
of the requirements for the degree of
Master of Science

By

KESHIA N. TORRES-MUNOZ

B.S., Wright State University, 2010

2012

Wright State University

Wright State University

SCHOOL OF GRADUATE STUDIES

May 17, 2012

I HEREBY RECOMMEND THAT THE THESIS PREPARED UNDER MY SUPERVISION BY Keshia N. Torres-Munoz ENTITLED Regulation of mitosis by nuclear speckle proteins BE ACCEPTED IN PARTIAL FULFILLMENT OF THE REQUIREMENTS FOR THE DEGREE OF Master of Science.

_____

Paula A. Bubulya, PhD

Thesis Director

_____

David Goldstein, Ph.D., Chair
Department of Biological Sciences
College of Science and Mathematics

Committee on

Final Examination

_____

Mill W. Miller, PhD

_____

Mark Mamrack, PhD

_____

Andrew Hsu, Ph.D.
Dean, School of Graduate Studies

Abstract

Torres-Munoz, Keshia N. M.S., Department of Biological Sciences, Wright State University, 2012. Regulation of Mitosis by Nuclear Speckle Proteins.

Mitosis is an intricate process that is monitored by multiple cell cycle regulator proteins. Errors in mitotic regulation have been linked to many types of cancer. Recently, evidence suggests an indirect regulation of mitosis by nuclear speckle proteins. Nuclear speckles are one of the multiple compartments found in the mammalian cell nucleus. They serve as assembly compartments for premRNA processing factors. Mass spectrometry analysis of purified nuclear speckles revealed 33 novel proteins including Son and TRAP150. The aim of my study was to determine how Son and TRAP150 can directly or indirectly impact mitosis. We and others recently reported that Son is required to maintain cell proliferation, as its depletion results in growth arrest in metaphase. We hypothesized that Son is required for the assembly of important mitotic structures such as the mitotic spindle and kinetochores. My results showed elongated and disorganized mitotic spindles in Son-depleted cells. In addition, my studies showed a novel localization pattern for Son in cytoplasmic foci following microtubule destabilization at metaphase. Son is important in the alternative splicing of transcripts that encode cell cycle regulators (Sharma et al., 2011). Therefore the

mitotic defects seen are most likely explained by alternative splicing defects that occur after Son depletion. In addition, preliminary evidence from the Bubulya lab showed the mitotic defects in TRAP-150 depleted cells suggesting a role for TRAP150 in mitosis. Given that TRAP150 did not colocalize with mitotic structures during mitosis, we hypothesized that TRAP150 depletion alters mitosis by altering the transcripts of mitotic regulators. My results indicated that TRAP150 is important in controlling abundance of transcripts that encode mitotic regulators.

Table of Contents

Page

List of Figures

List of Tables

List of Appendices

Chapter 1: Background

1.1 Introduction

Cell growth is enabled by the synthesis of new proteins, nucleic acids, carbohydrates and lipids. These are all necessary steps that precede cell division, the process in which one cell divides into two daughter cells. All of the genetic information of the parent cell must be duplicated and distributed through this process. To accomplish this, a cell must go through a series of steps, collectively known as the cell cycle. The cell cycle begins at the formation of two new cells and ends when these cells divide again into two cells. The division of the nucleus is known as mitosis while the division of the cytoplasmic components is known as cytokinesis. Both mitosis and cytokinesis comprise what is known as the M phase of the cell cycle (Jacobberger et al., 2004).

Each cell cycle needs to be regulated to meet the needs of each cell type. The molecular basis of this regulation is of major interest to researchers for it is important to understand the cell cycle regulation of normal cells as well as understanding how cancer cells escape the various regulatory control mechanisms. Most of the cellular components are synthesized continuously during interphase, so the cellular mass tends to increase as the cell approaches the division stage. DNA replication occurs during S phase. After S phase, the cell

enters G2 phase and then M phase. After M phase is completed, both daughter cells enter G1 (Jacobberger et al., 2004). For a mammalian cell, M phase usually takes less than one hour. Each chromosome pair consists of sister chromatids that are guided by the microtubules of the mitotic spindle; the sister chromatids are separated and move to opposite ends of the cell. The process of cytokinesis has usually begun by this point and the newly formed nuclear envelope surrounds the two groups of daughter chromosomes (Nasmyth et al., 2003).

Mitosis involves a reorganization of both the nucleus and cytoplasm and is monitored by the activation of various protein kinases. Each cell cycle event must occur with specific timing and regulation before progressing to the next phase. Checkpoints monitor intracellular conditions and stop the cell cycle if the conditions are not suitable. The first control point occurs during G1 and is called the restriction point. Cells need to have the necessary extracellular growth factors in order to move on to S phase. The second control point is at the G2-M transition also known as the DNA replication checkpoint. The DNA replication checkpoint makes sure that DNA synthesis is finished before proceeding to M phase. DNA damage checkpoints halt the cell cycle if DNA damage is detected. The third control point occurs during the metaphase to anaphase transition. This ensures that all chromosomes are properly aligned at metaphase before moving on to anaphase (Nigg et al., 2001).

The eukaryotic cell cycle is regulated by cylin dependent kinase (Cdk)-cyclin complexes. There are two major levels of regulation:

(1) Availability of cyclin molecules

(2) Phosphorylation of Cdks

Target mitotic proteins are phosphorylated by protein kinases and dephosphorylated by protein phosphatases. This mechanism is extremely important in regulating protein activity during the cell cycle. Many of these protein kinases become active when bound to a cyclin. These are referred to as cyclin-dependent kinases (Cdks). The concentration of cyclins oscillates during the cell cycle in order to control specific events. The concentration of the mitotic cyclins increases during G1phase, S phase, and G2 phase. At G2 phase, they reach a threshold value that is required to activate the mitotic Cdks which therefore triggers the onset of mitosis. Halfway through mitosis these cyclins are destroyed. The mitotic cyclins are those required for the G2-M transition as well as the other events that occur in mitosis. Likewise, there are G1 cyclins as well as S cyclins that function during G1 and S phase respectively. At the G2-M boundary, a Cdk-cyclin complex catalyzes the phosphorylation of proteins that promote nuclear envelope breakdown, chromosome condensation as well as spindle formation (Cross et al., 2007).

Many types of cancer are caused by a misregulation in the G1 and G2 phases. Cancer is a complex disease in which genetic changes lead to the production of cells that grow uncontrollably and can ultimately result in the death of the organism. Multiple genetic changes are required to transform a normal cell to a cancer cell. One aspect that can contribute to this transformation is the malfunction of the G2-M DNA damage checkpoint. For example, if damaged

sister chromatids get separated before they are repaired, it is impossible to correct this error after separation occurs. In addition, if M phase begins before DNA replication is completed, sister chromatid separation will result in major chromosomal damage (Coller et al., 2007).

1.2 Mitosis:

Even though mitosis has been studied for over a century, many aspects about mitotic regulatory mechanisms still remain unknown. Accurate chromosome segregation is required to ensure proper transmission of genetic information from one cell generation to the next. This process needs to be executed in perfect synchrony in order to avoid chromosome mis-segregation. Errors in segregation often lead to chromosomal instability which is linked to the formation of malignant tumor cells (Jallepalli et al.,2001; Haering, 2003; Walczak et al., 2010).

Mitosis is divided into 5 stages: prophase, prometaphase, metaphase, anaphase and telophase. During prophase, chromatin is reorganized into condensed chromosomes (Peters et al., 2004). This makes them easier to move within the cell (Wittman et al., 2001). Chromosome condensation is facilitated by histone modifications. These are in the form of phosphorylation, acetylation and methylation of histones. Phosphorylation of histone H3 at serine 10 correlates with chromosome condensation in mitosis and is required for error free chromosome segregation (Gurley et al., 1978). In addition, the nuclear lamina disassembles as a result of lamin hyperphosphorylation (Nigg, 1995; Nigg,

2001). When a cell enters prophase two main things happen: changes in microtubule dynamics result in a loss of individual microtubules and microtubule bundles begin to form. In addition, chromosomes undergo global condensation. Microtubules begin to search and capture kinetochores during prometaphase. Chromosome condensation continues throughout prometaphase. The cell is considered to be in metaphase once all the kinetochores are attached to microtubules and the chromosomes align at the metaphase plate. Chromosomes become shortened and the sister chromatids remain connected at the centromere. This is the location where kinetochores assemble and are then captured by microtubules (Peters et al., 2004). Replicated chromosomes remain associated and possess two kinetochores which allow them to become stably connected to microtubules extending from opposite poles (Kirschner and Mitchison, 1986; Wadsworth et al., 2004). After all chromosomes are bi-oriented on the metaphase plate, anaphase and cytokinesis inhibitors, securin and cyclin B, are removed from kinetochores and cells destroy the connections between sister chromatids. This triggers sister chromatid segregation toward opposite centrosomes during anaphase (Murray et al., 1985; Haering and Nasmyth, 2003). Anaphase can be divided into two sub-phases: anaphase A and anaphase B. Anaphase A is defined by the rapid separation of the sister chromatids which segregate to opposite poles of the mitotic spindle. Anaphase B is characterized by elongation of the spindle. During telophase, chromosomes begin to decondense, the nuclear envelope re-forms and the mitotic spindle disassembles. Towards the end of mitosis, cytokinesis ensues.

Although proper segregation of sister chromatids is not achieved until anaphase, the events that occur during prometaphase (attachment and initial alignment of chromosomes) represents the defining aspect of mitosis (Khodjakov et al., 2010). Mitotic progression is mostly regulated by two post-translational mechanisms: protein phosphorylation and proteolysis. The most important mitotic kinase is the cyclin dependent kinase 1 (Cdk-1). Cdk-1 becomes activated by de-phosphorylation of two neighboring residues in the ATP binding site. Cdk-1 then phosphorylates many substrates including microtubule binding proteins, kinesin-related motors and nuclear lamins. Cdk-1 phosphorylation is important for nuclear envelope breakdown, centrosome separation, spindle assembly and chromosome condensation. In addition, Cdk-1 is important for progression through anaphase as well as for mitotic exit and cytokinesis (Kimura et al., 1998; Lowe, M. et al., 1998; Andersen, S.S., 1999; Noton, E. and Diffley, J.F., 2000; Nigg, 2001).

Chromosome movement during mitosis is enabled by specialized machinery: the mitotic spindle which is comprised of microtubules and the centrosomes. The centrosomes are comprised of two centrioles, which are tiny, barrel shaped structures. A human centrosome contains over 100 different proteins including components that function in microtubule nucleation (e.g. gamma tubulin) as well as associated proteins (Andersen et al., 2003; Nigg, 2007). The centrosome is believed to be responsible for spindle morphogenesis through integrating preassembled spindle components and generating astral microtubules that continuously search for kinetochores (Wadsworth et al., 2004).

Generation of microtubules at the centrosome results in a polar radial array with microtubule plus ends extending toward the middle of the cell. In addition, centrosomes are attraction centers that recruit spindle components (Wadsworth et al., 2004). During interphase, centrosomes have a different function by serving as the main microtubule-organizing and nucleating centers (Winey, 1999; Wittman et al., 2001). Centrosomes undergo a cell cycle of their own that coincides with onset of DNA replication. Centrioles duplicate during S phase of the cell cycle but centrosome segregation does not occur until M phase. Centrosome duplication and segregation is required only once during each cell cycle (Mazia, 1987). If the centrosome gets duplicated more than once, there would be an abnormal number of centrosomes per cell. Abnormalities in this process result in aberrant centriole numbers which would lead to genome instability (Nigg, 2006; Nigg, 2007).

1.3 Kinetochores

The ability of chromosomes to achieve spindle bi-orientation is key to accurate chromosome segregation. The movement of chromosomes to the metaphase plate is aided by specialized structures known as kinetochores. Kinetochores are macromolecular complexes that assemble on the centromere of each sister chromatid during mitosis and interact with spindle microtubules (Chan et al., 2005). These structures must have the capability to maintain a grip on the dynamic ends of spindle microtubules in order to obtain accurate chromosome segregation (Davis et al., 2007). Kinetochores monitor attachments

and they possess control mechanisms that detect and correct defective attachments (Chan et al., 2005).

Kinetochore assembly is a complex, hierarchical process in which kinetochore proteins associate with either the centromere or the kinetochore-centromere structure. Many interdependencies between these proteins also promote kinetochore assembly (Kallio, 2006). Kinetochores form as a trilaminar stack in the interface between chromosomes and microtubules (Brinkley, B.R. and Stubblefield, E., 1966). In mammalian cells, kinetochores are divided into two regions called the inner and outer kinetochore. The inner kinetochore, which is immediately adjacent to the centromere, is composed of repetitive DNA sequences which assemble on a form of chromatin that contains the histone H3 variant CENP-A. The human kinetochore contains approximately 100 proteins. The inner kinetochore includes CENP-C that along with CENP-A are believed to behave as scaffolds and anchor protein components of the outer kinetochore to the centromeric heterochromatin. CENP-C or centromeric protein C is required for kinetochore assembly and proper segregation of sister chromatids (Saitoh et al., 1992; Tomkiel et al., 1994; Fukagawa and Brown, 1997; Kalitsis et al., 1998; Fukagawa et al., 1999). Recruitment of inner kinetochore proteins, CENP-C, CENP-H and CENP-I/MIS6, is mainly dependent on the presence of CENP-A (Howman et al., 2000; Oegema et al., 2001; Van Hooser et al., 2001; Fukagawa et al., 2001; Goshima et al., 2003). The outer kinetochore is a collection of more than 20 proteins that assemble on the inner kinetochore after nuclear envelope breakdown.

The majority of the known microtubule interacting proteins (CENP-E and dynein) and the checkpoint proteins are present on the outer plate of the kinetochore complex (Cooke et al., 1997). Different subgroups of outer kinetochore proteins leave the kinetochore at three points mitotic progression: microtubule capture, early anaphase and end of anaphase (Choo, 1997; Shah and Cleveland, 2000; McCleland et al., 2003). Locations of these various kinetochore proteins have been obtained through epistasis assays and protein-protein interaction data (Maiato et al., 2004; Foltz et al., 2006; Liu et al., 2006; Musacchio and Salmon, 2007; Cheeseman and Desai, 2008; Cheeseman et al., 2008; Wan, 2009). Evidence supporting a kinetochore assembly pathway demonstrated that there was a specific order in which proteins appear at kinetochores; hBub1-CENP-F-hBubR1-CENP-E. This order reflects in part the hierarchical relationship among them as well as the requirement of interaction between proteins that associate early and proteins that associate late (Kallio, 2006).

There are three protein complexes that assemble on the outer plate of the kinetochore and are important in forming the main attachment sites for kinetochores: Mis12 Complex, hKnl1/Blinkin and the Ndc80 complex. These protein complexes also serve as a scaffold for spindle assembly checkpoint proteins (Martin-Lluesma et al., 2002; DeLuca et al., 2005; DeLuca et al., 2006; Cheesema et al., 2006; Wei et al., 2007; Kemmler et al., 2009; Alushin, 2010). The evolutionarily conserved NDC80 complex plays an indirect role in organizing the structure of the kinetochore (DeLuca et al., 2005). The coiled coil regions of

the Ndc80 and Nuf2 subunits of the Ndc80 complex project toward the plus end of the microtubule (DeLuca et al., 2006). This action forces the Spc24 and Spc25 subunits to face in the opposite direction away from the plus end of the microtubule. This geometrical binding allows for the dynamic polymerization/depolymerization cycles that characterize microtubules (Wilson-Kubalek et al., 2008). Mutations in the Ndc80 complex in the absence of active Aurora B do not detach the kinetochores from the microtubules in metaphase, but weaken the attachments such that the kinetochores fall off during anaphase (Pinsky et al., 2006; Kutwaliwale, C. and Biggins, S., 2006). Defective NDC80 complexes as a whole result in elongated spindles, loss of tension across sister kinetochores and failure to align chromosomes (Martin-Lluesma et al., 2002; DeLuca et al., 2002; McCleland et al., 2003; Hori et al., 2003; Desai et al., 2003; Bharadwaj et al., 2004; McCleland et al., 2004; Maiato, 2004).

The kinetochore maintains attachment to microtubules despite the presence of thousands of tubulin subunits that are constantly being added or removed. The number of microtubules bound per kinetochore varies between the species; budding yeast have only a few microtubule attachments while humans have up to 20 microtubules attached per kinetochore (Rieder, 1982; Maiato et al., 2004; Wan, 2009). The kinetochores attach to spindle microtubules referred to as kinetochore microtubules and are re-arranged into bundles known as kinetochore fibres (K-fibres). Typically in vertebrate cells, a K-fiber is composed of 20-25 microtubules (McEwen et al., 1997). One set of K-fibers encircle the tip of the microtubule and another set of K-fibers attaches to the microtubule wall.

Kinetochore forces are not correlated to the number of microtubules in a K-fiber bundle. These forces become balanced when the chromosomes are positioned at the spindle equator (Khodjakov, 2010). Kinetochores in prometaphase undergo directional instability composed of alternating states of poleward and anti-poleward movements as well as kinetochore-microtubule polymerization/depolymerization states (Maiato, 2004).

Plus ends of microtubule protofilaments tend to curve away from the outer kinetochore making it rare for microtubules to penetrate centromeric heterochromatin (Maiato et al., 2006; Vandenbeldt et al., 2006; Dong et al., 2007; McIntosh et al., 2008; Wan, 2009). Initially, the kinetochore interacts with the lateral surface of the microtubule and then moves towards the spindle pole through sliding movements forming an end-on attachment. Kinetochores have multiple sites where microtubules attach end-on. These kinetochore-microtubule attachments are formed by weak lateral interactions by those particular attachment sites. The kinetochore continues to move closer to the spindle pole as the microtubule shrinks (Maure et al., 2011). The kinetochore assembled on the front of the moving chromosome is stretched as if the chromosome is pulled by the kinetochore (Skibbens et al., 1993; Walczak et al., 2010).

1.4 Mitotic Spindle

The events of cell division require a dynamic interplay of the cell's cytoskeleton. Microtubules rearrange from a uniform distribution to a highly intricate bipolar structure (Wittman et al., 2001; Ellenberg et al., 2010). Individual

chromosomes must be coordinated and integrated into a common structure that is known as the mitotic spindle (Wadsworth et al., 2004). The mitotic spindle is a macromolecular apparatus composed of approximately 800 proteins and it facilitates chromosome segregation (Sauer et al., 2005; Khodjakov et al., 2010). This structure positions the chromosomes in the equatorial plane of the spindle (Nicklas and Arana, 1992; Walczak et al., 2009).

Microtubules are polymers of alpha and beta dimers that are characterized by having a slow growing minus end and a fast growing plus end. The minus ends are anchored at the spindle poles while the plus ends project towards the chromosomes (Wittman et al., 2001). There are 3 different classes of microtubules within the mitotic spindle: kinetochore microtubules, interpolar microtubules and astral microtubules. Kinetochore microtubules extend from the centrosome and attach to kinetochores thereby attaching each sister chromatid to its respective spindle pole. Interpolar microtubules originate from the spindle poles and interact with other interpolar microtubules in an antiparallel way. This stabilizes the bipolar nature of the spindle and generates pushing forces that separate spindle poles in late anaphase. Astral microtubules project from centrosomes and into the cytoplasm. These serve to orient as well as position the mitotic spindle inside the cell (Wittman et al., 2001). Spindle orientation dictates the position of the cleavage plane. Many positive as well as negative regulators work in a coordinated fashion to form as well as maintain the mitotic spindle. Because of complexity in its regulation, depletion of one of these regulators does not greatly affect the mitotic spindle (Ellenberg et al., 2011).

Forces generated by motor proteins, chromosome arms as well as spindle microtubules also promote spindle formation (Wittman et al., 2001).

Amphitelic attachment of microtubules to kinetochores results in a tug of war dynamic which attempts to pull sister chromatids apart (Wittman et al., 2001). Microtubule attachments undergo a trial and error phase to selectively eliminate attachments that result in sister kinetochores being attached to the same pole (syntelic attachment) (Haering and Nasmyth, 2003). Sister chromatids are held together by cohesin ring complexes which resist the force generated by microtubules. The counteracting forces result in a tension that is believed to stabilize the attachments between kinetochores and microtubules as well as align the chromosomes at the metaphase plate (Haering and Nasmyth, 2003). In addition to stabilization, tension also increases the number of kinetochore-microtubule attachments (Nicklas and Ward, 1994; King and Nicklas, 2000; Nezi and Musacchio, 2009). The stabilization of microtubule-kinetochore attachments transforms the symmetric array of microtubules into the typical spindle shape (Wadsworth et al., 2004). In addition, to keep the spindle length constant during metaphase, there needs to be a balance between depolymerization of minus ends and polymerization of plus ends. After the chromosomes are aligned, the microtubule driven force move the sister chromatids to opposite poles of the cell during anaphase. Chromosome movements are caused by changes in the length of microtubules that are attached to kinetochores in an end-on attachment (Inoue and Salmon, 1995). In this way, the centrosome goes through synchronized poleward movement (Wittman et al., 2001).

1.5 Spindle Assembly Checkpoint

Checkpoints or feedback control mechanisms monitor the transition between the different cell cycle phases and ensure that key cellular events are executed error free (Hartwell et al., 1989). The spindle assembly checkpoint (SAC) monitors the metaphase to anaphase transition and ensures proper kinetochore-microtubule interactions during chromosome alignment at the metaphase plate (Musacchio and Salmon, 2007; Nezi and Musacchio, 2009). SAC triggers still remain controversial. One hypothesis is that the SAC monitors kinetochore-spindle interactions to a certain degree. Experiments performed on multiple organisms have shown that the SAC is activated by either lack of kinetochore-microtubule attachments (attachment-only hypothesis) or a defect in the tension generated by kinetochore-microtubules (Zhou et al., 2002; Pinsky and Biggins, 2005). The 'attachment-only' hypothesis of the SAC inactivation states that the kinetochore-microtubule attachment is the only important parameter monitored by the SAC. This hypothesis implies that all kinetochore-microtubule attachments, even incorrect ones, are sufficient to satisfy the SAC (Nezi and Musacchio, 2009). SAC activation inhibits Cdc20 thereby preventing ubiquitylation of securin and mitotic cyclins which delay anaphase onset (Zachariae and Nasmyth, 1999; Yu, 2002; King et al., 2007).

The anaphase promoting complex/ cyclosome (APC/C) is an E3 ubiquitin ligase. Its activity is inhibited by the SAC until all chromosomes are properly aligned at the metaphase plate. When the checkpoint is turned off, the APC/C

degrades securin and activates separase. Separase then cleaves centromeric cohesin so that sister chromatids are no longer attached.

The SAC involves a network of Mad and Bub proteins and it is inactivated when checkpoint proteins leave the kinetochore after microtubule attachment (Hardwick and Shah, 2010; Desai et al., 2011). The point at which the checkpoint becomes inactive marks a point of no return (Khodjakov and Rieder, 2009). Two other important kinetochore proteins are CENP-E and BubR1. CENP-E is a large kinesin that has plus end directed motor activity. It is believed to have a role in kinetochore capture of microtubules, chromosome congression to metaphase plate and maintenance of this movement. In addition, CENP-E also monitors kinetochore-microtubule attachments to ensure high segregation fidelity (Wordeman and Mitchison, 1995; Yen et al., 1992; Stever et al., 1990; Pfarr et al., 1990; Wittman et al., 2001). BubR1 is localized on the outer plate of the kinetochore where it is postulated to behave as a mechanosensor that monitors the activity of CENP-E (Chan et al., 1999). The checkpoint activity of BubR1 is therefore regulated by conformational changes in CENP-E when it interacts with microtubules (Howell et al., 2001). The dynamic interactions between the kinetochore and the spindle are monitored by other kinetochore proteins called Mad1, Mad2, Mad3, Bub1, Bub3 and Mps1 (found in budding yeast) (Maiato et al., 2004; Chan and Yen, 2003). Similar to BubR1, Mad1 and Mad2 also respond to conformational changes brought upon by CENP-E as they are displaced from kinetochores when microtubule attachments are made (Howell et al., 2001).

The mitotic checkpoint proteins as well as the microtubule motor proteins CENP-E and cytoplasmic dynein accumulate to higher levels in unattached kinetochores. Mad1 and Mad2 are detectable if the kinetochores are unoccupied by microtubules for a prolonged period of time. Therefore, Mad2 localization to unattached kinetochores correlates with an active SAC. Upon microtubule attachment, Mad2, Mad1, BubR1, Bub1, CENP-E, dynein/dynactin and Bub3 are released from the kinetochore at different rates after amphitelic attachments are made (Maiato et al, 2004). In addition, Aurora B, Aurora B kinase and Survivin are also involved in the SAC (Dimitrov et al., 2004). When cells were depleted of Aurora B, Aurora B Kinase or Survivin, mitosis was delayed due to the presence of unaligned chromosomes. A redistribution of these factors was also seen after depletion of any one of these proteins (Mollinari et al, 2003; Adams, R. et al., 2001; Speliotes, E.K., 2000; Kaitna, S. et al., 2000). The NDC80 complex is also responsible for stabilizing the MAD1/MAD2 and dynein association with kinetochores. Depletion of Ndc80/ Hec1 results in a 10-15% reduction of MAD1, MAD2 and dynein that leads to an inactivation of the spindle checkpoint (Martin-Lluesma et al., 2002; McCleland et al., 2003; Hori et al., 2003; DeLuca et al., 2002; Bharadwaj et al., 2004; McCleland et al., 2004). Alteration of these factors has been directly implicated in cancer (Dimitrov et al., 2004).

The SAC works to prevent aneuploidy. Erroneous inactivation of the SAC in mammalian cells leads to a rapid rise in aneuploidy and ultimately cell death (Dobles et al., 2000; Khodjakov and Rieder, 2009). Genetic as well as epigenetic alterations of spindle checkpoint genes lead to errors in chromosome

segregation, aneuploidy and polyploidy. These characteristics can be seen in cancer biopsies (Kops et al., 2005; Holland and Cleveland et al., 2009; Mattiuzzo, 2011). My study addresses an additional possibility that changes leading to altered expression (abundance or alternative splicing) of mRNAs coding for cell cycle regulators and/or SAC proteins will cause similar defects.

1.6 Nuclear Speckles

The mammalian cell nucleus is a highly complex and dynamic structure. It is compartmentalized into multiple subnuclear domains including nucleoli, paraspeckles, Cajal bodies and nuclear speckles (Matera et al., 2009; Spector, 2006). The premRNA splicing machinery is comprised of small nuclear ribonucleoprotein particles (snRNPs), spliceosome subunits, and other non-snRNP protein splicing factors, and this machinery displays a punctate localization in the nucleus. These subnuclear structures are termed nuclear speckles or interchromatin granule clusters (IGCs) (Phair, R.D. and Misteli, T., 2000; Lamond and Spector, 2010).

Speckles are highly dynamic structures; their size, shape, and number are dependent on the level of gene expression that occurs in a particular cell. They can measure anywhere from one to several micrometers in diameter and are made up of 20-25 nm granules that are interconnected by thin fibrils (Thiry, M., 1995). IGCs form throughout the nucleoplasm in areas containing little to no DNA. Speckles are usually found close to sites of high transcription activity. This occurrence suggests that speckles are somehow linked to gene expression. In

addition, some genes have been reported to localize in proximity with nuclear speckles (Thiry, M., 1995; Lamond and Spector, 2010).

Proteomic analysis of an IGC fraction provided the protein composition of nuclear speckles. These results identified 146 known proteins in addition to various uncharacterized proteins (Mintz, 1999; Saitoh, 2004). Among the known proteins found in speckles were snRNP proteins, SR proteins and several kinases and phosphatases that function in phosphorylating components of the splicing apparatus. Nuclear speckle purification also led to the identification of 33 novel proteins (12% of nuclear speckle proteins) for which little to no information was known (Mintz, 1999; Saitoh, 2004). SR proteins are a family of conserved splicing factors in metazoans and play diverse roles in RNA metabolism from premRNA splicing to mRNA export to protein translation. Classical SR proteins are characterized by having a bipartite structure containing at least one or two RNA recognition motifs (RRMs) at the amino-terminus and an RS domain enriched in arginine/serine dipeptide repeats at the carboxy-terminus (Lin, 2006).

Transcription and pre-mRNA processing coordination is essential for proper nuclear speckle integrity. Some evidence proposes that assembly of the nuclear speckles is based on a “self-association”, and speckle components are dynamically exchanged in response to phosphorylation signals (Mintz, 1999; Saitoh, 2004). The arginine/serine rich domain (RS domain) of the SR proteins is required for the assembly of these factors into nuclear speckles (Li and Bingham, 1991; Hedley et al., 1995; Caceres et al., 1997; Spector and Lamond, 2010). There are controversies regarding nuclear speckle function. Many do not believe

nuclear speckles are directly involved in transcription and pre-mRNA processing while others suggest that speckles are indeed linked to splicing as well as the transport of pre-mRNA (Spector and Lamond, 2010). A subset of the splicing proteins involved in pre-mRNA processing is associated with nuclear speckles in addition to being associated with transcription sites. Nuclear speckles become enlarged and increase in size when transcription is inhibited (Spector et al., 2003; Melcak et al., 2000; Spector et al., 1991; Spector and Lamond, 2010). This evidence supports the idea that IGCs are storage, assembly and modification compartments and function in the supplying of pre-mRNA processing factors to active transcription sites. It is believed that active genes come into close proximity with nuclear speckles increasing the efficiency with which proteins can travel between speckles and active transcription sites (Spector and Lamond, 2010).

Nuclear speckles also undergo dynamic regulation during mitosis. Once a cell enters mitosis and nuclear envelope break down (NEBD) begins, speckles disassemble and their components become diffusely distributed throughout the cell (Spector and Smith, 1986; Reuter et al., 1985; Ferreira et al., 1994; Thiry, M., 1995; Spector and Lamond, 2010). Once a cell is in metaphase, speckle components accumulate in structures known as mitotic interchromatin granules (MIGs) (Ferreira et al., 1994; Lesser et al., 1989; Verjeijen,R. et al., 1986; Prasanth et al., 2003; Spector and Lamond, 2010). MIGs are the mitotic counterpart of the IGCs. As the cell progresses from anaphase to telophase, the MIGs increase in number and size. Once the nuclear envelope is reformed,

speckle components diffuse into the newly formed daughter nuclei and MIG size decreases. Live cell studies demonstrated that most of these speckle components enter daughter nuclei within 10 minutes of nuclear envelope formation (Prasanth et al., 2003; Spector and Lamond, 2010). MIGs may have a role in either modifying components of the splicing machinery before their re-entry into daughter nuclei or facilitating protein-protein interactions between speckle components before their nuclear entry. Splicing factors are functional and able to undertake premRNA splicing functions immediately upon entry into daughter nuclei (Thiry, M., 1995; Lesser et al., 1989; Prasanth et al., 2003; Spector and Lamond, 2010). This finding supports that MIGs may have a role in splicing factor modification. It may be that splicing factors must be hyperphosphorylated to leave MIGs, analogous to their release from nuclear speckles in interphase nuclei (Spector and Lamond,2010).

1.7 SR Proteins and Alternative Splicing

Alternative splicing of pre-mRNAs is an important step in the diversification of gene function. Total gene number does not correlate with genome complexity, since mammalian genomes contain fewer protein coding genes than expected (Amaral et al., 2008; Mattick, 2009; Prasanth et al., 2010). The majority of the genes in the human genome undergo alternative splicing, which is regulated by various RNA binding proteins (Black, 2003; Fu et al., 2011). Alternative splicing is regulated by small nuclear ribonucleoproteins (snRNPs), the serine/arginine rich (SR) family of nuclear phosphoproteins (SR proteins), SR related proteins and heterogeneous nuclear ribonucleoproteins (hnRNPs)

(Blencowe, 2006; Long and Caceres, 2009; Prasanth et al., 2010). Intron removal is an important step in eukaryotic gene expression. In order to remove introns, the 5’ and 3’ splice site need to be recognized by the spliceosome (Screaton, 2000). The spliceosome is a dynamic structure comprised of approximately 300 proteins (Rappsilber et al., 2002; Zhou et al., 2002; Bessonov et al., 2008; Long and Caceres, 2009). The spliceosome is a complex composed of ribonucleoprotein splicing factors including U1, U2 snRNP and U2 auxiliary factor (U2AF). Spliceosomal assembly starts when U1 snRNP and U2AF recognize the 5’ and 3’ splice site and form the E complex. U2 snRNP is then recruited to the branchpoint which results in the formation of the A complex. Afterwards, the U4/U6.U5 tri-snRNP gets recruited and forms the B complex. Splice site consensus sequences are usually not enough to recruit the splicing machinery. Auxiliary elements such as ESEs (exonic splicing enhancers) and ISEs (intronic splicing enhancers) aid in constitutive as well as alternative splicing (Matlin and Moore, 2007; Long and Caceres, 2009). SR proteins recognize splicing enhancers (ESEs) and recruit the spliceosome to the neighboring intron (Graveley, 2000; Blencowe, 2000; Black, 2003; Shepard and Hertel, 2009). One model suggests that the RS domain of an SR protein bound to an enhancer interacts with other SR proteins and allows the recruitment of spliceosomal components (Graveley, 2000; Shepard and Hertel, 2009). The RS domain appears to be important for protein-protein interactions as well as protein-RNA interactions. Multiple SR proteins tend to bind to many ESEs in the same exon. Splice sites in the mammalian genome are recognized by the exon definition

mechanism, in which ESE bound SR proteins promote U2AF recognition of the 3' splice site and U1 binding to the downstream 5' splice site (Hertel, 2008). These complexes are then switched to intron assembly on the pre-mRNA. SR proteins mediate the switch between exon definition complexes to intron definition complexes (Fu, 2004; Fu et al., 2011). SR proteins stabilize the spliceosome assembly at the 3' splice site by recruiting U2AF and forming a bridge to connect the 5' and 3' splice sites (Tarn et al., 1995; Fu and Maniatis, 1992; Wu and Maniatis, 1993; Staknis and Reed, 1994; Screaton et al., 2000). Activation of splicing is proportional to the number of serine-arginine repeats in the RS domain of an SR protein (Graveley et al., 1998; Shepard and Hertel, 2009). Having a high number of serine-arginine repeats correlates with high levels of splicing activation. In addition, both up and down regulation of SR proteins affect alternative splicing in a similar fashion (Fu et al., 2011); altering the concentration levels of SR proteins result in the same alternative splicing defects.

SR proteins also have exon-independent functions. They are known to promote the pairing of 5' to 3' splice sites across an intron as well as mediate the addition of the tri-snRNP U4/U6.U5 into the spliceosome (Roscigno and Garcia-Blanco, 1995; Shepard and Hertel, 2009). Exonic splicing enhancers also have the ability to prevent exon skipping. SF2/ASF can inactivate the 3' splice site and prevent the recruitment of U2 to the branchpoint sequence (Roscigno and Garcia-Blanco, 1995; Shepard and Hertel, 2009). Some SR proteins are believed to function in mRNA export. SR proteins SF2/ASF, SRp20 and 9G8 are phosphorylated on specific residues within their RS domain and RNA binding

domain allowing them to shuttle continuously between the nucleus and cytoplasm (Caceres et al., 1998; Shepard and Hertel, 2009). Their shuttling ability also depends on their RNA binding activity (Kruys, 2011). Phosphorylation patterns of SR proteins are required for their transport throughout the cell.

SR proteins mediate the coupling of splicing to transcription by being recruited at the same time with U1 snRNP by RNA polymerase II. They are also deposited co-transcriptionally on the exon/5' splice sites of nascent transcripts (Das et al., 2007; Kruys et al., 2011). Phosphorylation of serine residues in SR protein RS domains regulates subcellular localization as well as overall SR protein activity. Phosphorylation/dephosphorylation cycles are required for pre-mRNA splicing and regulate alternative splicing patterns (Prasanth et al., 2010). Many kinase families have been shown to phosphorylate SR proteins, including the SR protein kinase family (SRPKs), the Clk/STY family, DNA topoisomerase I and AKT kinase (Rossi et al., 1996; Blaustein et al., 2005; Patel et al., 2005; Kruys et al., 2011). These kinases play a role in nuclear speckle disassembly and also have the ability to affect splicing efficiency (Duncan et al., 1995; Colwill et al., 1996; Yeakley et al., 1999; Prasad et al., 1999; Sacco-Bubulya and Spector, 2002).

Disturbances in SR protein levels as well as any changes in RS domain phosphorylation can modulate alternative splicing (Bourgeois et al., 2004; Calarco et al., 2009; Long and Caceres, 2009; Stamm, 2008; Prasanth et al., 2010). 15% of mutations that result in genetic disease are caused by pre-mRNA splicing errors (Long and Caceres, 2009). Recent evidence has shown that a

disturbance in the alternative splicing and mis-expression of SR proteins lead to the formation of cancerous tissue (Krawczak et al., 1992; Long and Caceres, 2009).

1.8 SON

Among the novel nuclear speckle proteins identified in Saitoh et al. (2004) was a large, 2530 amino acid protein called Son. Son localizes to nuclear speckles and is the largest known SR protein. Son is involved in the high fidelity RNA processing of various structural components of the cell cycle machinery such as HDAC6, KATNB1, MAP2, CDK6 and CDK2 (Ahn et al., 2011; Sharma et al., 2011). In addition, Son has been identified as a stem cell pluripotency factor and was among the top 10 most significant hits for stem cell maintenance (10^{th} place) (Ng et al., 2010).

Motif analysis demonstrated that Son contains an RS domain, a double stranded RNA binding domain and a G patch. In addition, one third of the primary sequence is composed of 6 different types of repeats that are unique to Son (Wynn et al., 2000; Sun et al., 2001; Saitoh et al., 2004). This feature sets this protein apart from other SR proteins. All of these structural features have been linked to pre-mRNA processing. For example: since the RS domain and the G patch that are found in multiple eukaryotic RNA binding proteins have important functions in splicing, this suggests putative roles of Son in RNA binding (Sharma et al., 2010). The multiple domains found in Son and their known roles in other SR proteins suggest that Son maybe responsible for various protein-protein as

well as protein-RNA interactions that work to enhance the process of co-transcriptional splicing (Ahn et al., 2011; Sharma et al., 2011).

The repeated heptad sequence in the carboxy-terminal domain of the largest subunit of RNA polymerase II showed that repetitive serine-rich sequence motifs have scaffolding roles (Hirose and Manley, 2000; Lewis and Tollervey, 2000; Phatnani and Greenleaf, 2004; Bentley, 2005; Egloff and Murphy, 2008). Similarly in Son, when the RS domain repeats are mutated or altered there is a disruption of nuclear speckle organization (Sharma et al., 2010). Live imaging studies of Son-depleted HeLa cells transfected with YFP-SF2/ASF showed that nuclear speckles undergo a morphological change and adopt a “doughnut” conformation over time. Nuclear speckles begin to change morphology until 15-16 hours after the depletion when these splicing factors form into doughnut shapes. Depletion of Son in a cell also causes a reorganization of nuclear speckle poly A+ RNA, snRNPs, SR proteins, pinin, and EJC core proteins. These findings demonstrated that Son has scaffolding properties and has organizational functions for pre-mRNA processing factors and other nuclear speckle proteins. However, the redistribution of splicing factors upon Son depletion does not affect global transcription activity or splicing factor levels (Sharma et al., 2010).

In addition to nuclear speckle structural changes upon Son depletion, microtubule biogenesis, organization and dynamics are affected after Son knockdown (Ahn et al., 2011; Sharma et al., 2011). Reduction of Son in HeLa cells results in a metaphase arrest (Huen et al., 2010; Sharma et al., 2010). This finding suggests that Son is an important component needed for normal cell

cycle progression. Son depletion leads to an increase of prometaphase and metaphase cells and an enhancement of the mitotic cell marker histone H3 (Ser10) P (Huen et al., 2010; Sharma et al., 2010). The mitotic machinery also underwent morphological changes. My thesis work also shows that absence of Son leads to disarrayed mitotic spindles with disorganized microtubules. This altered phenotype also exhibited longer interpolar distance measurements. On average, the interpolar distance was 2 to 3 μm longer in Son siRNA treated cells (Ahn et al., 2011; Sharma et al., 2011). Since previous evidence demonstrated that Son is needed for splicing factor integrity during interphase (Sharma et al., 2010) and MIG assembly begins at the onset of metaphase (Ferreira et al., 1994), there is a possibility that this metaphase arrest is due to Son being responsible for splicing factor organization into MIGs. Putatively, Son scaffolding functions during mitosis can be analogous to its scaffolding functions during interphase. Other lines of evidence indicate that Son is a phosphoprotein of the mitotic spindle machinery which could implicate that post-translational modification of Son could play a role in mitotic cells (Sharma et al., 2011).

More recent evidence demonstrated that Son plays an important role in regulating a large number of genes linked to the general regulation of cell cycle progression. Son depletion results in exon skipping or exon inclusion of 1061 genes as well as changes in transcript abundance of 927 genes (Sharma et al., 2011). This finding is the most likely explanation for the abnormal mitotic phenotypes seen in the absence of Son (Sharma et al., 2011).

Pre-mRNA processing in human nuclei is regulated in part by phosphorylation of the carboxy-terminal domain for the largest RNA polymerase II subunit. SR proteins help make up the spliceosome complex and play essential roles in splice site selection. They function by binding to exon splicing enhancers or intron splicing enhancers and recruiting the rest of the spliceosome machinery to the appropriate splice sites. Errors in pre-mRNA processing result in the production of defective proteins. Prevention of aberrant transcripts depends on proper assembly and function of large multimolecular splicing complexes and their accessory factors. Microarray studies of Son showed that there are multiple genes that undergo splicing level changes after Son depletion. These studies demonstrated that Son is involved in the regulated expression of many genes linked to genome stability as well as cell cycle progression (Ahn et al., 2011; Sharma et al., 2011). Microarray results showed statistically significant changes in transcripts for multiple cell cycle regulators like Katanin p80 subunit B1, microtubule associated protein 2 (MAP2), histone deacetylase 6 (HDAC6) and cyclin dependent kinases such as CDK6 and CDK2 (Sharma et al., 2011). HDAC6 functions in deacetylating histone tails to orchestrate gene expression (Narlikar et al., 2002) and also deacetylates tubulin at lysine 40. This last function influences the stability of the microtubule network which plays an important role in cell cycle progression (Zhao et al., 2010; Zhang et al., 2003). Katanin p80 subunit B1 (KATNB1) functions in microtubule depolymerization (Yu et al., 2005). In addition, Son is also involved in regulating the mRNA levels and splicing of

cyclin dependent kinases CDK6 and CDK2 which facilitate transition between the different phases of the cell cycle (Ekholm and Reed, 2000).

1.9 TRAP150

TRAP150 was identified in a proteomic analysis of purified nuclear speckles along with other pre-mRNA splicing factors (Mintz et al., 1999; Saitoh et al., 2004). TRAP150 shares approximately 62% sequence homology with another nuclear speckle protein called Bclaf1/Btf (Ito et al., 1999). Btf and TRAP150 are both type II SR proteins (meaning, they have an RS domain but do not have a RNA recognition motif). Both of these proteins also share approximately 30% similarity with an EJC core component called MLN51 (Macchi, P. et al., 2003; Tange, T.O., et al., 2005). It is unclear if Btf and TRAP150 have similar/synergistic functions or if they are antagonistic. Proteins having similar functions, or functioning together in the same complex, will typically colocalize within a cellular compartment. TRAP150 and Btf colocalize with EJC proteins at an actived transcription site in U2OS 2-6-3 cells (Figure 1.1) (Varia and Bubulya, unpublished). U2OS 2-6-3 cells contain a reporter gene array that allows gene expression to be monitored directly by visualizing DNA, RNA and protein (Janicki et al., 2004).

There is an inverse correlation between Btf and TRAP150 expression in human cells. When TRAP150 is depleted by treating cells with siRNAs, Btf expression increases. Likewise, when Btf is depleted, TRAP150 is upregulated. When both of these proteins are depleted, the cells die (Varia and Bubulya, unpublished). This data implies that TRAP150 and Btf may compensate for one

Figure 1.1: Btf and TRAP150 colocalize at the reporter locus

U2OS 2-6-3 cells were transfected with 2 μg of YFP-LacI, CFP-TRAP150 and pTet-ON. Dox was added 3 hours after transfection to start transcription of the locus. After Dox was added (2.5 hours), the cells were processed for immunofluorescence using rabbit anti-Btf antibody WU10. Arrows indicate de-condensed locus (Panel a). Bar= 5 μm. Figure provided by Sapna Varia.

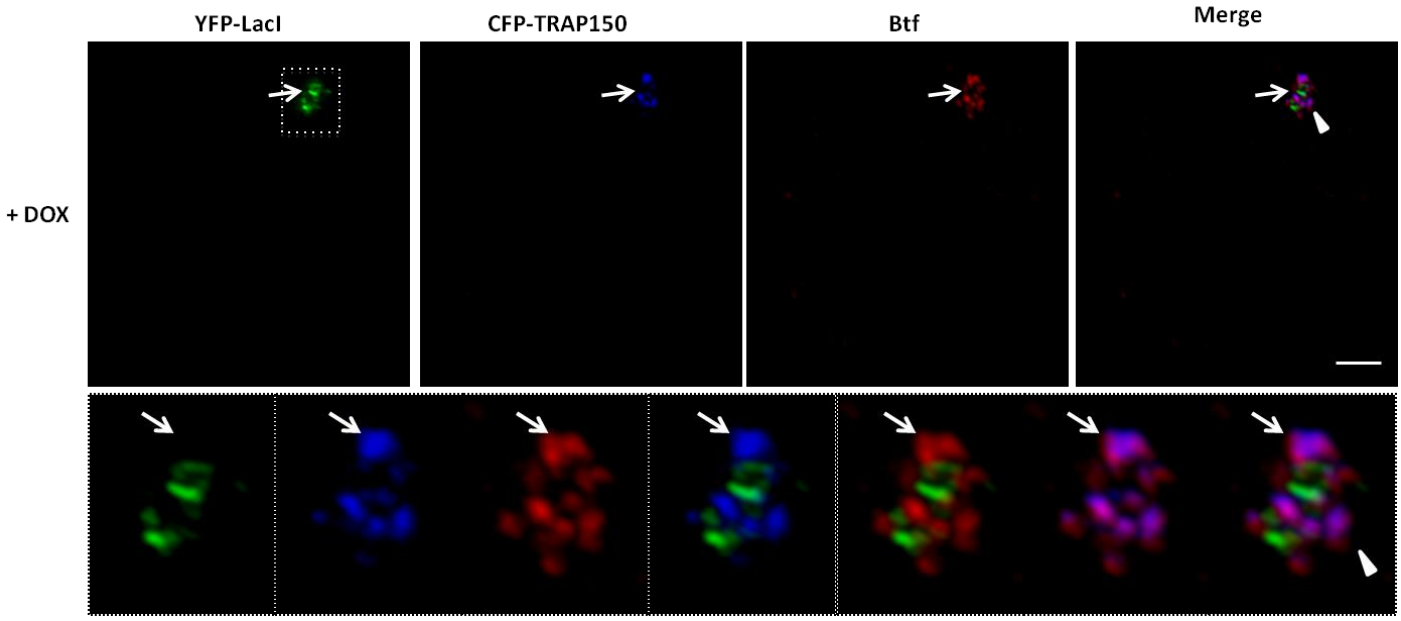
YFP-LacI
CFP-TRAP150
Btf
Merge
+ DOX

another when one of them is depleted from the cell. In addition, they both associate with the spliceosome suggesting a putative role in pre-mRNA splicing (Wahl, M.C. et al., 2009; Merz, C. et al., 2007). This data suggests that Btf and TRAP150 work together and perform pre-mRNA splicing functions.

Over expressing TRAP150 activates pre-mRNA splicing (Lee et al., 2010). It also has a splicing function in vivo; it associates with the spliceosomal complex in an ATP independent fashion (Lee et al., 2010). In addition, reduction of TRAP150 through RNA interference resulted in an inhibition of pre-mRNA splicing in vivo (Lee et al., 2010). It has been proposed that TRAP150 involvement in pre-mRNA processing may occur upon spliceosome assembly and may require ongoing transcription (Lee et al., 2010). In addition, TRAP150 behaves as a modular protein. TRAP150 has the ability to induce mRNA degradation when tethered to mRNA transcripts in the nucleus. However, this was not seen when tethered to pre-mRNA (Lee et al., 2010). TRAP150 induced mRNA decay in the nucleus is independent of ongoing translation. Mutant construct analysis demonstrated that alteration of the N terminus containing the RS domain resulted in a loss of its splicing ability but its RNA degradation activity was unaffected. However, depletion of the C terminal domain of TRAP150 gave opposite results. The mechanism of TRAP 150 mediated mRNA decay needs further study (Lee et al., 2010).

TRAP150 as well as glycogen synthase kinase 3 (GSK3), a signaling mediator that plays a role in alternative splicing, function as key components of the T cell receptor signaling pathway (Heyd et al., 2010). This pathway results in

the RNA binding of PSF and subsequent CD45 exon exclusion (Heyd et al., 2010). CD45 is a transmembrane tyrosine phosphatase and CD45 pre-mRNA processing is an example of signal-induced splicing regulation. PSF is an abundant RNA binding protein found in the nucleus. It functions in multiple RNA biogenesis processes and regulates the alternative splicing of various genes, one being CD45. In resting T cells, GSK3 regulates PSF via phosphorylation. In this modified phosphorylated form, TRAP150 binds PSF and forms a complex. The TRAP150/PSF complex prevents PSF interaction with the ESS1 sequence in CD45 exons and it therefore cannot participate in activation-induced CD45 exon skipping. Once T cells become stimulated, GSK3 levels are reduced which results in a lower concentration of phosphorylated PSF. Reduction of GSK3 levels allows PSF to be released from the TRAP150 complex and interact with CD45 exons. Additional evidence supports the interaction of PSF and TRAP150. Both TRAP 150 as well as Btf, another nuclear speckle protein that shares sequence homology with TRAP150 coprecipitate with PSF. Evidence suggests that TRAP150/GSK3 mediated regulation of PSF is probably responsible for influencing a wide spectrum of genes in addition to CD45 alternative splicing in T cells (Heyd et al., 2010). It is believed that TRAP150 performs a role in the alternative splicing of other genes via a similar mechanism.

In our lab, reduction of TRAP150 by RNAi in HeLa cells increased the number of abnormal mitotic phenotypes in prometaphase, metaphase, anaphase as well as telophase. The most common phenotypic abnormality was the presence of misaligned chromosomes in metaphase. In addition, exon array

analysis showed that TRAP150 depletion results in an alteration of transcript abundance of multiple genes including genes important for mitotic progression.

Chapter 2: Hypothesis and Experimental Aims

Mitotic progression mistakes often lead to aneuploidy which leads to the formation of cancerous tissue (Holland and Cleveland, 2009; Schvartzman et al., 2010). In addition, splicing errors accounts for 15% of genetic diseases (Long and Caceres, 2009). Nuclear proteins Son and TRAP150 affect mitosis after being depleted from cells by altering transcription and splicing patterns of transcripts coding for key mitotic regulators (Ahn et al., 2011; Sharma et al., 2011; Varia et al., unpublished).

Previous studies shown in Sharma et al. (2010) demonstrated that absence of Son leads to a metaphase arrest. I therefore hypothesized that depletion of Son results in an alteration of mitotic structures such as the mitotic spindle and kinetochores. Past immunofluorescence results showed Son localized to the chromatin region in metaphase cells in a pattern similar to a kinetochore pattern. This led to the hypothesis that Son may colocalize with kinetochores in a dynamic fashion. Son's interaction with kinetochores may be seen before a microtubule attaches to a kinetochore.

Previous studies done in the Bubulya lab showed mitotic defects after TRAP150 depletion (Figure 2.1). In addition, absence of Btf, another nuclear speckle protein that shares many sequence similarities with TRAP150 results in misaligned chromosomes during metaphase. This led to the hypothesis that TRAP150 depletion results in a disruption of cell cycle progression with many metaphase cells displaying misaligned chromosomes. Microarray studies from the Bubulya lab demonstrated that depletion of TRAP150 results in the alteration of multiple key molecules required for cell cycle progression. This suggests that TRAP150 impacts mitosis in an indirect way by altering transcript abundance of important mitotic regulators.

My specific experimental aims were as follows:

Aim I

To study mitotic spindle and kinetochore abnormalities after Son depletion

Aim II

To identify mitotic defects after TRAP150 depletion and correlate with changes in mitotic transcript abundance

Figure 2.1: Depletion of TRAP150 leads to metaphase and telophase defects. Immunostaining of HeLa cells that have been transfected with TRAP150 siRNA 4 oligo. Cells were stained with rabbit anti-TRAP150 (1:1000); microtubules were labeled with mouse anti-alpha tubulin (1:4000) and DNA was stained using DAPI (1:20,000). Merged alpha-tubulin and DAPI images are also shown. After TRAP150 depletion misaligned chromosomes were detected at metaphase and lagging chromosomes were detected at telophase. Arrows indicate misaligned or lagging chromosomes. Immunoblotting was performed to validate TRAP150 depletion. Beta-actin was used on all five lanes as a loading control (Blaza and Bubulya, unpublished).

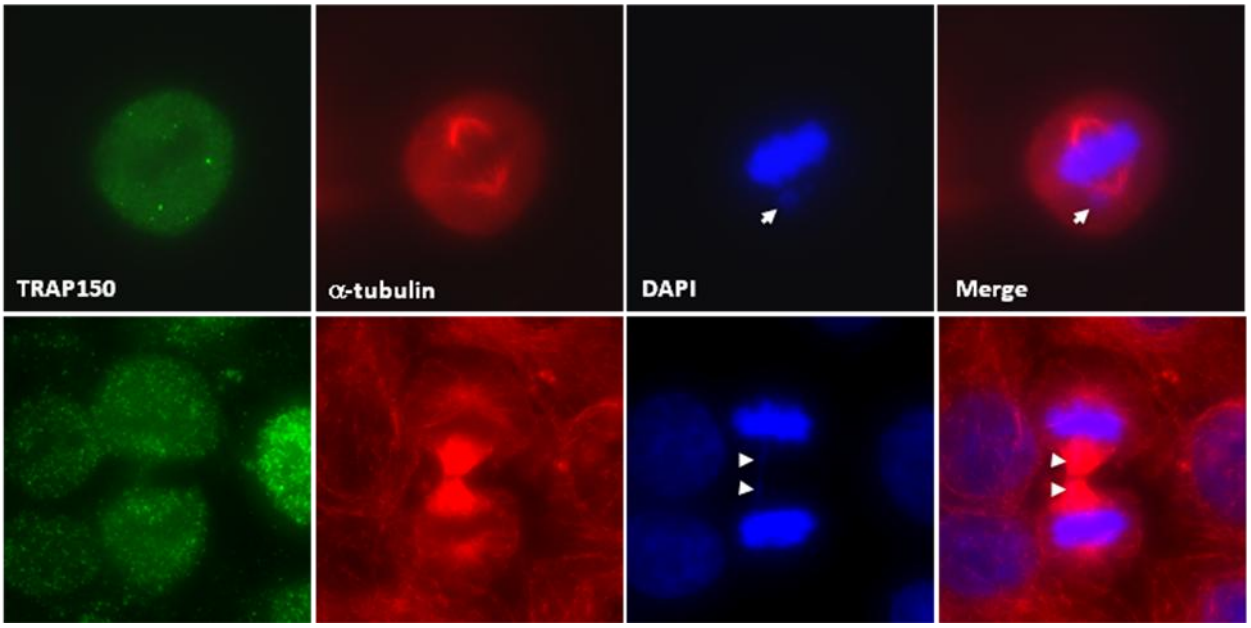
TRAP150
α-tubulin
DAPI
Merge

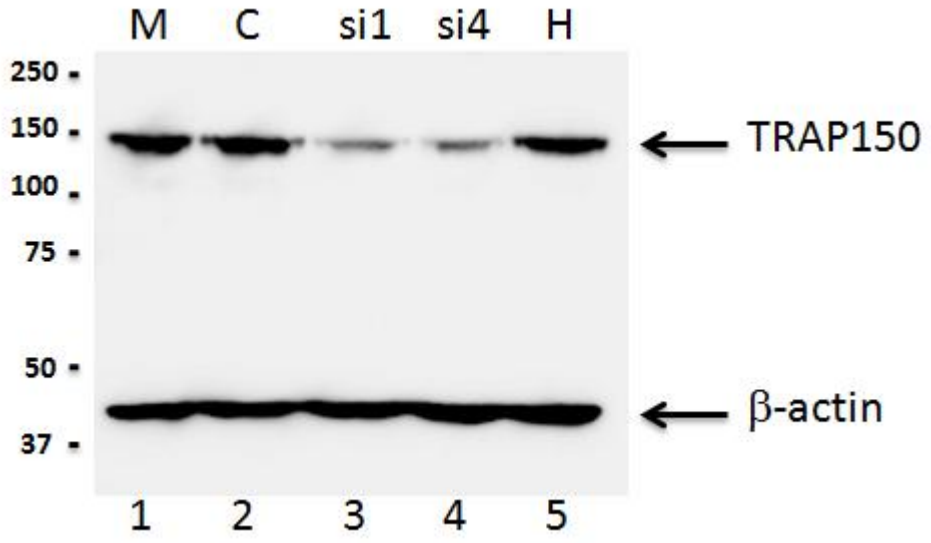
M
C
si1
si4
H
250
150
100
75
50
37
TRAP150
β-actin
1
2
3
4
5

Chapter 3: Materials and Methods

3.1 Cell Culture

HeLa cells and H2B-YFP cells were maintained in Dulbecco's Modified Eagles Medium (DMEM) supplemented with 1% penicillin/streptomycin and 10% fetal bovine serum. Cells were kept in a humidified 37^{o}C incubator injected with 5% carbon dioxide. To passage HeLa and H2B-YFP, cells were washed three times with phosphate buffered saline (PBS; 137mM NaCl; 2.7mM KCl; 4.3 mM Na2HPO4; 1.47 mM KH2PO4, pH 7.4). After washing, the cells were incubated with trypsin-EDTA (Invitrogen, 0.25% trypsin solution) for 2 minutes at 37^{o}C. Approximately 5 ml of DMEM was added to inactivate the trypsin and the suspension was transferred to a 15 ml conical tube and centrifuged at 1500 rpm for 2 minutes. The supernatant was removed by aspiration and the pellet was resuspended in 5 ml of DMEM. The cells were then either plated into new 100 mm X 20 mm culture dishes or counted and plated into 6 well dishes for experiments.

3.2 Plating Cells

To plate cells for immunofluorescence experiments, siRNA depletion experiments, flow cytometry experiments and live cell experiments, the cells were collected as previously described. Ten microliters of the cell

suspension was loaded onto each side of a Bright Line hemocytometer. The cells were counted to determine cell concentration. Cells were diluted with DMEM to a concentration of 1 X 10^5cells/ml. These were plated onto coverslips to process for immunofluorescence and live cell imaging or without coverslips for flow cytometry analysis and protein and RNA extraction. For all Son depletion experiments, cells were plated at a density of 5X10^5cells per well in 6 well plates. For live cell imaging experiments, cells were plated onto coverslips in 60 mm x 15 mm dishes.

3.3 Coverslip Preparation

All coverslips were cleaned thoroughly by washing in one part nitric acid and two parts hydrochloric acid for 2 hours with occasional stirring. They were rinsed in distilled water until the pH returned to 7.0. The coverslips were then stored in 70% ethanol and flamed prior to use.

3.4 Immunofluorescence

HeLa cells were washed briefly with PBS and fixed in 2% formaldehyde (for SF2/ASF, Son and ACA immunofluorescence experiments) or 4% formaldehyde (for alpha tubulin immunofluorescence experiments) for 15 minutes. Afterwards, they were washed three times for five minutes in phosphate buffered saline (PBS). Cells were then permeabilized using 0.2% Triton X-100 in PBS for five minutes. After permeabilization, the cells were washed 3 X 5 minutes with PBS/0.5% normal goat serum (NGS) and then the cells were incubated with primary antibodies at room temperature

for one hour. Primary antibodies used were WU14 (Anti-Son, 1:1000), Anti-tubulin (Sigma, 1:3000), Anti SF2/ASF (A. Krainer, 1:2500), Anti-U170K (1:200), Anti-ACA (1:3000) and Anti-TRAP150 (Bethyl catalog number: A300-956A, 1:1000). After the incubation time, the cells were washed 3 X 5 minutes with PBS/0.5% NGS. The cells then underwent a second incubation with either FITC-, Texas Red- or Cy5-conjugated secondary antibodies (min x; 1:1000; Jackson Immunoresearch Lab) for 1 hour at room temperature in a dark humidified chamber. Afterwards, the cells were washed with PBS for 5 minutes. After this wash, the cells were washed with DAPI (10 µg/ml) in PBS (1:20,000) for 5 minutes to stain the DNA. After the DAPI staining, the cells were again washed with PBS for 5 minutes and mounted on 8 µl of glycerol based mounting medium containing anti-fade (polyphenylinediamine), sealed with nail polish and stored at -80^{o}C.

3.5 Microscopy

Cells were imaged using a Delta Vision RT real time restoration system (Applied Precision) with PLAN-APO oil, 1.4 N.A. objectives (Olympus). HeLa and H2B-YFP cells were imaged with a 60X objective lens. Images were obtained with a cool snap CCD camera and SoftWorx Explorer Suite (Applied Precision, Issaquah, WA) was used for visualization and processing. Z-stacks containing of 0.25 µm increments through the z plane of the cells were displayed as a volume projection to include all images from the z-stack of interest. For live cell imaging, z-stacks (0.25

μm increments in z-plane) spanning the entire cell were collected every 2 minutes.

3.6 RNA Interference

Cells were plated as previously described in antibiotic-free DMEM supplemented with 10% FBS. Transfection of siRNA duplexes was done 24 hours after cells were plated. HeLa and H2B-YFP cells were transfected using Gibco 1X Opti-MEM, Invitrogen Oligofectamine Reagent, Dharmacon 1X siRNA buffer, 20 μM Luciferase Oligo (Dharmacon, catalog No. D-001210-02) and Son siRNA duplex 1 (Dharmacon, Catalog No. D-012983-01, target sequence GCUGAGCGCUCUAUGAUGU) and Son siRNA duplex 4 (Dharmacon, catalog No. D-012983-04, target sequence CAAUGUCAGUGGAGUAUCA) as well as TRAP150 siRNA duplex 1(Dharmacon, Catalog No. D-019907-01, target sequence GGUAUAAGCUCCGAGAUGAUU) and TRAP150 siRNA duplex 4 (Dharmacon, Catalog No. D-019907-04, target sequence GUUGAUCUCCGCCUUGAUAUU).

Table 3.1: RNA interference contents for all four conditions: Mock, Control, SiRNA1 and siRNA4.

Condition	Tube 1	Tube 2
Mock	250 µl Opti-MEM	15 µl Oligofectamine
	15 µl siRNA buffer	60 µl Opti-MEM
Control	250 µl Opti-MEM	15 µl Oligofectamine
	11 µl siRNA buffer	
	4 µl Luciferase oligo (50 µm)	60 µl Opti-MEM
SiRNA 1	250 µl Opti-MEM	15 µl Oligofectamine
	9 µl siRNA buffer	
	6 µl siRNA 1(50 µm)	60 µl Opti-MEM
siRNA 4	250 µl Opti-MEM	15 µl Oligofectamine
	9 µl siRNA buffer	
	6 µl siRNA 1(50 µm)	60 µl Opti-MEM

Contents were added to each tube and incubated for 5 minutes at room temperature. Afterwards, contents of tube 2 were added to tube 1 and incubated for 20 minutes at room temperature. 340 µl of the mixture was added to appropriate wells. Son depletion experiments were incubated for 48 hours and then processed. For TRAP150 depletion experiments cells

were incubated in the presence of siRNA duplexes for 72 hours and then processed.

3.7 RNA Extraction and DNase Treatment

Cells to be harvested for RNA extraction were plated as described previously. RNA was extracted using Qiagen RNeasy Extraction Kit. DMEM was removed from cells and collected in 15 ml conical tubes. The cells were washed briefly with PBS and incubated for 2 minutes with trypsin. Then they were collected using 1 ml of DMEM and centrifuged for 5 minutes at 1500 rpm. The supernatant was removed by aspiration and resuspended with 350 µl of Qiagen RNeasy RLT buffer and vortexed for 1 minute. Afterwards, 350 µl of 70% ethanol was added to the mixture and 700 µl of the sample was loaded into a RNeasy spin column. Then the samples were centrifuged for 15 seconds at 1500 rpm. 700 µl of Qiagen RNeasy RW1 buffer was added to the column and centrifuged for 15 seconds at 1500 rpm. Then 500 µl of Qiagen RNeasy RPE buffer was added to the column and centrifuged for 15 seconds at 1500 rpm. Additional 500 µl of RPE buffer was added to the spin columns and centrifuged for 2 minutes at 1500 rpm. To elute the RNA, 50 µl of RNAse free water was applied directly to the spin column membrane and centrifuged for 1 minute. The eluted RNA was then stored at – 80^{o}C.

The samples then underwent DNase treatment to degrade any leftover DNA using Ambien Turbo DNA free kit. The following was added to a fresh 1.5 ml eppendorf tube:

1) 5 µl of 10X Turbo DNAse buffer
2) 1 µl of Turbo DNAse
3) 5 µg RNA
4) Bring final volume to 50 µl with RNase free water.

The mixture was then incubated at 37^{o}C for 30 minutes. Afterwards, 5 µl of DNase inactivation reagent was added to each sample. They were incubated for 5 minutes at room temperature with occasional vortexing. The samples were then centrifuged for 1.5 minutes at 1500 rpm. 50 µl of the sample was then added to a fresh 1.5 ml eppendorf tube and stored at -80^{o}C.

3.8 RT-PCR

Son depletion validation

To assess Son mRNA knockdown, semiquantitative reverse transcription RT-PCR was performed. Reverse transcriptase reactions were performed on 100 ng of total RNA (SuperScript One Step RT-PCR System; Invitrogen). The linear range for amplification was verified after which 32 cycles were used to amplify both Son and glyceraldehyde-3-phosphate dehydrogenase (GAPDH) mRNAs). Son depletion was validated using

primers 5'-GTACCCTGAGCCAAGCACAT-3' and 5'-GGCTGCTCTGGCAATCTTAG-3'.

Cell Cycle gene validation

Quantitative RT-PCR was performed using BR1-Step Sybr Green qRT-PCR kit (Quanta) and 100 ng of total RNA. GAPDH primers 5'-ATGTTCGTCATGGGTGTGAA-3' and 5'-GGTGCTAAGCAGTTGGTGGT-3' were used as an internal control for all qRT-PCR reactions. Cell cycle genes tested were NDC80 (target sequence, 5'-AGTTGCAGACATTGAGCGAAT-3' and 5'-TGTTCAGCTTCCAGGTCCTT-3'), CENP-E (target sequence, 5'-TGGTCCTTGAGGAGAATGAGA-3' and 5'-GGTCTTCAAAGCACCCAAAC-3'), Bub1 (target sequence, 5'-AACTGAGAGCGCCATGTCTT-3'and 5'- CCAAAGGAGGAACAACAGGA-3'), CENP-F (target sequence, 5'- GTGGCAACAGAAGCTGACAA-3' and 5'- TCTTCTGTGTCGATGCCAAG-3' and Aurora B.

3.9 Microtubule Destabilization Experiment

HeLa cells were plated at 1x 10^5 per well in a 6-well dish with coverslips. After 48 hours, the cells were placed in 4^{o}C for 4-5 hours. Immunofluorescence was performed as previously described. Primary antibodies used were human anti-ACA (1:3000), mouse anti-tubulin (1:4000) and rabbit anti-Son (WU14) (1:1000). Secondary antibodies used were anti-mouse Cy5, anti-rabbit FITC and anti-human Texas Red.

Control cells that did not undergo cold treatment were also plated but were kept at 37^{o}C while the other samples were at 4 ^{o}C.

3.10 Protein extraction

The sample media was placed into 15 ml conical tubes. The cells were removed from the plate by applying cold PBS to the cells and scraping using a rubber policeman. The cells were then placed in an eppendorf tube and centrifuged for 5 minutes at 4^{o}C. Once the cells were centrifuged, they were resuspended in 100 µl of cold PBS and centrifuged for 2 minutes. Afterwards, the supernatant was removed and the pellet was resuspended in 100 µl of dH2O. The same amount of 2X Laemmli buffer (4% SDS, 20% glycerol, 1.4M β-mercaptoethanol, 0.125 M Tris-HCl) was added to each sample. The samples were boiled at 100^{o}C for 5 minutes. The samples were then stored for future immunoblotting analysis.

3.11 Protein Quantification (Bradford Assay)

Bradford reagent was purchased from Thermo Scientific (Product No. 1856210). The mass spectrometer was set to measure absorbance at 595 nm because it is the maximum absorbance wavelength for the Coomasie dye-protein complex.

Standards of known protein concentrations were prepared using bovine serum albumin (stock 10 µg/ µl) as follows:

- 0 µg (blank): 2 µl 1X Laemmli and 5 µl of dH2O
- 1 µg: 2 µl of 1X Laemmli, 0.5 µl of BSA and 4.5 µl of dH2O
- 2 µg: 2 µl of 1X Laemmli, 1 µl of BSA and 4 µl of dH2O
- 5 µg: 2 µl of 1X Laemmli, 2.5 µl of BSA and 2.5µl of dH2O
- 10 µg: 2 µl of 1X Laemmli and 5 µl of BSA

2 µl of protein extract was mixed with 2x Laemmli buffer for a total volume of 4 µl. 496 µl of water and 500 µl of Coomasie Plus Protein Assay Reagent (Thermo Scientific) were added to each sample for a final volume of 1 ml. Samples were loaded into 1 ml cuvettes and absorbance was measured on a Milton Roy Spectronic 1001 Plus. A graph of OD versus µg protein was plotted with the standard samples and a best fit line was applied using Microsoft Excel. Protein concentrations of experimental samples were obtained using the line equation obtained.

3.12 SDS-PAGE and Immunoblotting

The cell extracts were removed from -80°C and thawed to room temperature. The extracts were loaded into the wells of a 7% gel [resolving gel: 30% Degassed acrylamide/bis, 0.125 M Tris HCl (pH 8.8),

0.1% SDS; stacking gel: 30% Degassed acrylamide/bis, 0.125 M Tris HCl (pH 6.8), 0.1% SDS]. Precision Plus protein ladder (BioRad Catalog No. 161-0374) served as the molecular mass marker. The gel was run at 150V for one hour. The running buffer was prepared using 10X protein buffer (30.3 g Tris Base and 14.4 g glycine) and 10 ml of 10% SDS which was brought to a final volume of 1L. Once proteins were separated following electrophoresis, the proteins were then transferred from the polyacrylamide running gel to a nitrocellulose membrane at 200 mA for 90 minutes using chilled transfer buffer. Ponceau staining was used to confirm successful transfer (0.5% Ponceau S, 1% acetic acid) and to mark well lanes and mass markers. The nitrocellulose membrane was blocked against non-specific bonding using PBST (2.2 g sodium phosphate monobasic, 12.0 g sodium phosphate dibasic anhydrous, 85 g sodium chloride, and 1.0% Tween) and 5% non-fat dry milk. The nitrocellulose paper was then cut into strips such that the upper portion (>100 kDa) was probed with rabbit anti-TRAP 150 (1:250) and the lower portion was probed with mouse anti-actin (1:1000). The antibodies were diluted in 5% nonfat dry milk prepared with 1X PBST. Primary antibodies were applied to the membrane and incubated for 1 hour. The membrane was washed 3 X 5 minutes with PBST on a rotary shaker. Afterwards, secondary antibodies were applied to the membrane and incubated for 1 hour at room temperature on a shaker. Secondary antibodies used were anti-rabbit and anti-mouse horseradish peroxidase (HRP) (1:25000). The

membrane was then washed 3 X 5 minutes with PBST on a shaker. To detect species-specific antibodies conjugated with horseradish peroxidase (HRP) a chemiluinescence technique was used with Thermo Scientific Pierce ECL Western Blotting Substrate. The blot was then imaged on FUJI LAS-4000 Luminescent Image Analyzer (Fujifilm Life Science USA, Stamford, CT).

3.13 Flow Cytometry

TRAP150-depleted cells (treated with siRNA duplexes TRAPsi1 and TRAPsi4) as well as appropriate controls (mock and control) underwent flow cytometry analysis 72 hours after siRNA treatment using a FAC Scan flow cytometry system. Cells treated in parallel went through protein extraction 72 hours after siRNA treatment to confirm TRAP150 knockdown by western blotting. Untreated cells were used to set the gating on the flow cytometer and showed expected peaks at G1 and G2/M phase.

3.14 Live Cell Microscopy

HeLa and H2B-YFP cells were cultured and plated as described above. HeLa cells stably expressing H2B-YFP were plated at a density of $1x10^5$ on 60 mm coverslips 24 hours before RNAi. siRNA-mediated depletion of Son was done by transfection with siGENOME4. 72 hours after transfection, the cells were transferred to a live imaging chamber (Bioptechs, Butler, PA), perfused with L-15 medium (without phenol red) containing 20% fetal bovine serum and penicillin and streptomycin, and

placed into a 37^{o}C environmental chamber on the stage of a Delta Vision RT imaging system. Chromosome congression was observed by acquiring z stacks through the entire cell every 2 minutes for at least 1 hour.

3.15 Exon Array 1.0 ST

Five replicates the Human Exon Array 1.0 ST were performed using RNA samples isolated from five independent RNAi experiments (TRAP150-siRNA4 or control siRNA treated cells). Each RNA sample was subjected to DNase treatment as described above. RNA quality was determined by microfluidic analysis, using the Agilent 2100 Bioanalyzer, a RNA 6000 Nano Kit (PN-5067-151, Agilent, CA) to ascertain that the RNA was of sufficient quality for further analysis. RNA integrity numbers were all greater than 9.0. Whole Transcript (WT) Expression Array Kit (Ambion) was used to generate biotinylated sense strand DNA targets from the isolated RNA as described in the kit protocol. DNA quality and quantity was analyzed by nanodrop spectrophotometry (Thermo Scientific) and subjected to fragmentation and labeling using the Affymetrix GeneChip WT terminal labeling kit (Affymetrix) according to kit protocols. Each sample was hybridized and subjected to an automated washing, staining and scanning on the Fluidics Station 450 (Affymetrix) following fluidics protocol FS450-0001. Array results were analyzed for differential gene expression and alternative splicing in control versus Son-depleted samples. Ingenuity assessed genome wide changes in transcription as well as alternative splice events. Constitutive exons were used to detect

the changes in transcription, filtering out probe sets with a Detection Above Background (DABG) p-value of greater than 0.05 and probe sets with a non-log expression less than 70 (Sharma et.al, 2011).

Interkinetochore and Interpolar distance measurements

3.16 Statistics

The statistics were done by Dr.Melissa Schen using SPSS version 19. A Kruskal Wallis test was done on the interpolar distances, spindle width and interkinetochore distance measurements. A Kruskal Wallis test is a non-parametric alternative to a one-way anova test which requires equal variances in the sample. This test determines whether there is a significant difference between the different samples. A Games-Howell test was also performed. This test does pairwise comparisons between the samples.

Chapter 4: Identifying metaphase defects in the absence of Son

4.1 Son co-localizes with SF2/ASF through mitosis

To study the nature of the mitotic defect observed in Son-depleted cells, it was hypothesized that perhaps Son directly impacts mitotic progression through metaphase. To test this hypothesis, I examined Son localization throughout mitosis. For this purpose cells were plated and processed for immunofluorescence 48 hours later. Son as well as SF2/ASF (SRSF1) served as a marker to indicate nuclear speckle localization. This protein is known to localize in MIGs during anaphase (Lamond and Spector, 2003).

During interphase both Son and SF2/ASF localized in the typical speckled pattern (Figure 4.1, A, H). Once a cell enters prophase, the chromosomes start to condense but the nuclear speckles are still intact (Figure 4.1, B, I, P, W). As seen with the cells in interphase, both Son and SF2/ASF are present in prophase nuclear speckles (Figure 4.1, O). When a cell enters prometaphase, nuclear speckle disassembly as well as other significant morphological changes become more obvious. Chromosomes continue to condense and the nuclear envelope disassembles. Son, as well as SF2/ASF, starts to become diffuse throughout the cell (Figure 4.1, C, J, Q). A cell enters anaphase when the mitotic spindle begins to shorten pulling the aligned chromosomes apart (Figure 4.1, Z).

Figure 4.1: Son and SF2/ASF co-localize during mitosis.

Immunofluorescence of Son using rabbit anti-Son antibody WU14 (1:1000) (A-G); mouse anti-SF2/ASF (1:2500) (H-N); merged Son and SF2/ASF images are shown (O-U) and DNA stained with DAPI (1:20,000). Son and SF2/ASF co-localize during mitosis. After nuclear envelope breakdown, Son and SF2/ASF diffuse throughout the cell. In anaphase both proteins begin to accumulate in mitotic interchromatin granules (MIGs). In telophase, the MIGs increase in number and size. After the nuclear envelope reforms, Son and SF2/ASF are imported into the nucleus. Arrows indicate MIGs. Bar = 5μm.

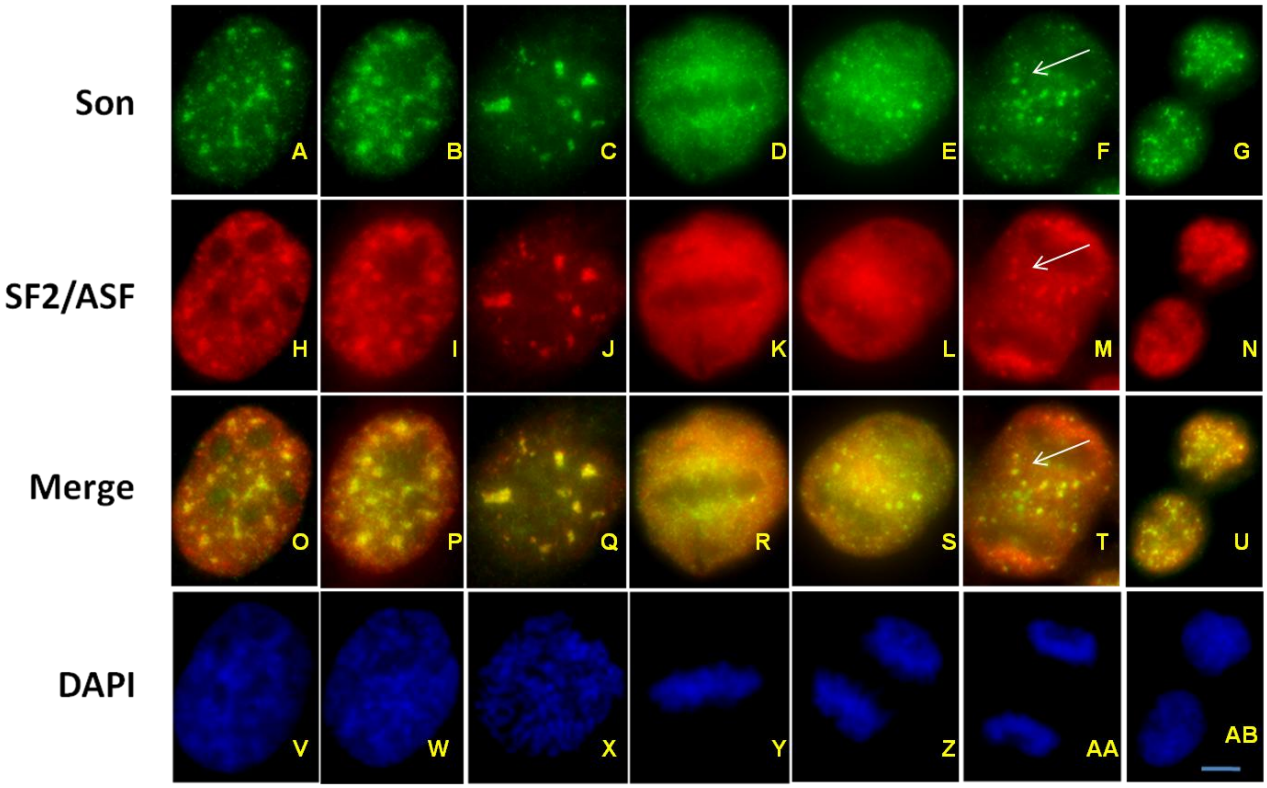
Son
SF2/ASF
Merge
DAPI
A
B
C
D
E
F
G
H
I
J
K
L
M
N
O
P
Q
R
S
T
U
V
W
X
Y
Z
AA
AB

During this phase, SF2/ASF starts assembling in regions analogous to the nuclear speckles known as MIGs. The MIGs can be described as bright dots found dispersed throughout the cytoplasm (Lamond and Spector, 2003).

In addition, the level of diffuse SF2/ASF found throughout the cell decreases once the MIGs begin to form. Son showed a similar pattern as SF2/ASF. Merged images indicated that Son and SF2/ASF colocalized in MIGs (Figure 4.1, S). When the cell enters telophase, these MIGs increase in number and size (Lamond and Spector, 2003). The amount of diffuse protein found throughout the cell also decreases. As the cell cycle progresses to G1, the nuclear envelope forms once again and the nuclear speckle proteins move from the cytoplasm to the nucleus (Lamond and Spector, 2003). Once import is complete, speckle components begin to assemble into nuclear speckles (Figure 4.1, G, N, U, AB).

Son was detected in other regions of the cell that were SF2/ASF deficient. Son was present in the chromatin region its localization pattern in this region (doublets of small foci) suggested possible localization within kinetochores.

4.2 Depletion of Son disrupts mitotic spindle formation

HeLa cells were treated with Son siRNA oligos (1 and 4) and harvested for immunofluorescence and RNA extraction 48 hours later. RT-PCR was performed in order to validate Son depletion in each experiment (Figure 4.2, M). Following

Figure 4.2: Depletion of Son results in disorganized and elongated mitotic spindles.

HeLa cells were transfected with control oligo (A-D), Son siRNA oligo 1 (E-H) or Son siRNA oligo 4 (I-L). Cells were processed for either immunofluorescence or RNA extraction 48 hours later after transfection. Microtubules were labeled using mouse anti-alpha-tubulin (B,F,J); Son was labeled using rabbit anti-Son antibody WU14 (A,E,I); merged Son and microtubule images are shown (C,G,K) and DNA stained with DAPI (1:20,000) (D,H,L). Son depletion was validated through RT-PCR (M). A separate set of cells underwent RNA extraction. RNA extracts were treated with DNase and used for RT-PCR to measure Son expression levels. Arrows indicate disorganized microtubules. Bar= 5 µm.

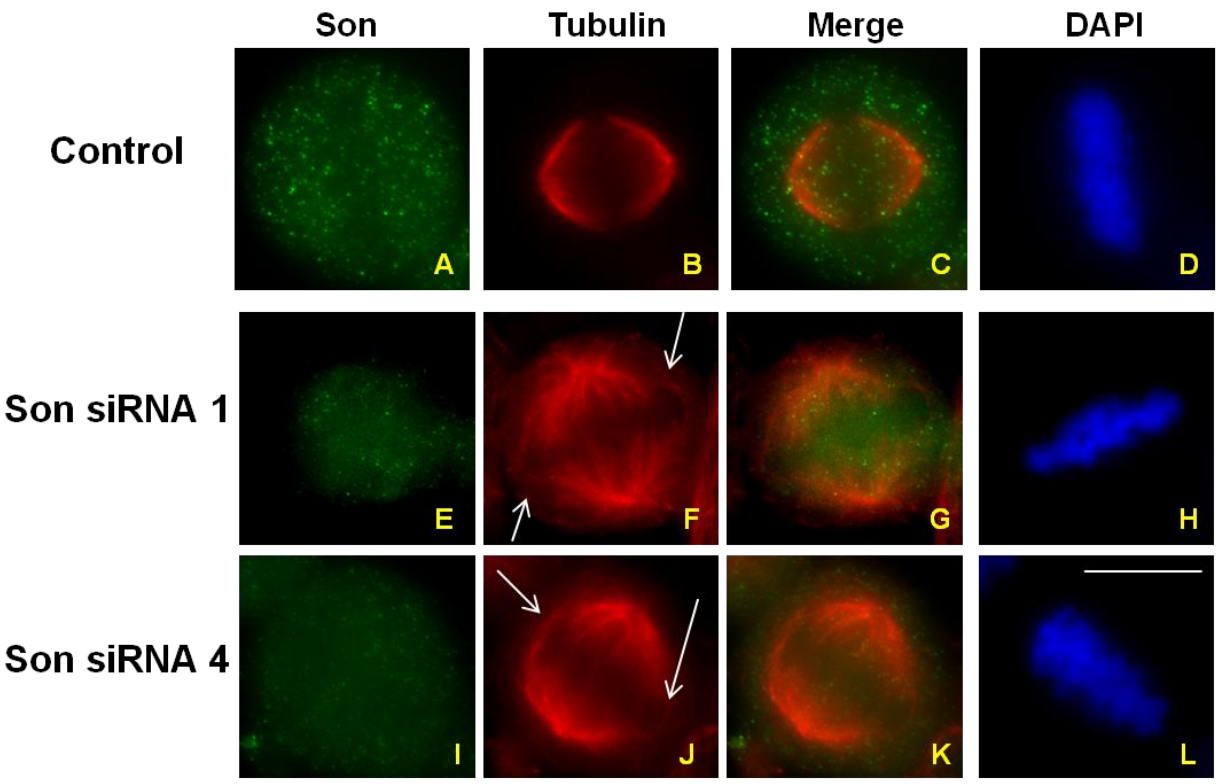
Son
Tubulin
Merge
DAPI
Control
Son siRNA 1
Son siRNA 4
A
B
C
D
E
F
G
H
I
J
K
L

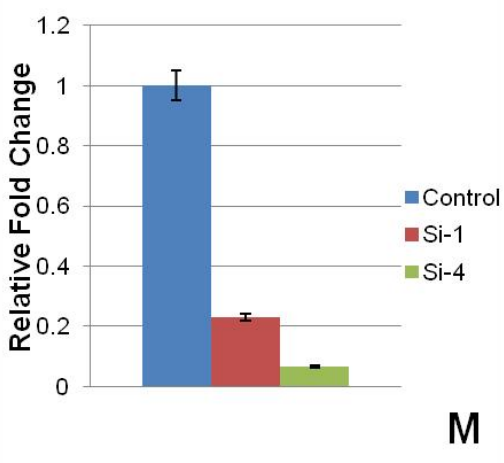
1.2
1
0.8
0.6
0.4
0.2
0
Relative Fold Change
Control
Si-1
Si-4
M

Son depletion, metaphase cells exhibited disarrayed microtubules (disorganized spindles) as well as elongated spindles (Figure 4.2 F, J). Microtubules in Son-deficient cells radiate from the centrosomes in a disorganized way. In order to quantify these defects, three replicates of Son siRNA experiments were performed. 150 metaphase cells in each sample (for mock, control, si1 and si4) for all replicates were scored to measure interpolar distance as well as spindle width using Delta Vision RT real time restoration system (Applied Precision) software measuring tools. On average, the interpolar distance was 2 to 3 μm longer in Son siRNA treated cells even though spindle width remained unchanged (Figure 4.3 A, B). Statistical analysis was done on interpolar distances as well as in the spindle width measurements in the form of a Kruskal Wallis test. Results showed that there is a significant difference in spindle widths and interpolar distances between the samples ($p<0.000$). A Games-Howell test was done to do pairwise comparisons. All of the samples had spindle widths that were statistically significant from each other ($p< 0.05$) except for si4 and control. All of the samples had interpolar distances that were statistically significant from each other ($p<0.05$).

To further characterize these defects, interkinetochore distances were measured in control as well as Son depleted cells. RT-PCR was performed to confirm Son depletion in each experiment (Figure 4.4 B). A total of 600 interkinetochore distances were measured in two separate Son siRNA experiments. Interkinetochore distance measurements were not dependent on the presence of

Figure 4.3: Son depletion results in elongated spindles but it does not alter spindle width

(A) HeLa cells were transfected with control control oligo, Son siRNA1 or Son siRNA4. After 48 hours of transfection, cells were processed for immunofluorescence or RNA extraction. A total of 150 mitotic spindles were measured in Mock, Control, Son siRNA1 and Son siRNA4 cells. After Son depletion, interpolar distances were 2 to 3 μm longer than control cells ($p<0.000$). (B) Spindle width distances were also measured in these cells. However, after Son depletion spindle width measurements remained unchanged. (C) Son depletion was validated through RT-PCR. RNA was extracted from a duplicate set of cells and the RNA extracts were treated with DNase. The RNA extracts were then used for RT-PCR.

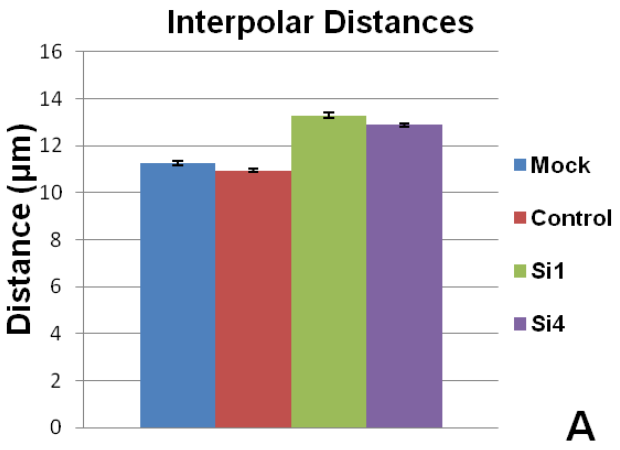
Interpolar Distances
Distance (µm)
16
14
12
10
8
6
4
2
0
Mock
Control
Si1
Si4
A

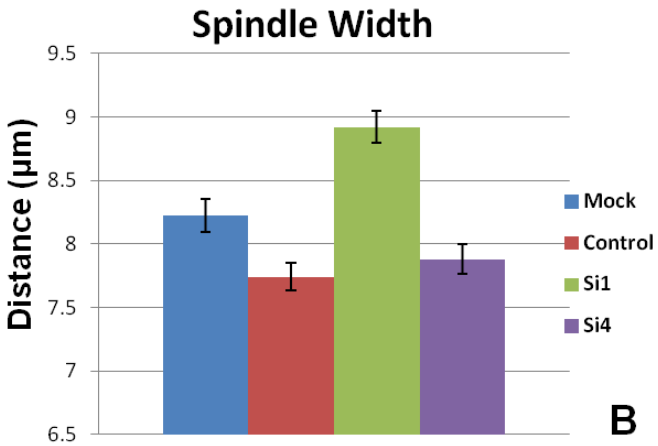
Spindle Width
Distance (µm)
9.5
9
8.5
8
7.5
7
6.5
Mock
Control
Si1
Si4
B

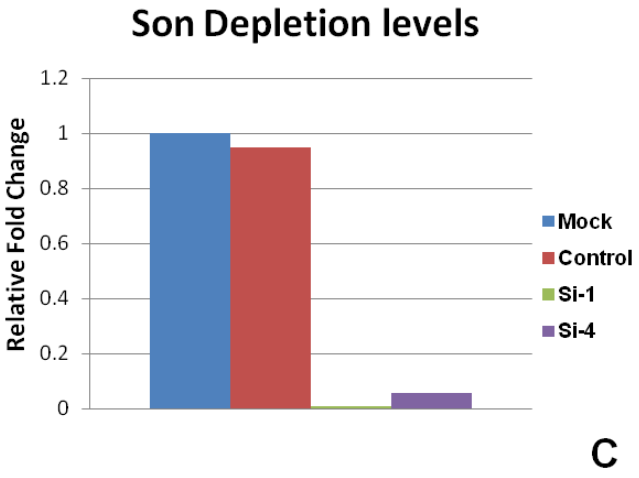
Son Depletion levels
Relative Fold Change
1.2
1
0.8
0.6
0.4
0.2
0
Mock
Control
Si-1
Si-4
C

Figure 4.4: Son depletion does not alter interkinetochore tension

(A) HeLa cells were transfected with control oligo, Son siRNA1 oligo or Son siRNA oligo4 and processed for either immunofluorescence or RNA extraction. A total of 1200 interkinetochore distances were measured for mock, control, Son siRNA1 and Son siRNA4. After Son depletion, interkinetochore distances remained unchanged ($p<0.000$). (B) Son depletion was validated through RT-PCR. RNA was extracted from a duplicate set of cells and the RNA extracts were treated with DNase. The RNA extracts were then used for RT-PCR. (C) Immunofluorescence image of kinetochores (labeled using human anti-ACA, 1:3000; DNA was stained with DAPI, 1:20,000). Inset indicates examples of what was measured as an interkinetochore distance.

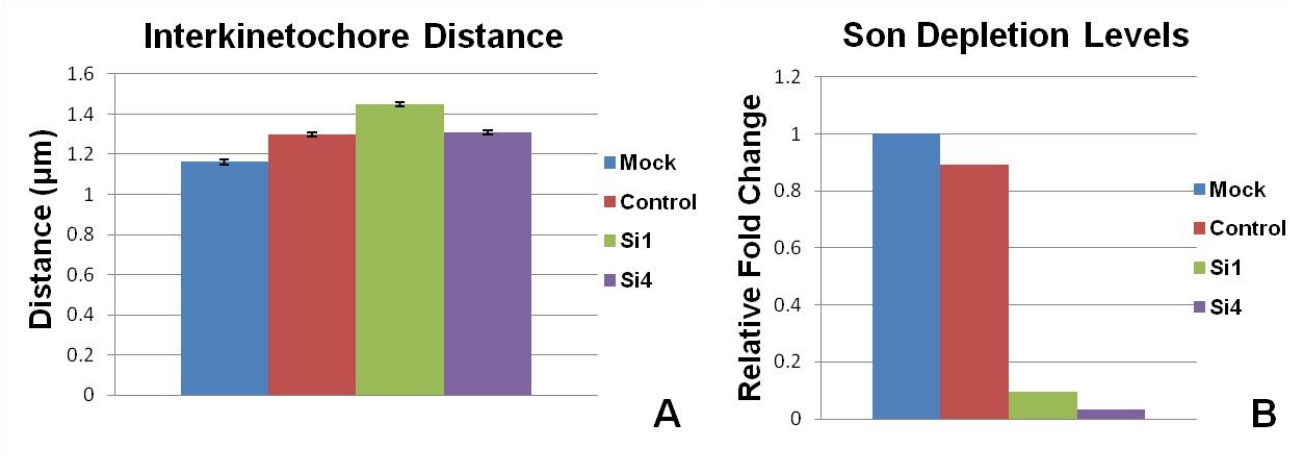
Interkinetochore Distance
Distance (µm)
1.6
1.4
1.2
1
0.8
0.6
0.4
0.2
0
Mock
Control
Si1
Si4
A
Son Depletion Levels
Relative Fold Change
1.2
1
0.8
0.6
0.4
0.2
0
Mock
Control
Si1
Si4
B

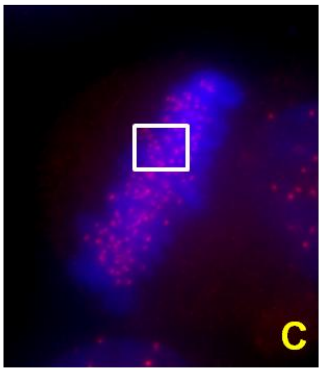
C

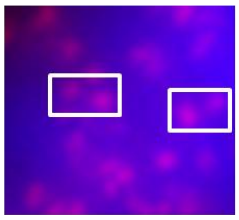

Son (Figure 4.4 A). Variability was seen through all four samples; regardless of Son levels. Kruskal Wallis test using SPSS (version 19) was performed on the interkinetochore distance measurements in order to confirm statistically significant results. Results showed there is a significant difference between the samples. A Games-Howell test was done to do pairwise comparisons. All of the samples had interkinetochore distances that were statistically significant from each other ($p<0.05$) except for si4 and control.

4.3 Son does not co-localize with kinetochores

Previous results demonstrated that Son exhibited a pattern similar to a kinetochore pattern during metaphase. To further study possible Son-kinetochore interactions, immunofluorescence experiments were performed immunolabeling Son (WU14) and ACA (anti-centromere antibody) (Figure 4.5). Colocalization studies did not reveal any colocalization between Son and kinetochores at any point during mitosis. To rule out a dynamic role of Son in kinetochores, cold tubulin destabilization was performed to detect an enhancement of Son at the kinetochore (Figure 4.6). However, destabilization did not enhance Son localization at the kinetochore. Instead, Son morphology seemed to change following cold treatment, aggregating in MIG-like structures. To determine if this was a characteristic typical of nuclear speckle proteins, the same experiment was performed with SF2/ASF and U170K (Figure 4.7 and 4.8). SF2/ASF and U170K did not change distribution in response to cold treatment. In order to determine whether Son's cellular localization was changing as a response to cold or in response to the destabilization of microtubules, cells were arrested using

Figure 4.5: Son does not co-localize to kinetochores during mitosis

HeLa cells were plated and processed for immunofluorescence 48 hours later. Son was labeled using rabbit anti-Son antibody WU14 (1:1000) (A-F); kinetochores were labeled using human anti-ACA (CREST) (1:3000) (G-L); merged Son and kinetochore images are shown (M-R); merged kinetochores and DNA images are shown (S-X); DNA stained with DAPI (1:20,000). Son and kinetochores did not co-localize during mitosis. Insets of Son and kinetochore images are shown below (AE, AF). Insets indicate several Son foci that do not overlap with ACA (AE-AP). Bar= 5 µm.

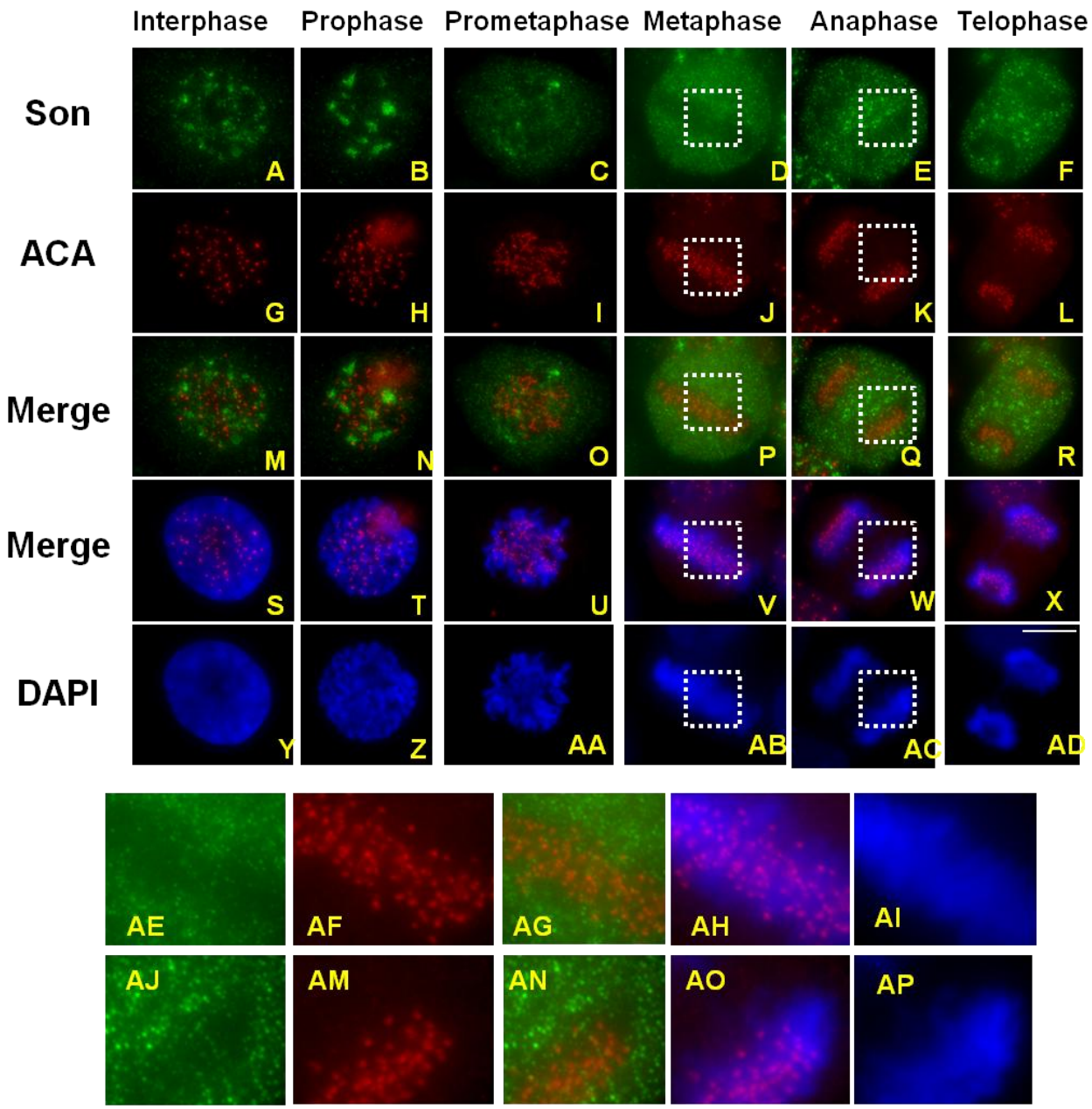
Interphase
Prophase
Prometaphase
Metaphase
Anaphase
Telophase
Son
ACA
Merge
Merge
DAPI
A
B
C
D
E
F
G
H
I
J
K
L
M
N
O
P
Q
R
S
T
U
V
W
X
Y
Z
AA
AB
AC
AD
AE
AF
AG
AH
AI
AJ
AM
AN
AO
AP

Figure 4.6: Cold destabilization of microtubules did not enhance Son localization to the kinetochore but revealed novel Son localization

HeLa cells were placed in 4^{o}C for 4 hours and then processed for immunofluorescence. A duplicate experiment that did not undergo cold treatment were processed for immunofluorescence and served as control. Son was labeled using rabbit anti-Son antibody WU14 (1:1000) (A,F,K,P); kinetochores were labeled using human anti-ACA (CREST) (1:3000) (B,G,L,Q); microtubules were labeled using mouse anti-tubulin (1:4000) (C,H,M,R); merged ACA and Son images are shown (D,I,N,S) and DNA was stained with DAPI (1:20,000) (E,J,O,T). After cold destabilization, Son did not co-localize with kinetochores but it did exhibit a novel localization resembling MIGs (indicated by arrows). Insets of of prometaphase (U-X) and metaphase cells (Y-AC) after cold treatment are shown. Bar= 5 µm.

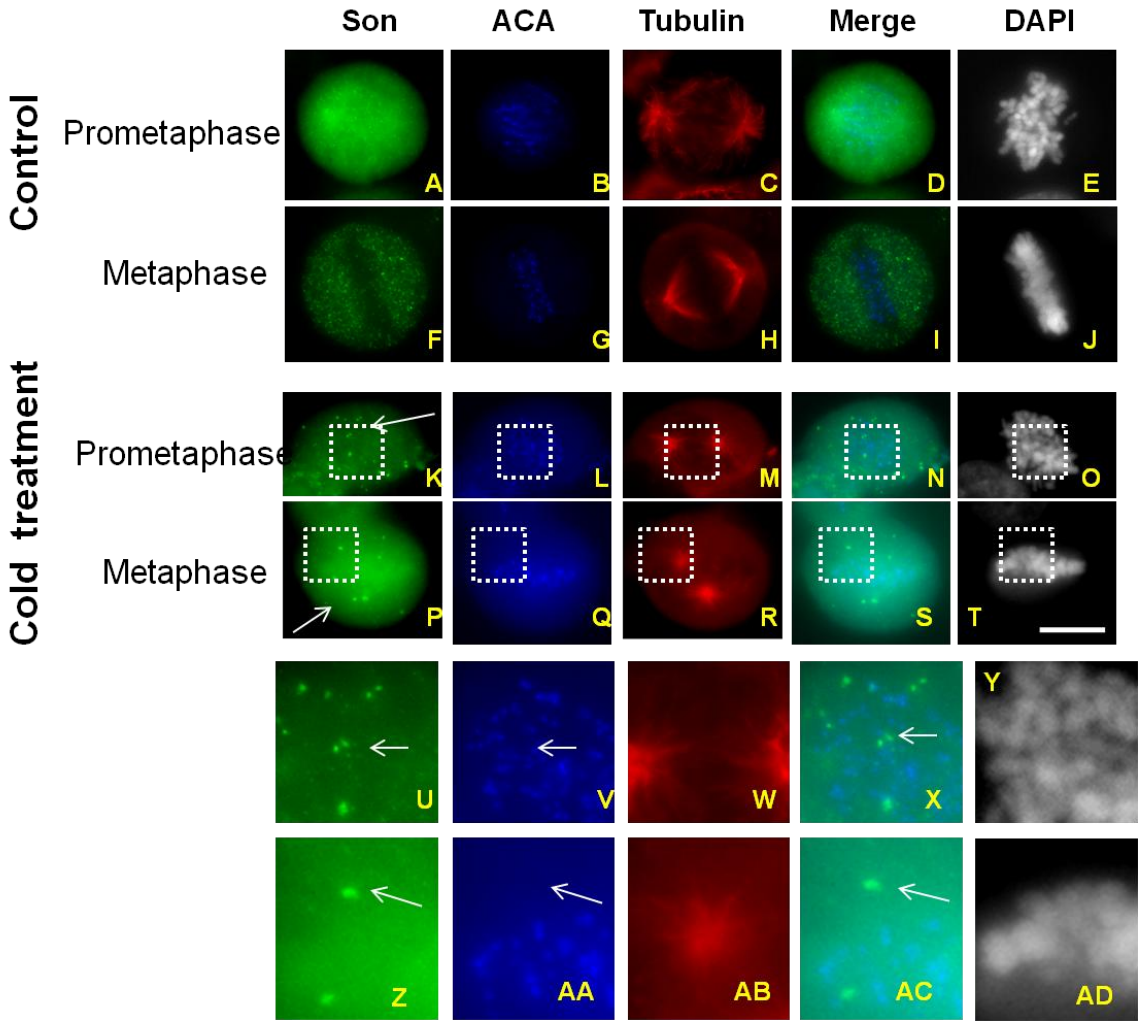
Son
ACA
Tubulin
Merge
DAPI
Control
Prometaphase
Metaphase
Cold treatment
Prometaphase
Metaphase
A
B
C
D
E
F
G
H
I
J
K
L
M
N
O
P
Q
R
S
T
U
V
W
X
Y
Z
AA
AB
AC
AD

Figure 4.7: Cold destabilization of microtubules changed Son morphology in the cell but it did not alter SF2/ASF morphology

HeLa cells were placed in 4^{o}C for 4 hours and then processed for immunofluorescence. A duplicate experiment that did not undergo cold treatment were processed for immunofluorescence and served as control. Son was labeled using rabbit anti-Son antibody WU14 (1:1000) (A,F,K,P); kinetochores were labeled using human anti-ACA (CREST) (1:3000) (C,H,M,R); SF2/ASF was labeled using mouse anti-SF2/ASF (B,G,L,Q); merged ACA and Son images are shown (D,I,N,S) and DNA was stained with DAPI (1:20,000) (E,J,O,T). Insets of metaphase cell after cold treatment are shown (U-Y). After cold destabilization, Son morphology exhibited a change in localization but SF2/ASF did not undergo any morphological change. Arrows indicate novel Son cytoplasmic foci but this was not seen with SF2/ASF. Bar= 5 µm.

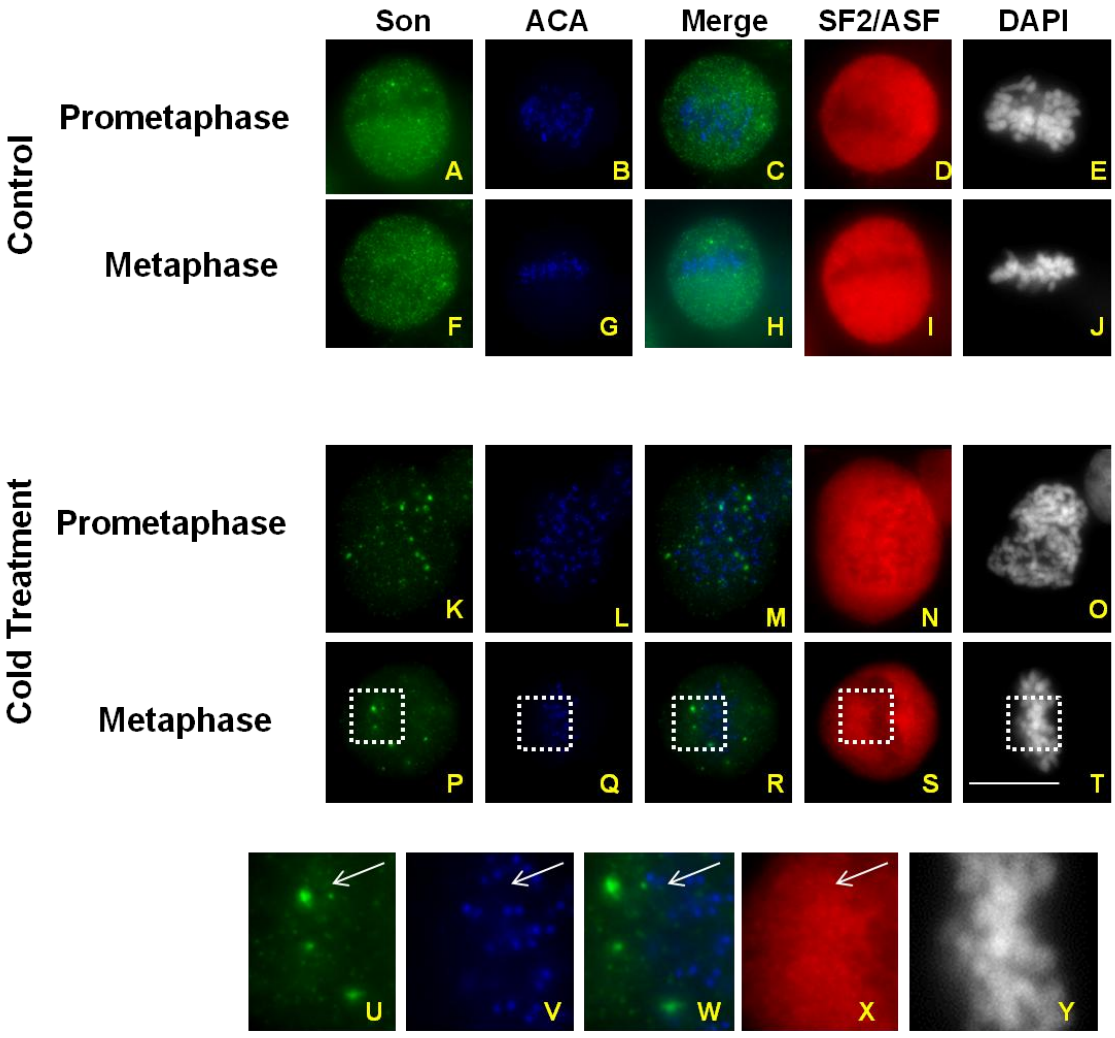
Son
ACA
Merge
SF2/ASF
DAPI
Control
Prometaphase
Metaphase
Cold Treatment
Prometaphase
Metaphase
A
B
C
D
E
F
G
H
I
J
K
L
M
N
O
P
Q
R
S
T
U
V
W
X
Y

Figure 4.8: Cold destabilization of microtubules changed Son morphology in the cell but it did not alter U170K morphology

HeLa cells were placed in 4^{o}C for 4 hours and then processed for immunofluorescence. A duplicate set of cells that was not exposed to cold treatment was processed for immunofluorescence and served as control. Son was labeled using rabbit anti-Son antibody WU14 (1:1000) (A,F,K,P); kinetochores were labeled using human anti-ACA (CREST) (1:3000) (C,H,M,R); U170K was labeled using mouse anti-U170K (B,G,L,Q); merged ACA and Son images are shown (D,I,N,S) and DNA was stained with DAPI (1:20,000) (E,J,O,T). Insets of a metaphase cell after cold treatment are shown (U-Y). After cold destabilization, Son exhibited a change in localization (indicated by arrow) but U170K did not undergo any change (indicated by arrow). Bar= 5 µm.

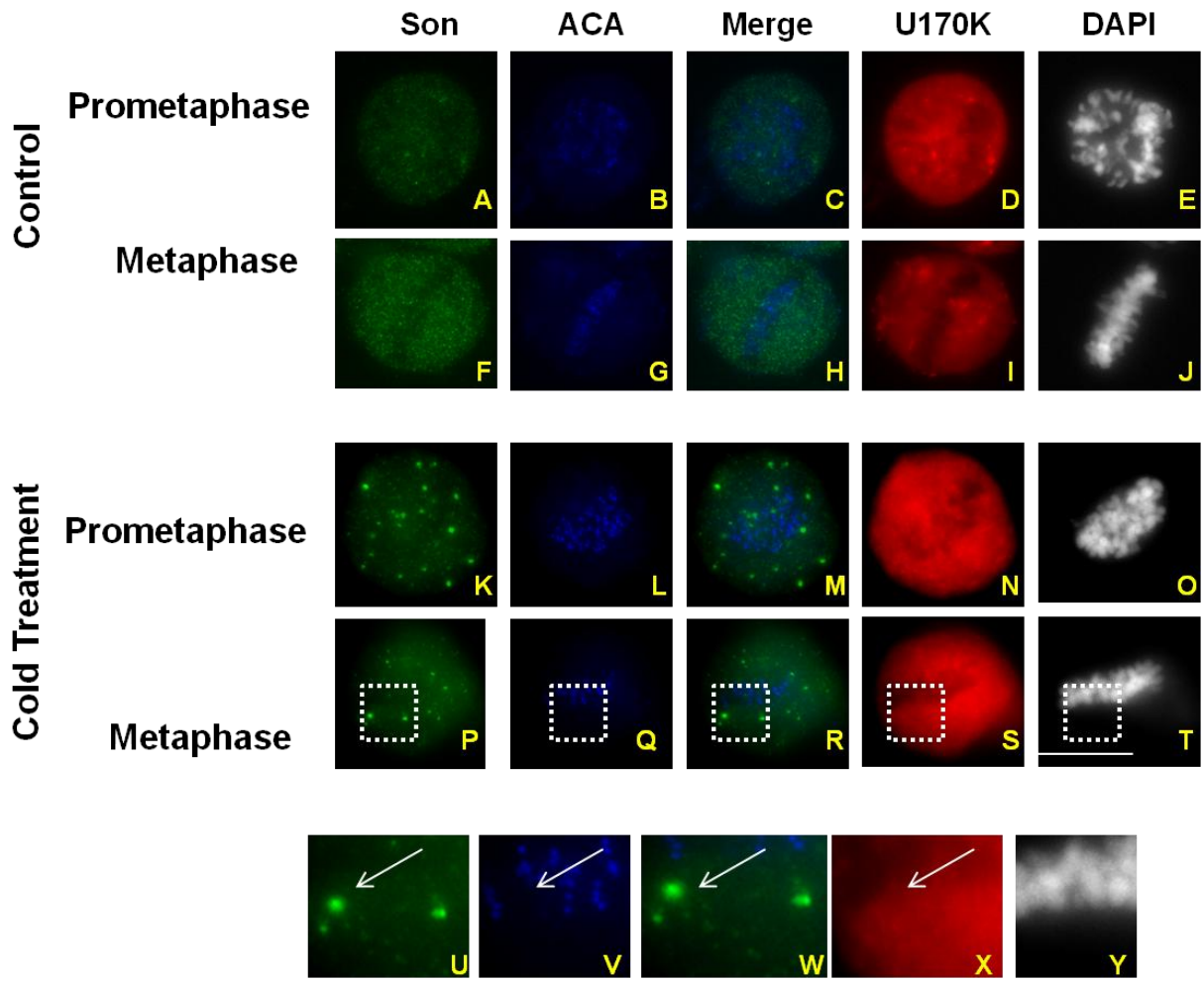
Son
ACA
Merge
U170K
DAPI
Control
Prometaphase
Metaphase
Cold Treatment
Prometaphase
Metaphase
A
B
C
D
E
F
G
H
I
J
K
L
M
N
O
P
Q
R
S
T
U
V
W
X
Y

nocodazole and then processed for indirect immunofluorescence labeling of Son as well as alpha-tubulin (Figure 4.9). Destabilization of microtubules using nocodazole resulted in the same son phenotype that occurred following cold destabilization of microtubules (Figure 4.9, I, M, Q). After the nocodazole treatment, Son accumulated into cytoplasmic foci that resemble MIGs. This was seen in prometaphase as well as metaphase cells.

Figure 4.9 Microtubule destabilization using nocodazole caused a change in the localization of Son

HeLa cells were treated with nocodazole (100 ng/ml) and processed for immunofluorescence 6 hours later. Control cells that were not treated with the drug were plated and processed at the same time. Son was labeled using rabbit anti-Son antibody WU14 (1:1000) (A,E,I,M,Q); microtubules were labeled using mouse anti-alpha-tubulin (1:4000) (B,F,J,N,R); merged Son and microtubule images are shown (C,G,K,O,S) and DNA was stained with DAPI (D,H,L,P,T). Microtubule destabilization using nocodazole altered Son's localization pattern in the cell. Arrows indicate Son aggregates that form after microtubule destabilization. Bar= 5 µm.

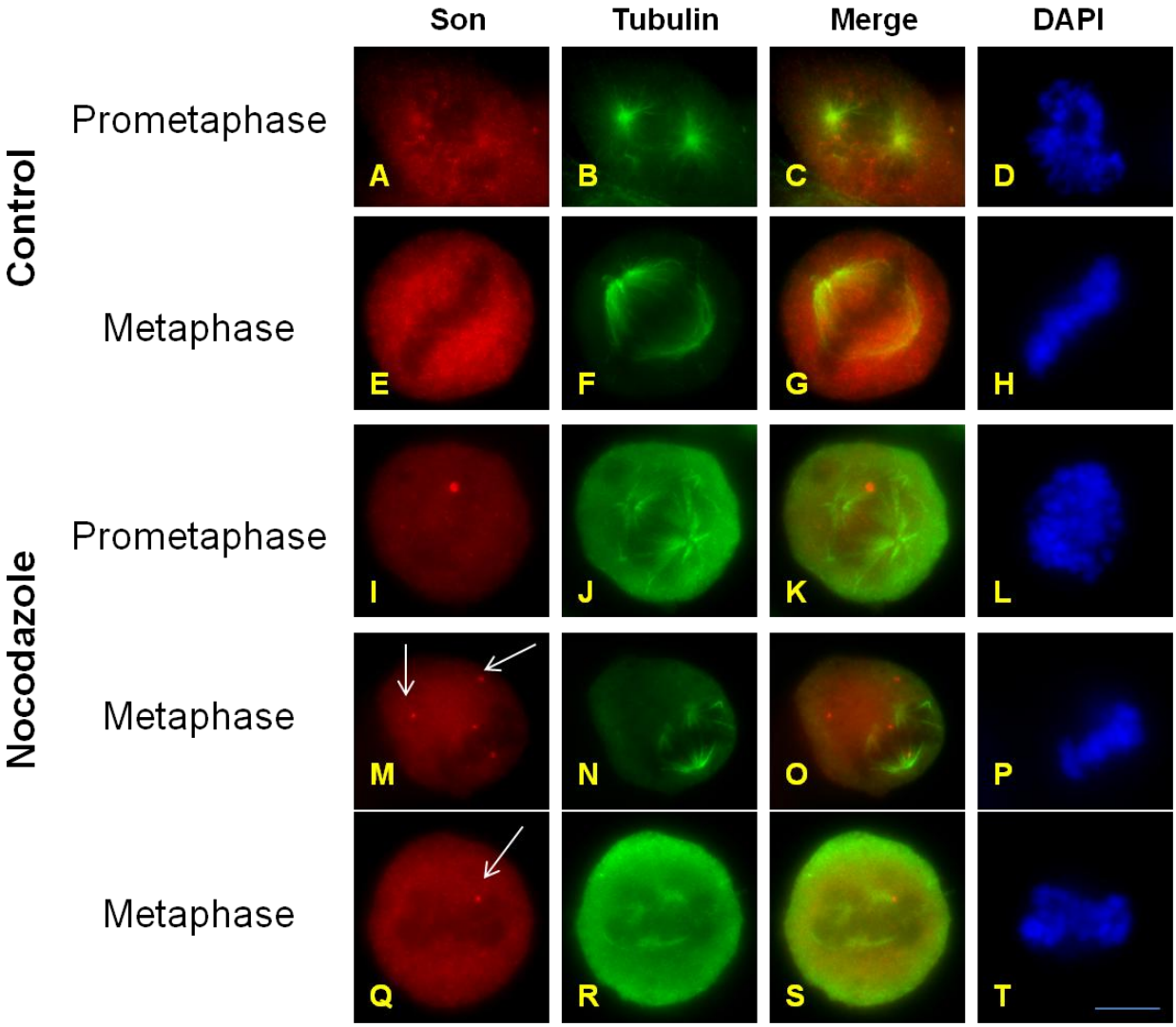
Son
Tubulin
Merge
DAPI
Control
Prometaphase
Metaphase
Nocodazole
Prometaphase
Metaphase
Metaphase
A
B
C
D
E
F
G
H
I
J
K
L
M
N
O
P
Q
R
S
T

Chapter 5: Studying mitotic defects after TRAP150 depletion

5.1 TRAP150 depletion results in mitotic defects

To detect whether TRAP150 showed any colocalization with mitotic structures, HeLa cells were plated and processed for immunofluorescence 48 hours later. TRAP150 and alpha-tubulin were immunolabeled and their localization was compared throughout mitosis (Figure 5.1). Results did not show localization of TRAP150 at the mitotic spindle, but showed that TRAP150 in MIGs as expected for a nuclear speckle protein.

HeLa cells were treated with TRAP150 siRNA oligos 1 and 4 and they were harvested for immunofluorescence and protein extraction 72 hours later. Western blotting was performed to validate TRAP150 depletion. TRAP150-depleted cells showed multiple mitotic defects at various mitotic stages. Defects were seen at all stages of mitosis except prophase (Figure 5.2). The most common defect was misaligned chromosomes in metaphase cells. To further study this defect, mitotic distribution as well as mitotic index were calculated in control and in TRAP150-deficient cells. To calculate mitotic distribution, 300 mitotic cells of each sample (3 replicates performed) were scored and categorized into the different mitotic stages. Defective mitotic cells were also scored and categorized (Figure 5.3). After TRAP150 depletion, the mitotic distribution changed. In control samples, metaphase cells were

Figure 5.1: TRAP150 does not co-localize with any mitotic structure during mitosis

HeLa cells were plated and processed for immunofluorescence 48 hours later. TRAP150 was labeled using rabbit anti-TRAP150 (1:1000) (A, E, I, Q, U); microtubules were labeled using mouse anti-alpha-tubulin (B,F,J,N,R,V); merged TRAP150 and microtubule images are shown (C,G,K,O,S,W) and DNA was stained with DAPI (D,H,L,P,T,X). TRAP150 did not co-localize with any mitotic structures during mitosis. Bar = 5μm.

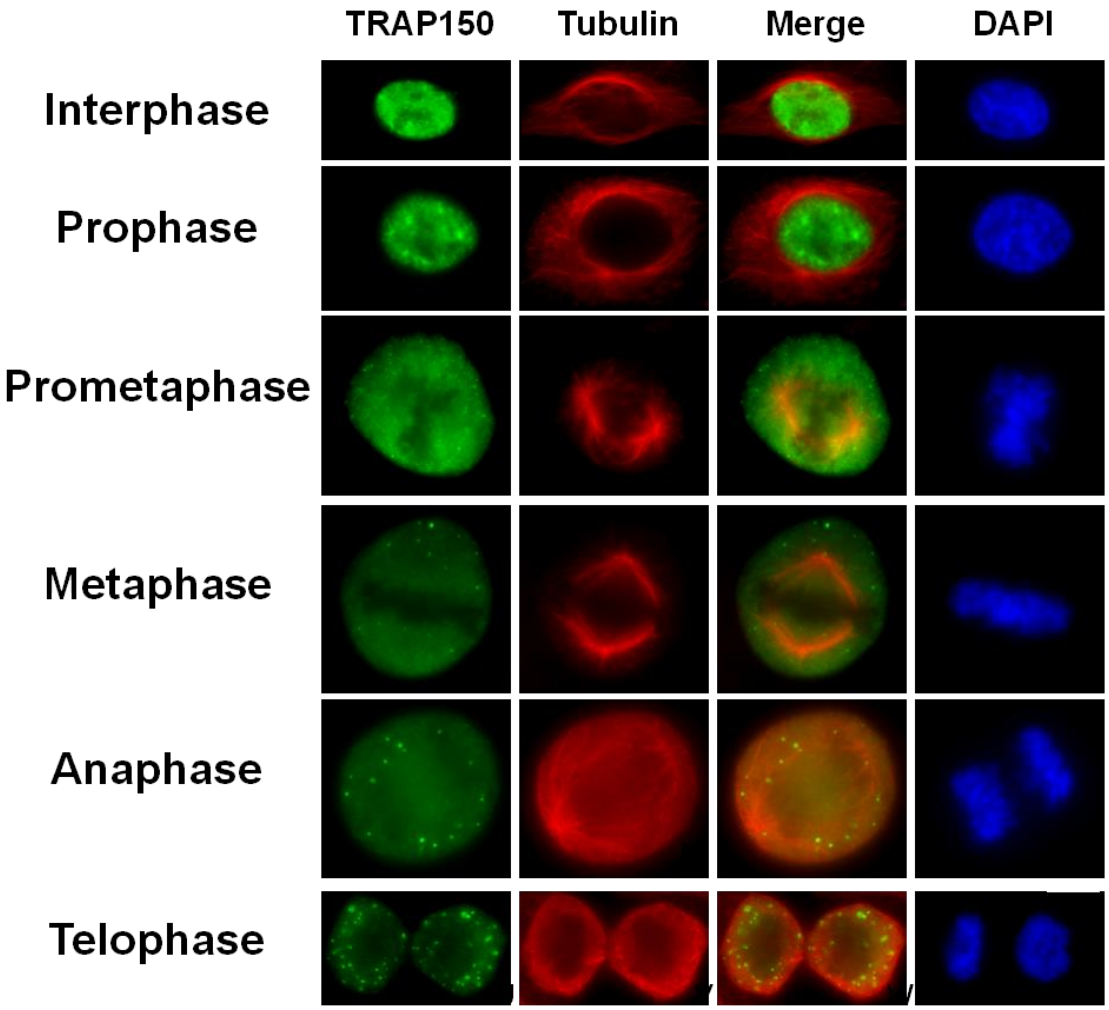
TRAP150
Tubulin
Merge
DAPI
Interphase
Prophase
Prometaphase
Metaphase
Anaphase
Telophase

Figure 5.2: TRAP150 depletion results in multiple mitotic defects

HeLa cells were transfected with control oligo or TRAP150 siRNA4. After 72 hours, the cells were processed for immunofluorescence or protein extraction. TRAP150 was labeled using rabbit anti-TRAP150 (1:1000) (A,E,I,M); microtubules were labeled using mouse anti-alpha-tubulin (1:4000) (B,F,J,N); merged TRAP150 and microtubule images are shown (C,G,K,O) and DNA was stained with DAPI (1:20,000) (D,H,L,P). Bar= 5 µm. Arrows indicate misaligned chromosomes. (Q) TRAP150 depletion was validated through immunoblotting. A duplicate experiment underwent protein extraction. Protein extracts were then used for western blot. Control immunofluorescence images are also shown in the figure. These cells were not treated with TRAP150 siRNA4 oligo.

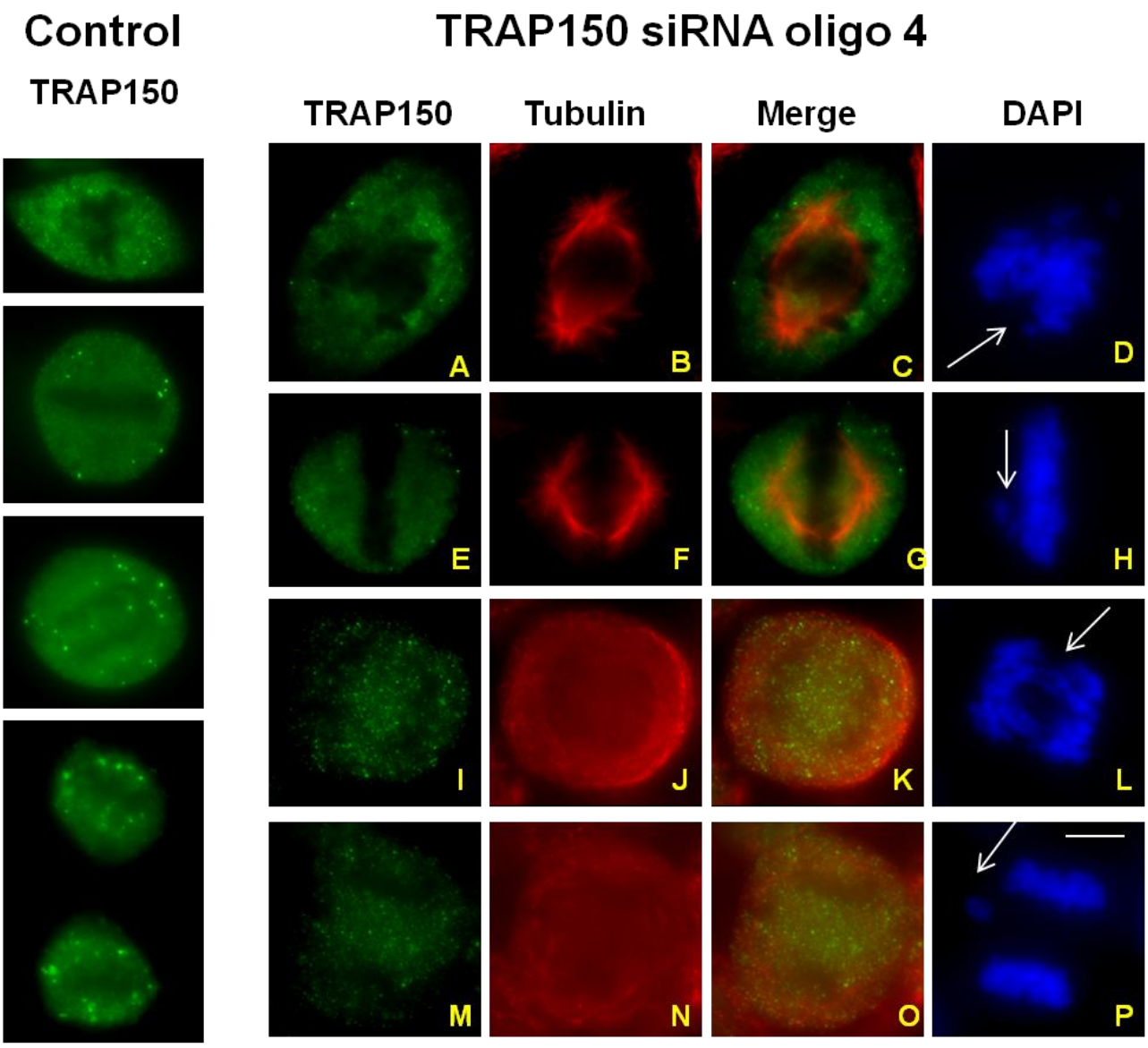
Control
TRAP150
TRAP150 siRNA oligo 4
TRAP150
Tubulin
Merge
DAPI
A
B
C
D
E
F
G
H
I
J
K
L
M
N
O
P

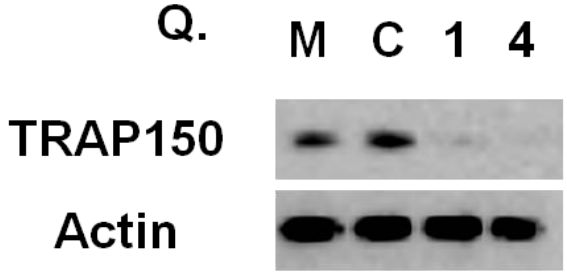
Q.
M C 1 4
TRAP150
Actin

more abundant than any other mitotic phase with prometaphase cells being the second most abundant. In TRAP150 depleted samples however, there was an increase in prometaphase cells and a decrease in metaphase cells. The mitotic stages that were the most defective in TRAP150-deficient cells were prometaphase and metaphase. There were no prophase defects and a few anaphase and telophase defects. The mitotic index was determined by counting the number of mitotic cells out of 100 cells and averaging that percentage (n=10). In TRAP150-depleted samples, mitotic index decreased by approximately 1% (Figure 5.3). A one-way anova test was performed on this data in order to determine if the difference seen after TRAP150 depletion is significant. The samples were not statistically different from one another ($p>0.05$).

5.2 TRAP150 depletion does not cause a mitotic arrest

Flow cytometry was performed on controls and TRAP150-depleted samples in order to detect if a mitotic arrest occurs after TRAP150 depletion. Cells were plated in parallel and protein was extracted from them in order to validate TRAP150 depletion via western blotting. This experiment was performed a total of three times. TRAP150 depletion did not result in a mitotic arrest. There was no arrest in mitosis in the absence of TRAP150. No major changes were seen except a slight increase in G1 and a decrease in S phase (Figure 5.4).

Figure 5.3: TRAP150 depletion results in multiple mitotic defects with metaphase defects being the most abundant.

(A) HeLa cells transfected with either control oligo, TRAP150 siRNA1 oligo or TRAP150 siRNA4 oligo. After 72 hours the cells were processed for immunofluorescence or protein extraction. (A) Mitotic distribution was determined for mock, control, siRNA1 and siRNA4 cells by scoring 300 mitotic cells and dividing them by mitotic phase (3 replicates total). (B) From these 300 mitotic cells, the defective cells were also scored and categorized between the different mitotic phases. Defects were seen in prometaphase, metaphase, anaphase and telophase with metaphase defects being the most abundant. (C) Mitotic index was determined by counting mitotic cells out 100 total cells (n=10). After TRAP150 depletion, the mitotic index was slightly lower. One-way Anova test and Games-Howell post hoc test determined that differences between the samples were not statistically significant from one another ($p>0.05$). TRAP150 depletion was validated through immunoblotting. Western blot validating depletion is shown in Figure 5.2, Q.

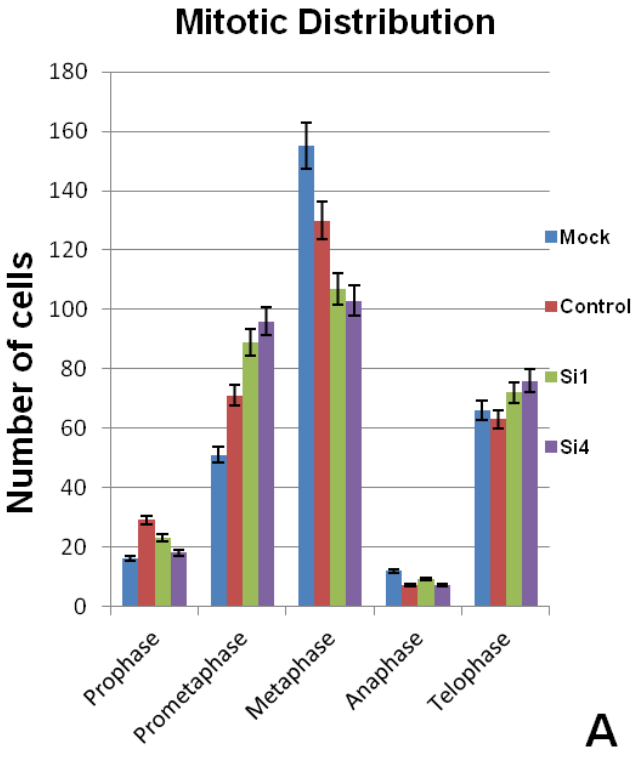
Mitotic Distribution
Number of cells
180
160
140
120
100
80
60
40
20
0
Prophase
Prometaphase
Metaphase
Anaphase
Telophase
Mock
Control
Si1
Si4

A

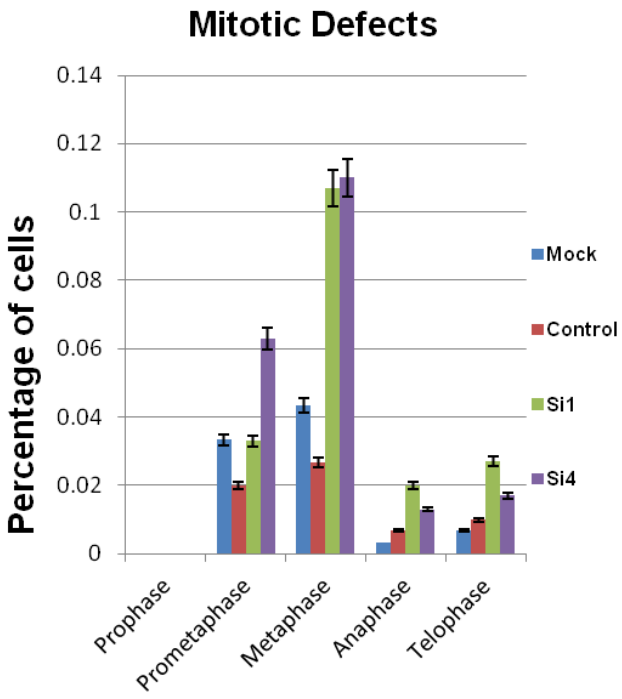
Mitotic Defects
Percentage of cells
0.14
0.12
0.1
0.08
0.06
0.04
0.02
0
Prophase
Prometaphase
Metaphase
Anaphase
Telophase
Mock
Control
Si1
Si4

B

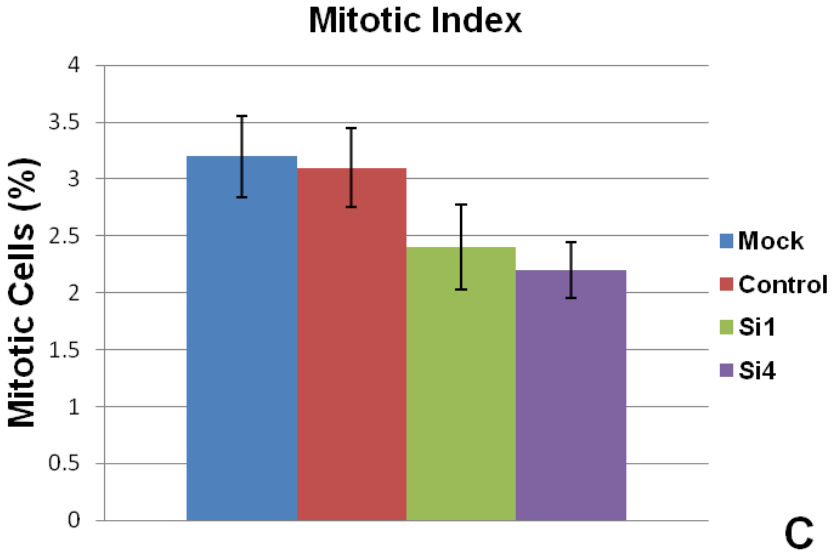
Mitotic Index
Mitotic Cells (%)
4
3.5
3
2.5
2
1.5
1
0.5
0
Mock
Control
Si1
Si4

C

Figure 5.4: TRAP150 depletion results in a slight increase of the G1 peak

HeLa cells were transfected with either control oligo, TRAP150 siRNA1 oligo or TRAP150 siRNA4 oligo. After 72 hours cells were extracted and processed for flow cytometry or protein extraction. Cells were fixed with ethanol and stained with propidium iodide. Flow cytometry machine measures DNA content of the samples. (A) Flow cytometry performed on mock sample. (B) Flow cytometry done on control sample. (C) Flow cytometry done on TRAP150 siRNA1 sample. (D) Flow cytometry done on TRAP150 siRNA4 sample. Table: Average values for each phase according to DNA content (average taken out of three replicates). (F) TRAP150 depletion was validated by immunoblot. A duplicate experiment underwent protein extraction. Protein extracts were used for western blotting.

	G1	S	G2/M	SubG1	Aneuploidy
Mock	59%	11.4%	15.5%	3.7%	7.2%
Control	59.9%	11%	15.2%	3.9%	6.8%
Si1	62.3%	9.9%	14.7%	3.9%	6.2%
Si4	63.5%	9.7%	14.6%	3%	6.3%

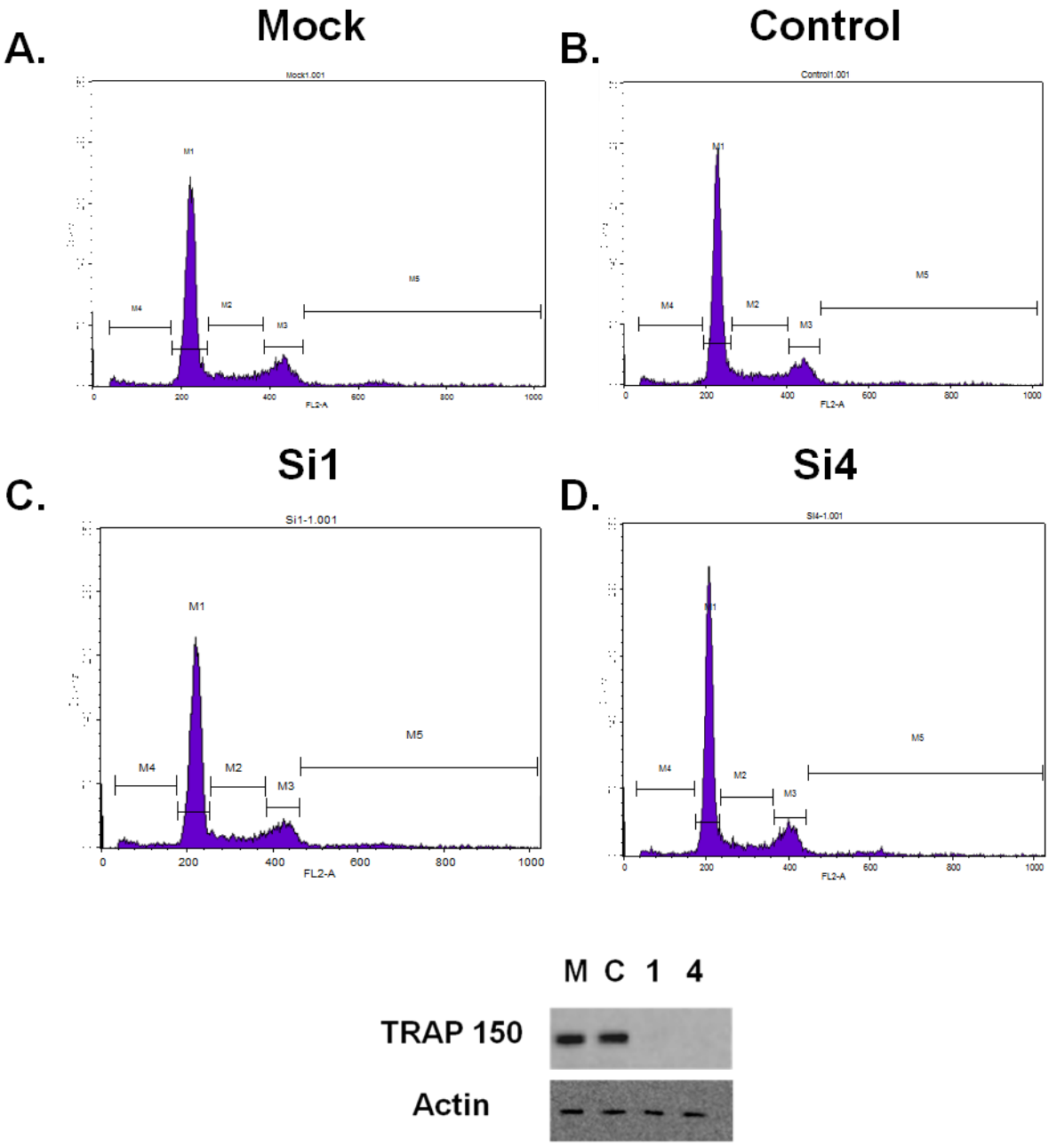

5.3 TRAP150 depletion does not alter chromosome movement

Untreated cells as well as cells treated with control oligo and TRAP150 SiRNA 4 oligo were imaged from prometaphase to the end of telophase. Even though both oligos depletete TRAP150, past experiments have shown that

siRNA oligo 4 has a higher depletion capacity than siRNA oligo 1. For this reason, I chose to perform the live cell experiments using TRAP150 siRNA oligo 4. HeLa cells were plated and treated with TRAP150 siRNA oligo 4 24 hours later. After 72 hours they were placed in a live cell chamber or harvested for protein extraction. Western blot was performed in order to validate TRAP150 depletion. A total of 10 movies were obtained per condition. Chromosome congression was timed from prometaphase to metaphase, metaphase to anaphase and anaphase to telophase. The average was obtained and compared between populations. Prometaphase to metaphase was timed from nuclear envelope breakdown to chromosome alignment. Metaphase to anaphase was timed from chromosome alignment to separation of sister chromatids. Anaphase to telophase was timed from separation of sister chromatids to end of mitosis. Chromosome congression from prometaphase to metaphase was approximately the same in all three conditions (Table 5.3, 5.4 and 5.5). On average, the prometaphase to metaphase transition lasted 19.3 minutes, 30.1 minutes and 38.6 minutes in untreated, control and TRAP150 si4 samples respectively. In addition, the timing between metaphase to anaphase and anaphase to telophase remained unchanged after TRAP150 depletion. The metaphase to anaphase transition took 18.5 minutes, 15.4 minutes and 16.4 minutes in untreated,

Table 5.1 TRAP150 depletion leads to a longer mitotic process

HeLa cells that are stably expressing H2B-YFP were transfected with either control oligo or TRAP150 siRNA4 oligo. After 72 hours, the cells were placed in a live cell chamber or underwent protein extraction. Live cell movies were imaged from early prometaphase until the end of mitosis. Chromosome movements were timed from prometaphase to metaphase, metaphase to anaphase and anaphase to telophase in untreated, control and TRAP150 siRNA4 samples. A total of 10 movies were collected per condition. TRAP150 depletion did not alter chromosome congression however the process of mitosis did take longer. TRAP150 depletion was validated by immunoblotting. A duplicate experiment underwent protein extraction. Protein extracts were used for western blotting.

Table 5.2 Untreated H2B-YFP Cells				
Cell	prometaphase to metaphase (mins)	metaphase to anaphase (mins)	anaphase to telophase (mins)	total time (mins)
1	22	10	9	42
2	14	6	6	28
3	13	18	10	44
4	30	7	6	47
5	16	20	18	59
6	18	16	10	50
7	12	4	6	29
8	22	54	12	96
9	34	40	8	91
10	12	10	8	40
Average	**19.3**	**18.5**	**9.3**	**47.1**
H2B-YFP cells treated with control oligo				
1	22	10	8	41
2	63	20	16	101
3	26	10	10	49
4	15	36	10	65
5	36	28	12	81
6	14	12	12	44
7	17	8	10	42
8	59	4	8	79
9	19	20	10	58
10	30	6	20	36
Average	**30.1**	**15.4**	**11.6**	**57**
H2B-YFP cells treated with TRAP150 siRNA oligo				
1	19	40	12	72
2	101	5	6	114
3	27	8	10	48
4	33	26	8	71
5	37	16	8	66
6	49	8	16	79
7	49	11	4	71
8	17	19	8	52
9	27	23	10	69
10	27	8	12	30
Average	**38.6**	**16.4**	**9.4**	**64**

control and TRAP150 si4 samples respectively. The anaphase to telophase transition took 9.3 minutes, 11.6 minutes and 9.4 minutes in untreated, control and TRAP150 siRNA oligo 4. However there was a difference in the total time that the cells stayed in mitosis. The total time was 47 minutes, 57 minutes and 64 minutes for untreated, control and TRAP150 si4 samples respectively. The difference seen between untreated and control samples is probably due to the transfection process. Even though there was no large difference in the transitions described before, the average total time the cells were in mitosis was longer in TRAP150-depleted cells than the untreated cells and control cells.

In many cases, after TRAP150 depletion the cells would start out with prometaphase defects but seem to get fixed as mitosis progressed (Figure 5.7).

In addition, many of the mitotic defects seen in fixed cells were also seen in live cells (Figure 5.8 and 5.9). These defects were not seen in the untreated and control samples (Figure 5.5 and 5.6). These cells were unable to progress to anaphase and remained in metaphase for more than 30 minutes. However, mitotic defects were still detected in anaphase and telophase.

5.4 TRAP150 alters a subset of mitotic pre-mRNAs

Microarray studies demonstrated that depletion of TRAP150 results in an alteration of key mitotic regulators. Analysis done with Ingenuity software showed that multiple genes including NDC80, BUB1, BUBR1, CENP-E, CENP-F and Aurora B are up-regulated after TRAP150 depletion (Table 5.3). This data was validated by using quantitative RT-PCR. Primers were designed for

Figure 5.5: Time lapse imaging of untreated H2B-YFP HeLa cells

HeLa cells stably expressing H2B-YFP were plated and placed in a live cell chamber 48 hours later. Live cell movies were imaged from early prometaphase until the end of mitosis. Mitosis took approximately 22 minutes.

Untreated H2B-YFP Cells

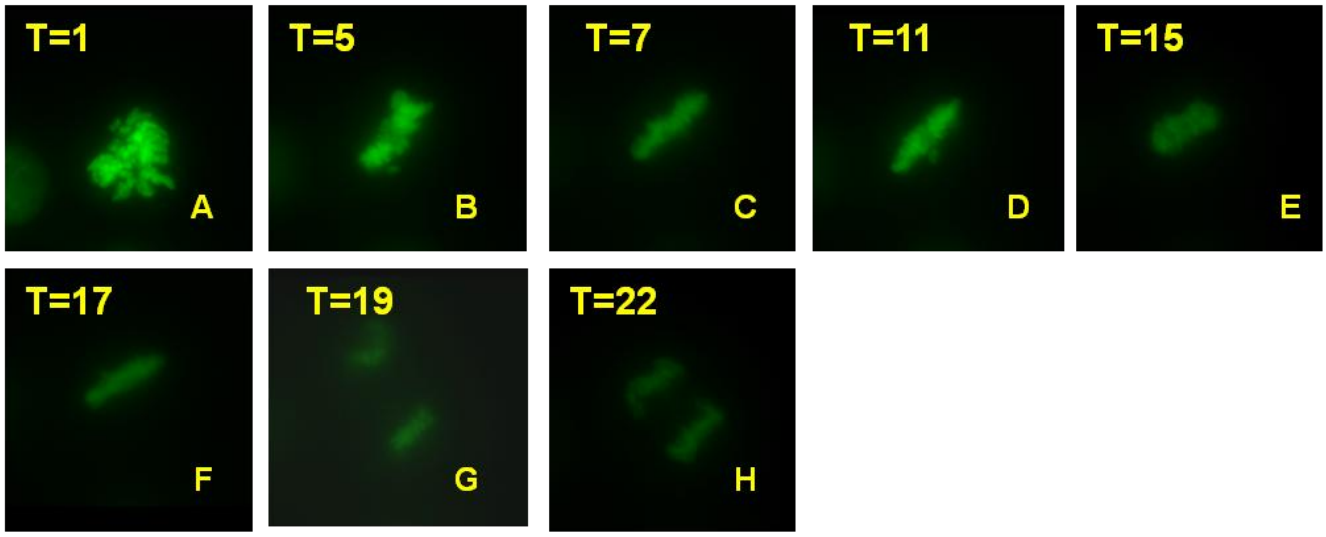

Figure 5.6: Time lapse imaging of H2B-YFP HeLa cells treated with control oligo

HeLa cells stably expressing H2B-YFP were transfected with control oligo and then placed in a live cell chamber 72 hours later. Live cell movie was imaged from early prometaphase until the end of mitosis. A duplicate experiment was done to perform protein extraction. Mitosis took approximately 43 minutes.

H2B-YFP Cells treated with Control oligo

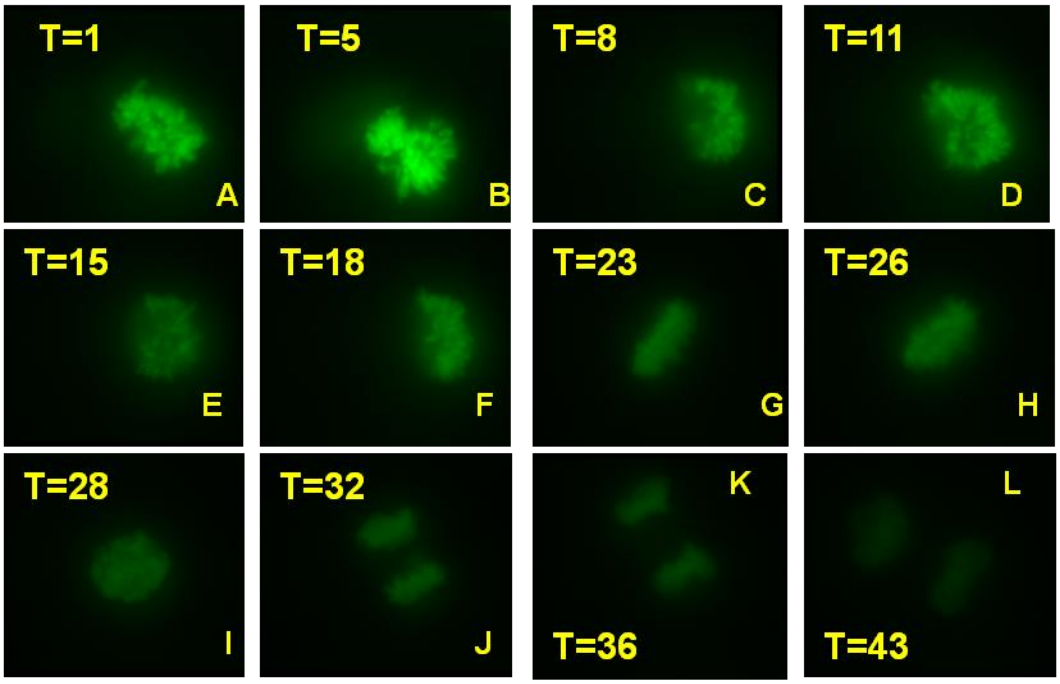

Figure 5.7: Time lapse images of H2B-YFP HeLa cells treated with TRAP150 siRNA oligo 4

HeLa cells stably expressing H2B-YFP were transfected with TRAP150 siRNA 4 oligo. After 72 hours, the cells were either placed in a live cell chamber or processed for protein extraction. Live cell movie were imaged from early prometaphase until the end of mitosis. Mitosis took approximately 40 minutes. TRAP150 depletion was validated by immunoblotting. Protein extraction was done in a duplicate set of cells; protein extracts were used for western blotting.

H2B-YFP Cells treated with TRAP150 SiRNA oligo

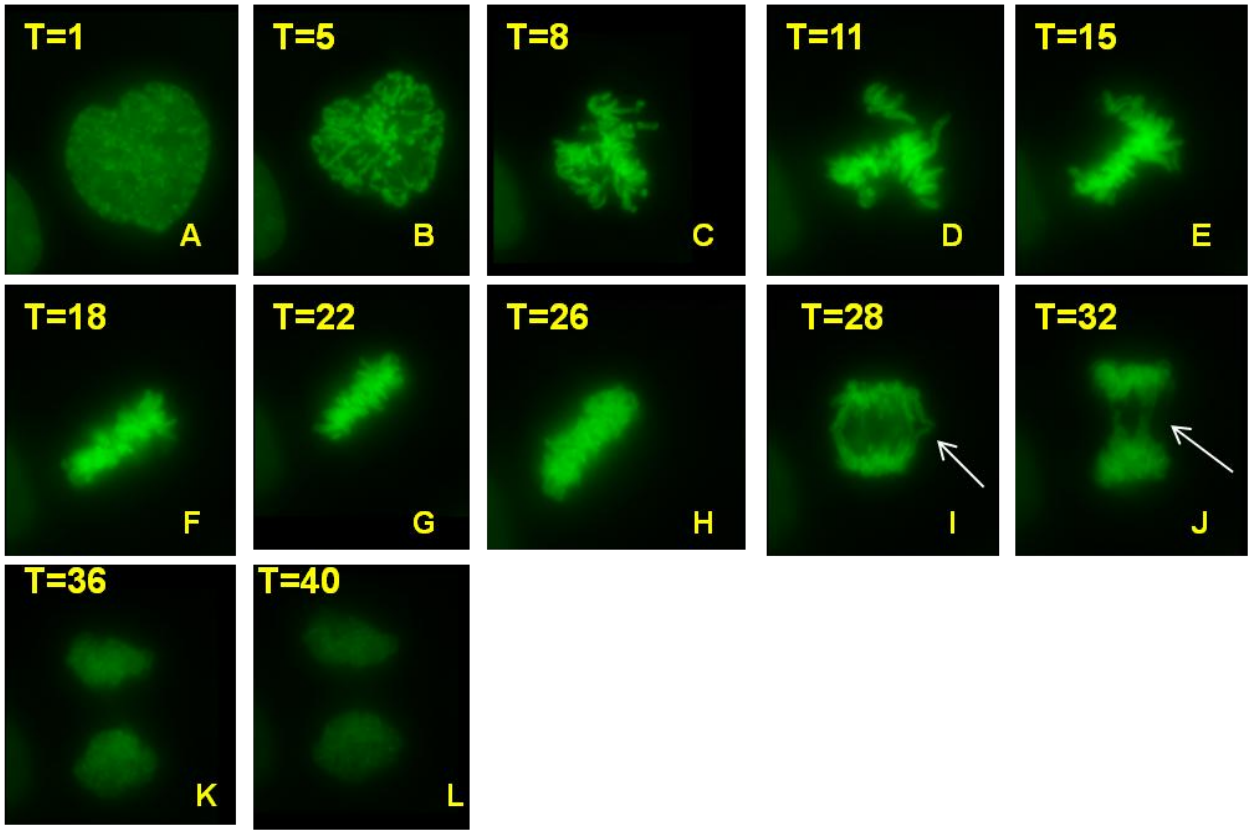

Figure 5.8: TRAP150-depleted H2B-YFP cells show mitotic defects through live cell microscopy

HeLa cells stably expressing H2B-YFP were transfected with TRAP150 siRNA oligo 4. After 72 hours, cells were either placed in a live cell chamber or processed for protein extraction. Live cell movie was imaged from anaphase to end of telophase and it took approximately 9 minutes. After TRAP150 depletion, some mitotic cells exhibited anaphase and telophase defects in the form of lagging chromosomes. Arrows indicate lagging chromosomes. TRAP150 depletion was validated by immunoblotting. A duplicate set of cells was used for protein extraction. Protein extracts were then used for western blotting.

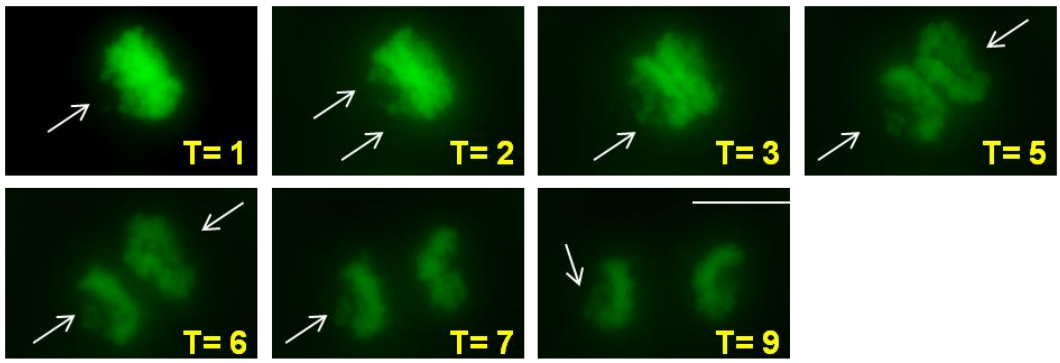
T= 1
T= 2
T= 3
T= 5
T= 6
T= 7
T= 9

Figure 5.9: TRAP150-depleted H2B-YFP cells with misaligned chromosomes were unable to progress through mitosis

HeLa cells stably expressing H2B-YFP were transfected with TRAP150 siRNA oligo 4. After 72 hours, cells were either placed in a live cell chamber or processed for protein extraction. Live cell movie was imaged at metaphase and remained at this phase for 15 minutes. Arrows indicate misaligned chromosomes. TRAP150 depletion was validated by immunoblotting. A duplicate set of cells was used for protein extraction. Protein extracts were then used for western blotting.

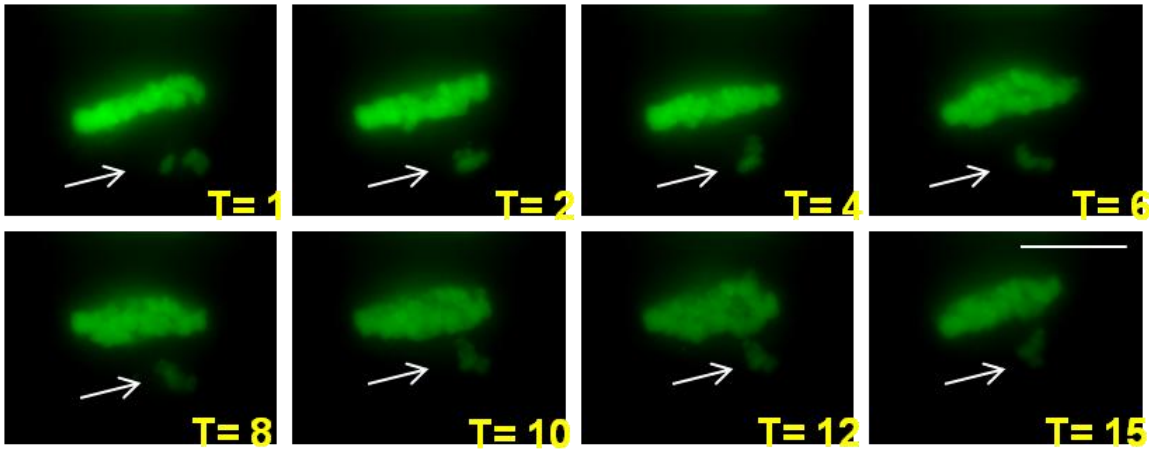
T= 1
T= 2
T= 4
T= 6
T= 8
T= 10
T= 12
T= 15

Table 5.2: Mitotic genes coding for kinetochore proteins are up-regulated after TRAP150 depletion

An exon array was performed by the Bubulya lab on TRAP150-depleted samples. Analysis by Ingenuity software revealed that approximately 1800 genes are affected after TRAP150 depletion. Many of these genes affected code for proteins that play an important role in mitotic progression. A subset of these genes was validated through RT-PCR. The genes validated code for kinetochore proteins.

Gene	TRAP150 Upregulation	P-Value
AURKB	Up-regulated 2.035	1.94 e^{-32}
CENPE	Up-regulated 2.62	1.94 e^{-32}
CENPF	Up-regulated 4.009	1.94 e^{-32}
NDC80	Up-regulated 2.781	1.94 e^{-32}
BUB1	Up-regulated 3.071	1.94 e^{-32}
BUB1B	Up-regulated 3.07	1.94 e^{-32}

Figure 5.10: Graph depicting kinetochore protein interactions

Kinetochore proteins all interact with one another. Aurora B phosphorylates NDC80. Aurora B also interacts with Bub1 which phosphorylates and recruits CENP-F. CENP-F recruits CENP-E. These two proteins stabilize each others binding at the kinetochore. CENP-E activates BubR1.CENP-F reduction leads to an increase of Mad1 and Mad2 recruitment to the kinetochore.

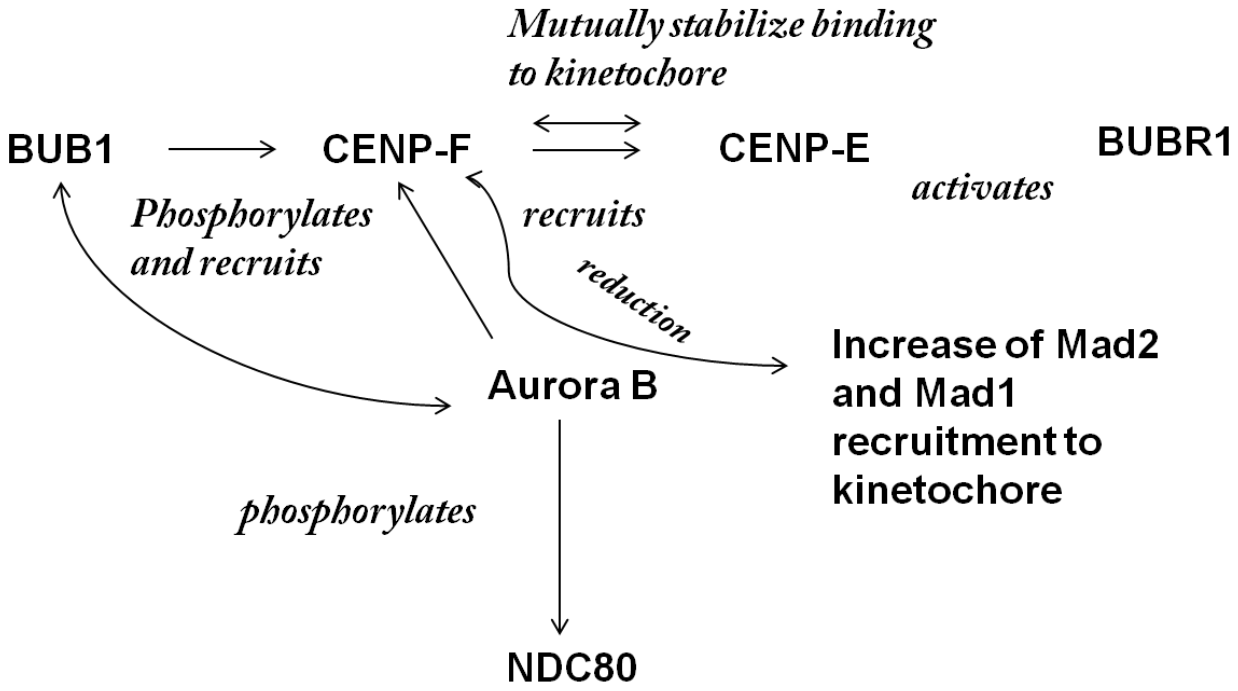
Mutually stabilize binding
to kinetochore
BUB1
CENP-F
CENP-E
BUBR1
activates
Phosphorylates
and recruits
recruits
reduction
Increase of Mad2
and Mad1
recruitment to
kinetochore
Aurora B
phosphorylates
NDC80

each of these genes and qRT-PCR was performed on RNA samples isolated from TRAP150 deficient cells as well as on RNA from control cells (Figure 5.11). Western blotting was performed in order to confirm TRAP150 depletion. All of these genes were up-regulated at least two fold. The difference in upregulation levels seen with the siRNA oligos is due to the efficiency in which the oligo depletes the protein. Even though both oligos deplete TRAP150, siRNA oligo 4 is more efficient than siRNA oligo 1. The most up-regulated gene from the group that was validated was CENP-F which was up-regulated fourfold following TRAP150 depletion. In addition, a single immunoblotting experiment was performed in order to detect if the protein levels of these genes also increased after TRAP150 depletion (Figure 5.11). After Btf depletion, aurora B levels were 5% and 29% upregulated when using siRNA oligo 1 and oligo 2 respectively. After TRAP150 depletion, aurora B levels were 17% and 50% upregulated when using siRNA oligo 1 and 4 respectively. However, Mad 2 levels were downregulated when using Btf siRNA oligo1 (downregulated 12%) and upregulated when using Btf siRNA oligo 2 (upregulated 17%). After TRAP150 depletion, Mad2 levels increased 10% and 33% when using siRNA oligo1 and siRNA oligo 4 respectively.

Western blotting was performed to examine if the changes in abundance of mitotic regulator mRNAs correlates with changes in their respective proteins. I also examined the expression of Btf in TRAP150-depleted cells, and the expression of TRAP150 in Btf-depleted cells. HeLa cells treated with siRNA duplexes for either TRAP150 or Btf were extracted for immunoblot analysis.

Interestingly, after TRAP150 depletion, BTF was upregulated, and after Btf depletion, TRAP150 was upregulated (Figure 5.13; also observed by S.Varia).

Another way to examine changes in protein expression is by performing immunofluorescence experiments. This approach can be useful in detecting local accumulation of protein in single cells that would not be detectable by immunoblot. To this end, I examined immunofluorescence localization of several mitotic regulator proteins in TRAP150-depleted cells, including mad2, aurora B, CENP-E and CENP-F. An increase in Aurora B was detected at kinetochores in TRAP150-depleted cells that had misaligned chromosomes (Figure 5.14)

Figure 5.11: Genes coding for kinetochore proteins get upregulated after TRAP150 depletion

Microarray RNA was treated with DNase to purify the sample. These RNA extracts were then used for RT-PCR. Primers were designed for each one of the genes that were upregulated. These primers were tested with two different sets of TRAP150-depleted RNA before the microarray RNA was used. The difference seen between the siRNA oligos are due to the efficiency in which they deplete TRAP150 from the cells. This work was done in collaboration with Sapna Varia.

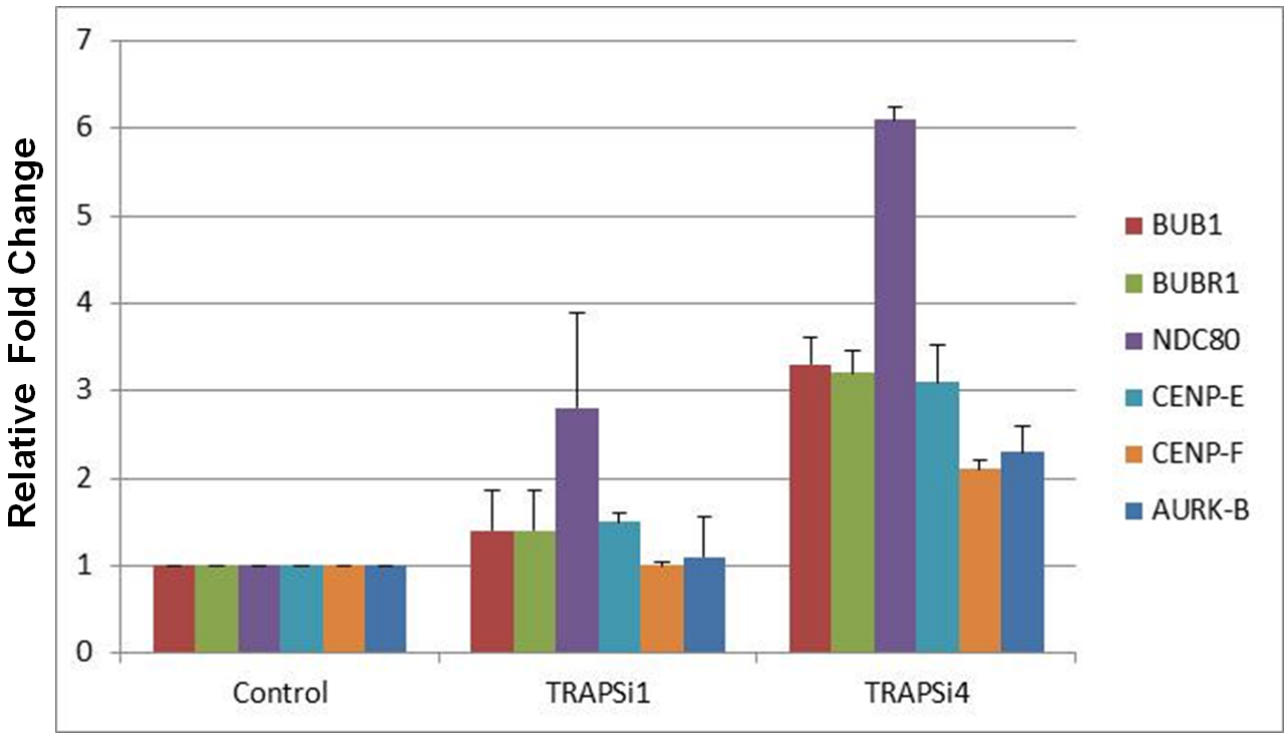
Relative Fold Change
7
6
5
4
3
2
1
0
Control
TRAPSi1
TRAPSi4
BUB1
BUBR1
NDC80
CENP-E
CENP-F
AURK-B

Figure 5.12: Aurora B and Mad2 protein levels increase after TRAP150 and Btf depletion

HeLa cells were transfected with either control oligo, TRAP150 siRNA1 oligo, TRAP150 siRNA4 oligo, Btf siRNA1 oligo or Btf siRNA4 oligo. After 72 hours the cells were processed for protein extraction. Protein extracts were used for immunoblotting. The blot was later probed for Aurora B with mouse anti-Aurora B antibody (1:1000) and Mad2 using mouse anti-Mad2 antibody (1:1000). Actin served as a loading control. Actin was probed with mouse anti-beta-actin (1:1000). TRAP150 was probed using rabbit anti-TRAP150 antibody (1:1000) and Btf was probed using rabbit anti-Btf antibody (1:1000). Densitometry was done on the blot to analyze the intensity of the bands and determine if protein concentrations had increased after depletion of TRAP150 or Btf. Graph shows densitometry results.

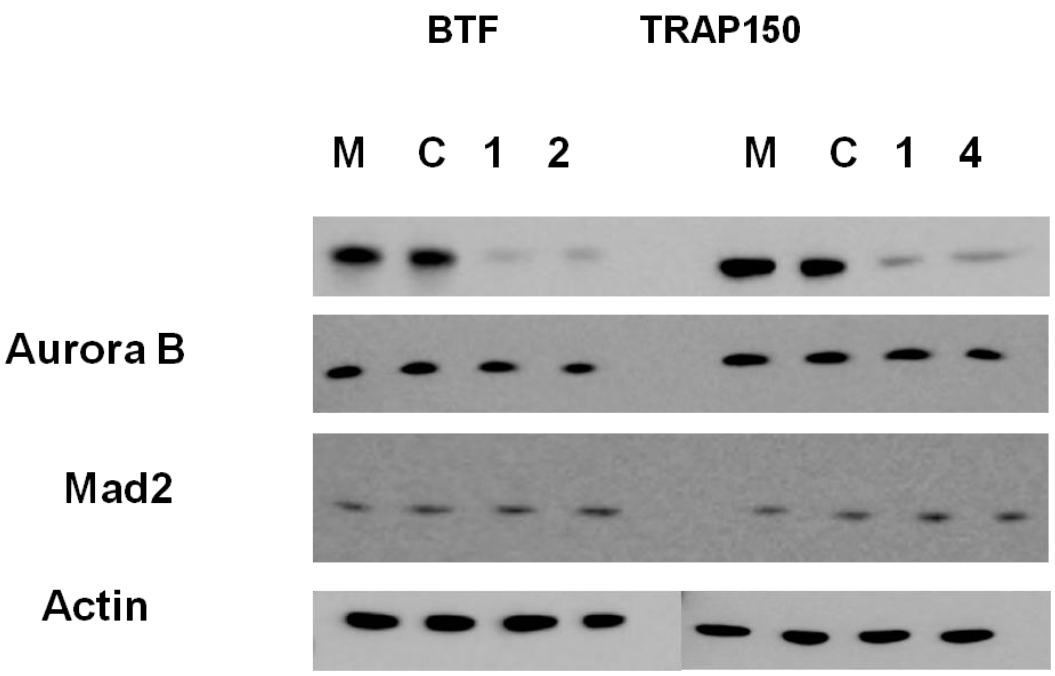
BTF
TRAP150
M C 1 2
M C 1 4
Aurora B
Mad2
Actin

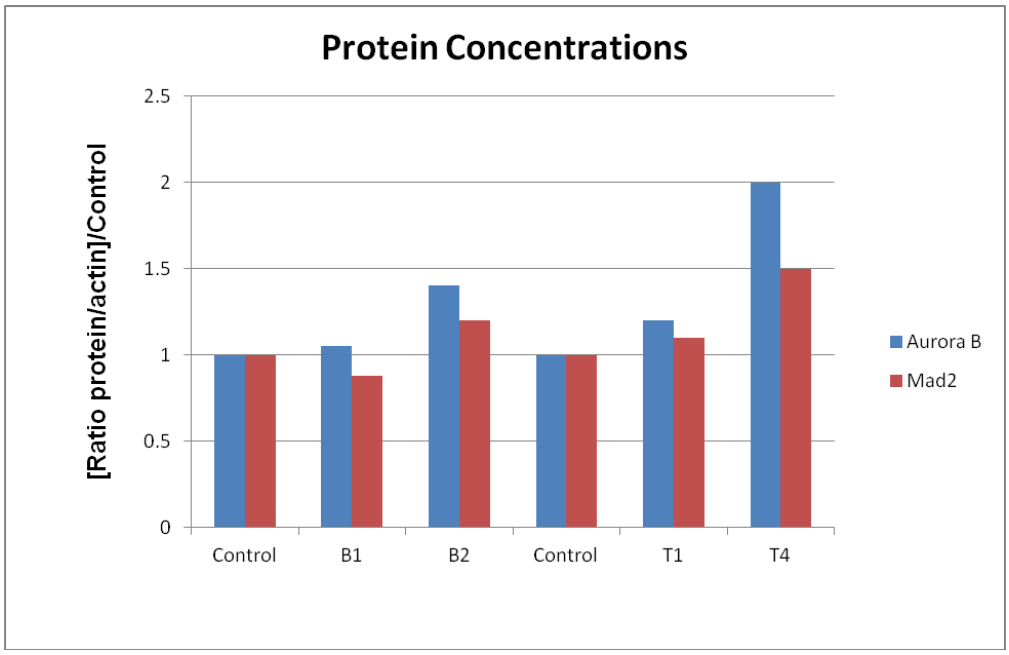
Protein Concentrations
[Ratio protein/actin]/Control
2.5
2
1.5
1
0.5
0
Control
B1
B2
Control
T1
T4
Aurora B
Mad2

Figure 5.13: Btf increases after TRAP150 depletion; TRAP150 increases after Btf depletion

HeLa cells were transfected with either control oligo, TRAP150 siRNA1 oligo, TRAP150 siRNA4 oligo, Btf siRNA1 oligo or Btf siRNA4 oligo. After 72 hours the cells were processed for protein extraction. Protein extracts were used for immunoblotting. Extracts that had undergone TRAP150 depletion were probed for Btf using rabbit anti-Btf antibody (1:1000). Extracts that had undergone Btf depletion were probed for TRAP150 using rabbit anti-TRAP150 antibody (1:1000). Densitometry was done on the blot image to analyze the intensity of the bands and determine if protein concentrations had increased after depletion of TRAP150 or Btf. Graph shows densitometry results.

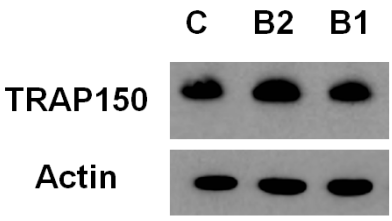
C
B2
B1
TRAP150
Actin

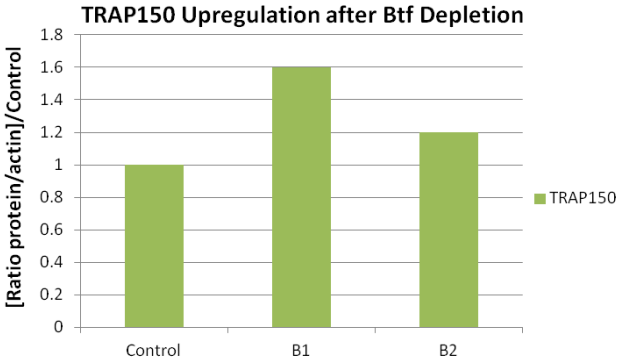
TRAP150 Upregulation after Btf Depletion
[Ratio protein/actin]/Control
1.8
1.6
1.4
1.2
1
0.8
0.6
0.4
0.2
0
Control
B1
B2
TRAP150

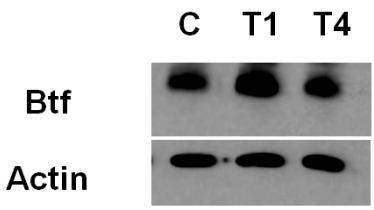
C
T1
T4
Btf
Actin

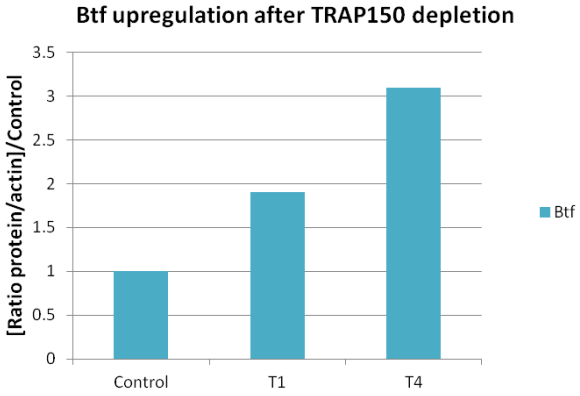
Btf upregulation after TRAP150 depletion
[Ratio protein/actin]/Control
3.5
3
2.5
2
1.5
1
0.5
0
Control
T1
T4
Btf

Figure 5.14: Aurora B levels increase in TRAP150-depleted cells that have misaligned chromosomes

HeLa cells were transfected with either control oligo, TRAP150 siRNA1 oligo or TRAP150 siRNA4 oligo. After 72 hours the cells were processed for immunofluorescence or protein extraction. TRAP150 was labeled using rabbit anti-TRAP150 antibody (1:1000) (A, F,K, P); Aurora B was labeled using mouse anti-Aurora B antibody (1:1000) (B,G,L,Q); merged Aurora B and TRAP150 images are shown (C,H,M,R); merged Aurora B and DAPI images are shown (D,I,N,S); DNA was stained with DAPI (E,J,O,T). TRAP-150 depleted cells showed an increase of Aurora B in misaligned chromosomes. Arrows indicate misaligned chromosomes. Bar= 5 µm. TRAP150 depletion was validated by immunoblot (U). A duplicate experiment underwent protein extraction. Protein extracts were used for immunoblotting.

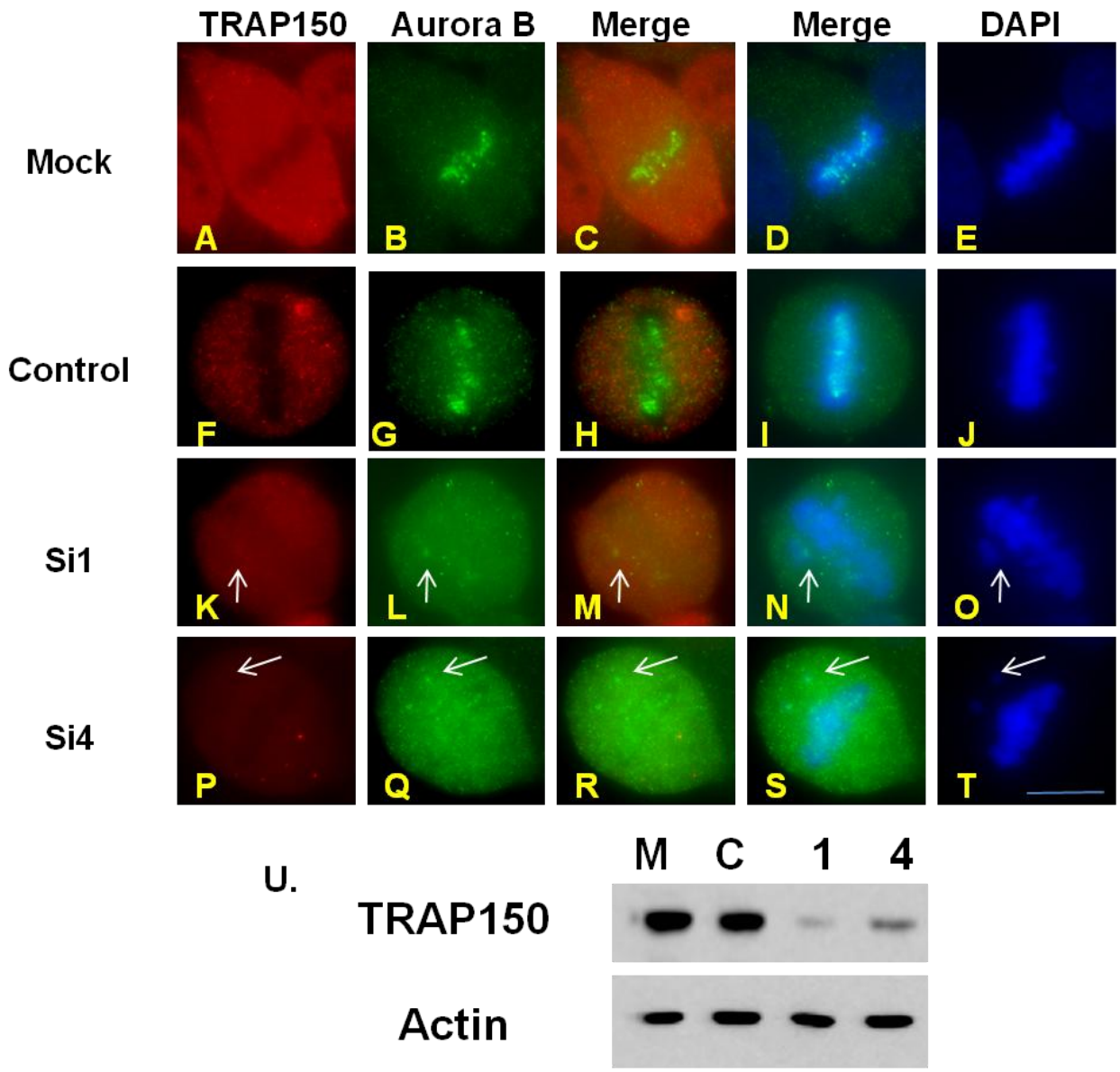
TRAP150
Aurora B
Merge
Merge
DAPI
Mock
Control
Si1
Si4
A
B
C
D
E
F
G
H
I
J
K
L
M
N
O
P
Q
R
S
T

U.
M
C
1
4
TRAP150
Actin

However, no change was seen when labeling CENP-E, CENP-F or mad2 (Figure 5.15, 5.16 and 5.17).

Figure 5.15: CENP-E levels increase in TRAP150-depleted cells that have misaligned chromosomes

HeLa cells were transfected with either control oligo, TRAP150 siRNA1 oligo or TRAP150 siRNA4 oligo. After 72 hours the cells were processed for immunofluorescence or protein extraction. TRAP150 was labeled using rabbit anti-TRAP150 antibody (1:1000) (A, F,K, P); CENP-E was labeled using mouse anti-CENP-E antibody (1:1000) (B,G,L,Q); merged CENP-E and TRAP150 images are shown (C,H,M,R); merged CENP-E and DNA images are shown (D,I,N,S); DNA was stained with DAPI (E,J,O,T). TRAP-150 depleted cells showed an increase of CENP-E. Arrows indicate misaligned chromosomes. Bar= 5 µm. TRAP150 depletion was validated by immunoblot. A duplicate experiment underwent protein extraction. Protein extracts were used for immunoblotting. Western blot is shown in figure 5.14, U.

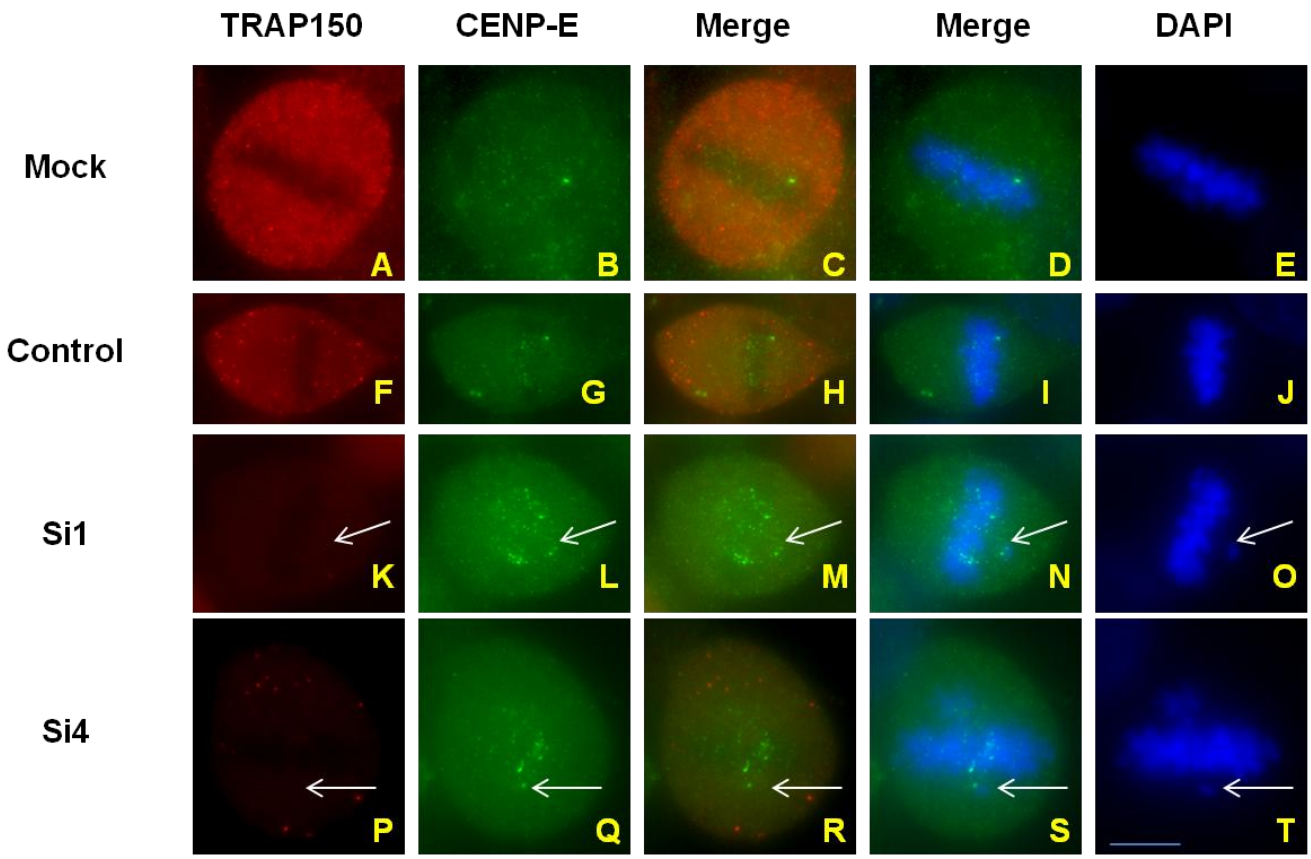
TRAP150
CENP-E
Merge
Merge
DAPI
Mock
Control
Si1
Si4
A
B
C
D
E
F
G
H
I
J
K
L
M
N
O
P
Q
R
S
T

Figure 5.16: Mad 2 protein levels decrease after TRAP150 depletion

HeLa cells were transfected with either control oligo, TRAP150 siRNA1 oligo or TRAP150 siRNA4 oligo. After 72 hours the cells were processed for immunofluorescence or protein extraction. TRAP150 was labeled using rabbit anti-TRAP150 antibody (1:1000) (A, F,K, P); Mad2 was labeled using mouse anti-Aurora B antibody (1:1000) (B,G,L,Q); merged Mad2 and TRAP150 images are shown (C,G,M,R); merged Mad2 and DNA images are shown (D,I,N,S); DNA was stained with DAPI (E,J,O,T). TRAP150-depleted cells caused a decrease of Mad2 in metaphase cells. Arrows indicate misaligned chromosomes. Bar= 5 µm. TRAP150 depletion was validated by immunoblot. A duplicate experiment underwent protein extraction. Protein extracts were used for immunoblotting. Western blot shown in Figure 5.14, U.

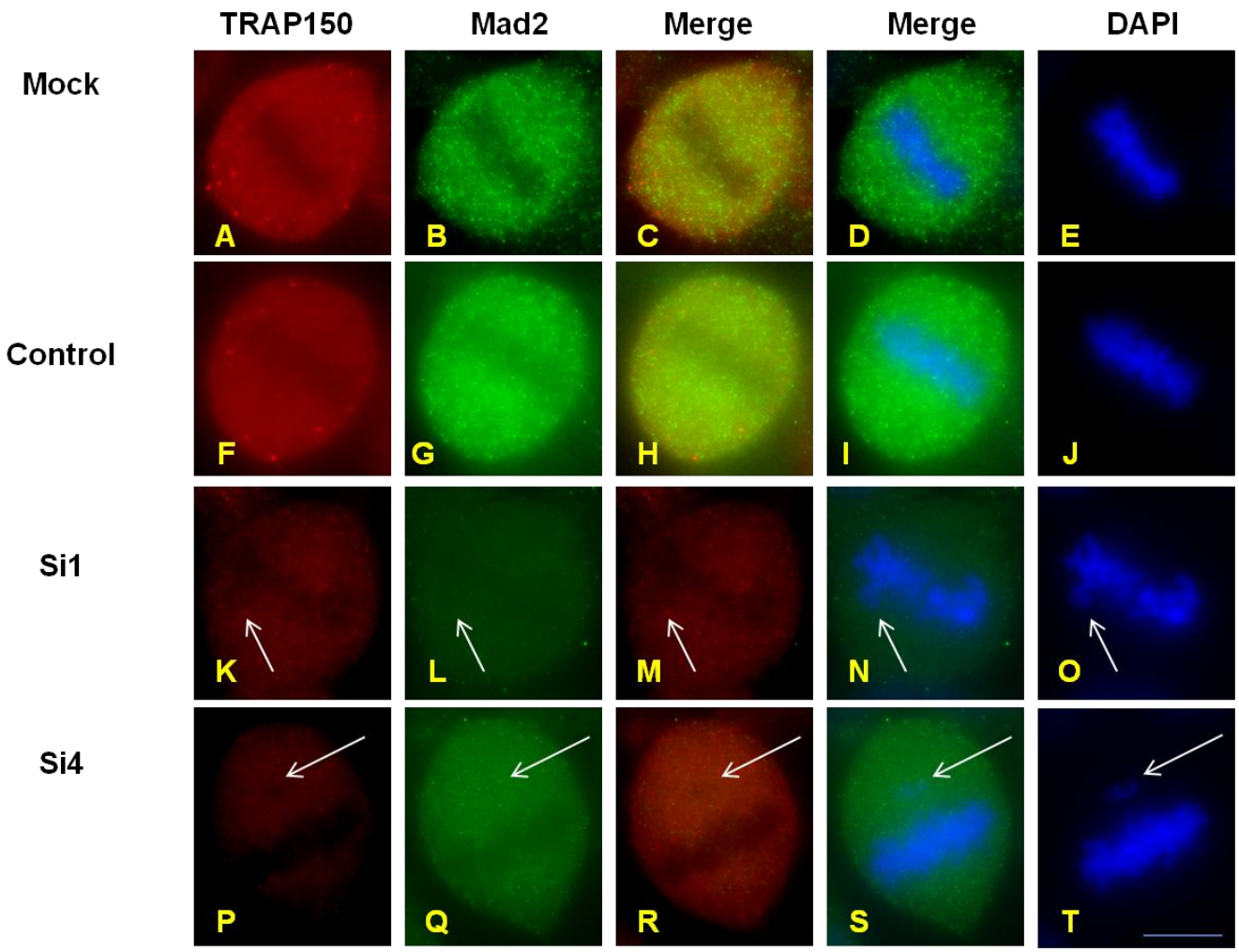
TRAP150
Mad2
Merge
Merge
DAPI
Mock
Control
Si1
Si4
A
B
C
D
E
F
G
H
I
J
K
L
M
N
O
P
Q
R
S
T

Figure 5.17: CENP-F levels remain unchanged after TRAP150 depletion

HeLa cells were transfected with either control oligo, TRAP150 siRNA1 oligo or TRAP150 siRNA4 oligo. After 72 hours the cells were processed for immunofluorescence or protein extraction. CENP-F was labeled using rabbit anti-CENP-F antibody (1:1000) (A,D,G,J); merged CENP-F and TRAP150 images are shown (B,E,H,K); DNA was stained with DAPI (C,F,I,L). CENP-F levels did not change in metaphase cells that were depleted of TRAP150. Arrows indicate misaligned chromosomes. Bar= 5 µm. TRAP150 depletion was validated by immunoblot. A duplicate experiment underwent protein extraction. Protein extracts were used for immunoblotting. Western blot is shown in figure 5.14, U.

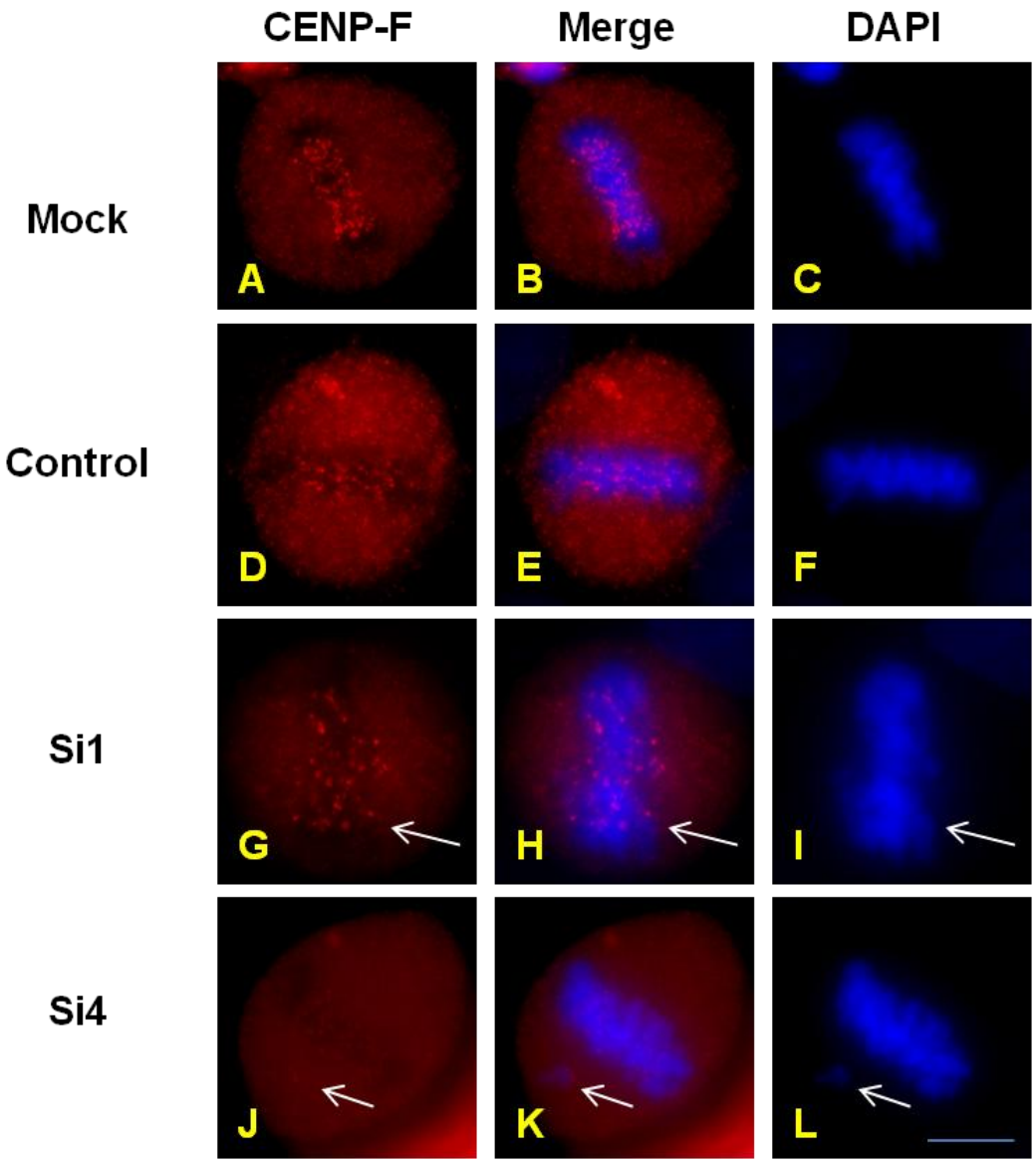
CENP-F
Merge
DAPI
Mock
Control
Si1
Si4
A
B
C
D
E
F
G
H
I
J
K
L

Chapter 6: Discussion

One of the conditions that cause cancer is aneuploidy. Having an abnormal number of chromosomes has been linked to malignant tumor cells (Holland and Cleveland, 2009; Schvartzman et al., 2010). For that reason, accurate chromosome segregation during mitosis is required for daughter cells to receive the proper number of chromosomes. Because of the importance of mitosis, this process is highly regulated by various structures and multiple proteins. Many of these proteins do not become activated until they are bound to other molecules known as cyclins. Phosphorylation and dephosphorylation cycles also play an important role in the regulation of mitosis. Concentrations of mitotic regulators oscillate up and down throughout the cell cycle in order to control mitotic progression (Cross et al., 2007).

Many aspects about mitotic regulation still remain unknown. It is becoming clearer now that other proteins other than those recognized as mitotic regulators can also impact cell cycle progression. My thesis project and other studies (Huen et al., 2010; Sharma et al., 2011; Ahn et al., 2011) have shown that nuclear splicing factors affect mitosis in an indirect way. Depletion of nuclear speckle proteins, Son and TRAP150, result in an alteration of mitotic progression.

Sharma et al. (2010) as well as Huen et al. (2010) revealed that depletion of Son resulted in a metaphase arrest. To elucidate a possible direct role for Son in

mitosis, I performed immunofluorescence experiments to examine localization of Son and SF2/ASF at each stage of mitosis (Figure 4.1). I observed that SF2/ASF and Son co-localize throughout the cell cycle. During interphase, both Son and SF2/ASF co-localize in nuclear speckles. Son and SF2/ASF show diffuse distribution throughout the cell after nuclear envelope breakdown and both proteins accumulate in mitotic interchromatin granules during early anaphase that increase in number and size at telophase. These findings were published by Huen et al. (2010). One difference that I observed between Son and SF2/ASF localization was that during metaphase, Son is present in small foci within the chromatin region, whereas SF2/ASF localized entirely out of this region in MIGs. Son exhibited patterns similar to kinetochore patterns; it was present in doublets throughout the chromatin region. This finding suggested that perhaps Son somehow interacts with the kinetochore and this interaction is important for mitotic progression. Kinetochore proteins are important for chromosome alignment to the metaphase plate by establishing proper kinetochore-microtubule attachments. If Son were important for establishing kinetochore-microtubule attachments, its absence could contribute to metaphase arrest.

To elucidate Son's possible co-localization with the kinetochore, an immunofluorescence experiment labeling Son (WU14) and the kinetochore (ACA) was performed. Kinetochore proteins can be specifically labeled by using antibodies against centromere antigens collected from patients with CREST variant of scleroderma (Earnshaw and Rothfield, 1985). These studies, however, did not show any co-localization between these two structures. The majority of

Son and kinetochore signals were adjacent to each other, although a few kinetochores overlapped with Son (Figure 4.5). Kinetochores are very large dynamic structures having a large number of proteins that are exchanged upon microtubule binding. For example, CENP-E is a directed motor protein that has shown transient kinetochore binding kinetics (Putkey et al., 2002; Kallio, 2006). Therefore, I hypothesized that Son's presence at the kinetochore may be transient, happening only at some brief point prior to MT attachment, and this would not have been readily detected in fixed cells via immunofluorescence. In order to study this possibility, destabilization of microtubules was performed in an attempt to promote enhancement of Son at the kinetochore (Figure 4.6). Results did not reveal the expected outcome. After microtubule destabilization, Son was still not observed to co-localize with the kinetochore. Instead, there was an unexpected change in Son localization. After cold treatment, Son changed from the typical diffuse pattern and accumulated into MIG-like aggregates. To address whether this occurrence is a characteristic that is common of nuclear speckle proteins, the cold destabilization experiment was repeated to examine SF2/ASF and U170K response. SF2/ASF and U1-70K are two different types of nuclear speckle proteins. SF2/ASF is a classical SR protein and U1-70K is part of the snRNP complex. After cold treatment, SF2 and U1-70K did not exhibit a similar phenotype as Son (Figure 4.7 and 4.8). I concluded that Son does not localize to the kinetochores at any point during mitosis but somehow the cold destabilization of microtubules affects Son's overall cellular distribution. This could be a novel mechanism or outcome of the cold environment. Another hypothesis is that

destabilizing the microtubules causes an early onset of MIGs. This would suggest that Son seeds assembly of MIGs in the same way that has been hypothesized to seed assembly of nuclear speckles in interphase cells. To study this further, microtubules were destabilized using nocodazole (Figure 4.9). This would help us understand if the change in morphology is brought upon by the cold temperature or by the destabilization of microtubules. When microtubules were disrupted using nocodazole, I observed a similar change in Son's distribution when microtubules were cold destabilized. This finding suggests that disruption of the microtubule network affects Son's localization in mitotic cells. Destabilizing microtubules may cause Son to assemble into cytoplasmic structures prematurely. While Son may be important in seeding assembly of MIGs, the redistribution of Son induced upon microtubule destabilization is unlikely to reflect true MIGs, since SF2/ASF and U1-70K were not present in those structures. This preliminary data can be used as the basis for a future project in the Bubulya lab.

Abnormal mitotic machinery can lead to problems in mitotic progression. Malformation of the mitotic spindle can activate the spindle assembly checkpoint (SAC) and cause the cells to arrest at metaphase. Since Son-depleted cells show metaphase arrest, this led to the hypothesis that Son depletion alters mitotic machinery such as the mitotic spindle and the kinetochores. To study this further, I measured several parameters including interpolar distance, spindle width and interkinetochore distance in control as well as in Son-depleted cells (Figure 4.3 and 4.4). Son depletion studies revealed that absence of Son

resulted in elongated mitotic spindles as well as disarrayed microtubules. On average, Son depleted cells exhibited mitotic spindles that were 2 to 3 µm longer than in control cells (Figure 4.3, A). This finding was published in Sharma et al. (2011) and Ahn et al. (2011). Altering the interpolar distance changes the tension across the mitotic spindle, because if the mitotic spindle is longer, there is presumably less tension on the mitotic spindle that would in turn shorten the interkinetochore distance. We would therefore expect to see a change in the interkinetochore distance. However, spindle width and interkinetochore distances remained unchanged after Son depletion (Figure 4.3, B; Figure 4.4, A). It is possible that the lengthening of the mitotic spindle that occurs after Son depletion is not enough to cause a change in the interkinetochore tension. The lengthening of the mitotic spindle can interfere with mitotic progression by activating the spindle checkpoint (Yu et al., 2003). It is possible that the size and overall role of the mitotic spindle plays a role in silencing the spindle assembly checkpoint. After all kinetochores become attached to microtubules and the connections between sister chromatids are destroyed, the mitotic spindle shortens as it brings the chromosomes closer to the spindle poles. If the mitotic spindle is elongated, it may not be able to shorten enough to separate these sister chromatids. In addition, the cell may have a way to detect this abnormality and prevent SAC inactivation.

Despite our vast knowledge about the human genome, it is still unknown all of the genes that are required for the basic functions of life (Ellenberg et al., 2010). Microarray studies done in the Bubulya lab demonstrated that Son is

essential for abundance and alternative splicing of many important transcripts coding for cell cycle regulators (Sharma et al., 2011; Ahn et al., 2011). Some of these genes are Katanin p80 subunit B1, microtubule associated protein 2 (MAP2), histone deacetylase 6 (HDAC6) and cyclin dependent kinases such as CDK6 and CDK2. HDAC6 functions in deacetylating tubulin at lysine 40. This plays a role in stabilizing the microtubule network (Kingston et al., 2002). Katanin plays a role in tubulin depolymerization (Baas et al., 2005). CDK6 and CDK2 mediate the transition between the different phases of the cell cycle (Ekholm and Reed, 2000). Son is an important factor in the processing of these mRNAs. Absence of Son leads to aberrantly processed transcripts that could be translated into mutated and probably nonfunctional versions of their respective protein. This evidence strongly suggests that Son's role in mitosis is due to an indirect effect in regulation of these various transcripts (Sharma et al, 2011; Ahn et al., 2011).

Another nuclear speckle protein, TRAP150 is a known splicing factor as well as an important factor in mRNA degradation (Lee et al., 2010). Preliminary evidence from the Bubulya lab revealed that depletion of TRAP150 from HeLa cells caused mitotic defects including misaligned chromosomes and lagging chromosomes (Blaza and Bubulya, unpublished). In order to elucidate a possible role of TRAP150 in mitosis, I examined TRAP150 localization throughout mitosis and compared this to alpha-tubulin localization through this process (Figure 5.1). This study led to my hypothesis that TRAP150 was not affecting mitosis in a direct manner. Immunofluorescence results did not show any co-localization

between TRAP150 and the mitotic spindle or any other mitotic structure. These results suggested that TRAP150 affects mitosis in an indirect way.

TRAP150 depletion studies were done in order to characterize and elucidate mechanisms for mitotic defects. TRAP150-depleted cells exhibited a greater number of prometaphase, metaphase, anaphase and telophase defects when compared to control samples (Figure 5.2). This finding suggests that TRAP150 may regulate spindle checkpoint activation. There are various checkpoints throughout the cell cycle that allows a cell to detect mistakes and fix them before moving on to the next phase. The spindle assembly checkpoint (SAC) ensures that all chromosomes are properly aligned at the metaphase plate before moving on to anaphase. The checkpoint gets activated when there are misaligned chrosomosomes and mitotic progression stops until this problem is fixed. When TRAP150 is depleted, there are defects present at each phase except prophase suggesting that the spindle checkpoint is being silenced prematurely. There is a possibility that the defects seen in prometaphase are simply chromosomes that have not yet aligned at the metaphase plate. I therefore hypothesized that a problem in chromosome alignment occurs at metaphase but in the absence of TRAP150 the spindle checkpoint gets silenced prematurely and that leads to the defect continuing all throughout mitosis. A possible way I could test this was by calculating mitotic index and performing flow cytometry studies on TRAP150-depleted samples. This would determine whether there is an increase in the mitotic population after TRAP150 depletion suggesting a mitotic arrest.

Mitotic index was calculated for TRAP150 depleted cells and compared to control cells (Figure 5.3). There was only a slight difference between the two, TRAP150-depleted cells had a mitotic index that was approximately 1% lower than in control cells. One-way Anova analysis demonstrated that the difference seen between the samples were not statistically significant from one another ($p>0.05$). Previous results obtained until this point suggested an increase in the mitotic population. The data that was obtained up to this point demonstrates that there are many misaligned chromosomes after TRAP150-depletion. A mitotic arrest would be expected given the nature of the spindle assembly checkpoint. It is possible that a different cell cycle checkpoint like the DNA structure checkpoint gets activated and halts the defective TRAP150 depleted cells hence making the mitotic index lower. The DNA structure checkpoint monitors the G2/M transition by halting cell cycle progression in response to unreplicated DNA or DNA damage (Nigg et al., 2001).

In order to further study these mitotic abnormalities, flow cytometry was performed on TRAP150-depleted cells as well as control cells. This type of analysis should reveal whether or not there is a mitotic arrest after TRAP150 depletion. However, flow cytometry results did not show a mitotic arrest after TRAP150 depletion. There was a slight increase in G1 and a slight decrease in S phase. This finding is consistent with the mitotic index results that show that TRAP150 depleted samples have a lower mitotic index. In addition, it further supports the hypothesis that another cell cycle checkpoint is getting activated. An

alternative possibility is that defective cells override the SAC somehow and proceed despite problems.

In order to detect these defects on living cells, live cell studies were performed using H2B-YFP cells. This type of study allows a more detailed interpretation of mitotic phenotypes (Ellenberg et al., 2010). Chromosomes can be fluorescently labeled and phenotypes such as chromosome segregation defects can be studied in great detail. In addition, time lapse imaging can detect mitotic delays rather than mitotic arrests (Ellenberg et al., 2006). Untreated, control and TRAP150-depleted samples were imaged from prometaphase to telophase. Immunoblotting was performed in order to validate TRAP150 depletion. The timing for individual phases of mitosis was determined (Table 5.3). Results showed that chromosome congression (time to alignment) and remained unchanged in all three conditions. There were differences in timing between prometaphase to metaphase, metaphase to anaphase and anaphase to telophase. The average timing from prometaphase to metaphase was 19, 30 and 38 minutes for untreated, control and si4 samples respectively. The difference between untreated and control samples is most likely due to the presence of an oligo in the control cells. The siRNA procedure can be a harsh treatment on the cells and this could have therefore affected the mitotic timing. However, when comparing prometaphase to metaphase transition in control and si4 samples, there is approximately an 8-minute difference. Because the timing of mitotic phases fell over a wide range, I cannot determine outliers or determine if the difference in timing of mitotic phases between control and TRAP150-depleted

cells is statistically significant. The average timing from metaphase to anaphase was 18, 15 and 16 minutes for untreated, control and si4 samples respectively (Table 5.3). The timing of the metaphase to anaphase transition did not differ in these different conditions. The average timing from anaphase to telophase was 9, 11 and 9 minutes in untreated, control and si4 samples respectively (Table 5.3). Overall, this finding suggests that TRAP150 depletion does not alter chromosome movements and mitotic transitions. However, when comparing total time that a cell remained in mitosis (47, 57 and 64 minutes for untreated, control and TRAP150 siRNA duplex 4 respectively), cells that were depleted of TRAP150 remained in mitosis longer than untreated and control cells (Table 5.3).

In addition, the chromosome alignment defects that were seen in fixed TRAP150-depleted cells were also seen in live cells (Figure 5.8 and 5.9). In some of the cases, cells that showed misaligned chromosomes (Figure 5.9) they remained in metaphase for more than 30 minutes before progressing through metaphase. This suggests that the SAC is indeed getting activated in the presence of misaligned chromosomes in TRAP150-depleted cells. However, anaphase and telophase defects were seen in cells that progressed through mitosis and entered G1 (Figure 5.8). This suggests that even though the majority of the defects seen in fixed cells were metaphase defects, these cells seem to correct the chromosome alignment defect before progressing through metaphase. It also suggests that TRAP150 does not alter the activation or silencing of the SAC. However, the defects seen in anaphase are not corrected by the cell and the defect continues on through mitosis. Another aspect that

needs to be considered is the occurrence of inappropriate microtubule attachments. A desired kinetochore-microtubule attachment is an amphitelic attachment in which each kinetochore of a pair binds to microtubules that radiate from the pole it is facing. However, there are other types of attachments (syntelic, merotelic and monotelic attachments) that lead to chromosome mis-segregation if not corrected (Pinsky and Biggins, 2005). Syntelic attachments occur when both kinetochores within a pair face the same pole and attach to microtubules that radiate from that pole. Monotelic attachments occur when kinetochores are facing opposite directions but only one of the kinetochores binds to a microtubule (Pinsky and Biggins, 2005). Merotelic attachments occur when both kinetochores of a pair bind to microtubules that emanate from both spindle poles (Pinsky and Biggins, 2005). This type of attachment most often leads to lagging chromosomes in anaphase (Cimini et al., 2008). Syntelic and monotelic attachments have been reported to activate the SAC (Lampson et al., 2004; Nezi and Musacchio, 2009). However, merotelic attachments are usually undetected by this checkpoint (Cimini et al., 2008; Nezi and Musacchio et al., 2009). Even though anaphase defects were not the most abundant in the fixed samples, they prove to be the most important when analyzing the effects of TRAP150 depletion in mitosis. This type of defect cannot be detected by the SAC and does not cause a mitotic delay (Cimini et al., 2003) but it still results in mitotic defects that can affect cell cycle progressin.

The Bubulya lab performed exon microarray analysis on TRAP150-depleted samples. Results showed that multiple key mitotic regulator transcripts

were significantly upregulated in the absence of TRAP150. Some of these affected genes were: Aurora B, CENP-F, CENP-E, BUB1 and NDC80 (Table 5.2; Figure 5.10). Even though these were not in the top 10 genes up or down regulated by TRAP150 depletion. These genes were studied further because they are linked to mitotic progression (see Appendix 1). All of these genes encode for kinetochore proteins. These proteins are essential in mediating chromosome movements to the metaphase plate. In order to do so, they all interact with one another to perform their functions properly (Figure 5.10).

NDC80, shown by exon array to be upregulated 2-fold after TRAP150 depletion, forms part of the NDC80 complex. This complex is essential for microtubule kinetochore attachments. Studies show that the number of NDC80 complexes directly correlates with the number of microtubules in a K-fibre (DeLuca et al., 2005; Walczak et al., 2009). The NDC80 complex has both a microtubule and kinetochore binding site (Martin-Lluesma et al., 2002; DeLuca et al., 2002; McCleland et al., 2003; Cheeseman et al., 2006). Disturbance of this complex results in a disruption of K-fibre formation and chromosome alignment (DeLuca et al., 2002; Deluca et al., 2005; Walczak et al., 2009). Overexpression of Ndc80 results in an overactivation of the SAC and aneuploidy. Upregulation of Ndc80 also leads to an upregulation of Mad2 and Securin (Diaz-Rodriguez et al., 2008).

According to our exon array data, CENP-E is upregulated 2-fold after TRAP150 depletion. CENP-E is an activator of kinetochore bound BUBR1. CENP-E is a very large kinesin that has plus end directed motor activity. It has

been linked to kinetochore capture of microtubules, congression of chromosomes at the metaphase plate and maintenance of chromosome congression. Unattached chromosomes are positioned at the metaphase plate through CENP-E mediated forces (Walczak et al., 2009). Microtubule-kinetochore interactions are very dynamic. They rely on tethering dynein and CENP-E, and these proteins are usually regulated by phosphorylation (Rieder and Salmon, 1998; Nigg, 2001). Depletion of CENP-E results in a failure of chromosome congression (Skibbens et al., 1993; Wood et al., 1997; Yen et al., 1991).

CENP-F is a 350 KDa transient kinetochore protein that is upregulated four-fold after TRAP150 depletion, according to our exon array data. CENP-F accumulates at kinetochores at late G2 suggesting a role in the initiation of kinetochore assembly. Recruitment of CENP-F is followed by recruitment of BUBR1, CENP-E and Mad2. CENP-F associates with CENP-E. Depletion of CENP-F leads to a decrease of CENP-E, BUBR1 and Mad1 at the kinetochore. It remains in the outer kinetochore until the metaphase-anaphase transition. Afterwards, it translocates to the central spindle and accumulates at the intracellular bridge between daughter cells. At the end of telophase, CENP-F is degraded. Depletion of CENP-F leads to chromosome alignment defects, improper kinetochore-microtubule attachments, abnormal spindle morphology and failure of chromosome segregation and cytokinesis but still proceeded through mitosis thus resulting in aneuploid cells (Kallio et al., 2006). Overexpressed CENP-F is found in many types of cancer. Upregulation of

CENP-F is linked to disruptions in kinetochore assembly and mitotic checkpoint function (De La Guardia et al., 2001).

BUB1 exon array is upregulated 3-fold after TRAP150 depletion. It associates with kinetochores very early in mitosis and it is required for CENP-F recruitment at the kinetochore. Evidence suggests that BUB1 phosphorylates CENP-F to promote its binding to the kinetochore (Jablonski et al., 1998). In addition, BUB1 protects sister chromatid cohesion and is essential for proper kinetochore-microtubule attachments (Kijatima et al., 2005; Johnson et al., 2004; Meraldi and Sorger, 2005; Kallio et al., 2006). Upregulation of Bub1 leads to an upregulation of BubR1 (Pinto et al., 2008). Overexpressing Bub1 can disrupt mitotic checkpoint function (Taylor et al., 1997) by causing chromosome misalignment and lagging chromosomes (Ricke et al., 2011). Studies have shown that these effects are caused in an Aurora-B dependent manner (Ricke et al., 2011). Upregulation of Bub1 and BubR1 are found in 80% of gastric cancer cases (Grabsch et al., 2003).

Aurora B is upregulated 2-fold after TRAP150 depletion according to our exon array data. Aurora B is responsible for regulating amphitelic kinetochore attachment and spindle checkpoint functions, spindle assembly and disassembly, anaphase chromosome condensation and cytokinesis (Pinsky and Biggins, 2005). It corrects merotelic attachments (Andrews et al., 2004; Kline-Smith et al., 2004) by regulating MCAK and Ndc80/Hec1 (Cheeseman et al., 2006; Knowlton et al., 2006). It is also required for recruitment of various SAC proteins as well as for maintaining the integrity of the chromosome passenger complex (CPC) of

which it is a subunit. The CPC is very important for SAC signaling (King et al., 2007; Nezi and Musacchio, 2009). The CPC has a dynamic localization; first it appears in the inner centromere between sister kinetochores then moves to the elongating spindle and concentrates in spindle midzone (Pinsky and Biggins, 2005). Aurora B is localized at the centromere but it is able to promote recruitment of SAC proteins to kinetochores through phosphorylation. Aurora B phosphorylates substrates such as NDC80 and CENP-A. The phosphorylation of NDC80 by Aurora B decreases the binding affinity of NDC80 for microtubules. Aurora B also contributes to the destabilization of improper kinetochore-microtubule interaction (DeLuca et al., 2006; Ciferri et al., 2008; Cheeseman et al., 2006). Upregulation of Aurora B leads to multinucleation and aneuploidy due to an increase of mitotic H3 phosphorylation at serine-10 (Ota et al., 2012). Aurora B is the essential target through which upregulation of Bub1 causes aneuploidy (Ricke et al., 2011).

These results contradict the hypothesis that the SAC is not getting activated after TRAP150 depletion. All of the genes discussed activate the spindle checkpoint when absent in a cell however, TRAP150 depletion results in an up-regulation of these factors not a down-regulation. A possible explanation can be a compensatory mechanism that occurs after TRAP150 depletion. When TRAP150 levels are decreased, another protein that shares sequence homology with TRAP150, Btf, is shown to be up-regulated (Figure 5.13). In the same way, when Btf is depleted from the cell, TRAP150 compensates for this absence and is upregulated (Figure 5.13). There is a possibility that Btf upregulation mediates

an up-regulation of all of these different factors (Figure 6.1). TRAP150 results in an upregulation of Btf which may lead to an upregulation of Bub1, BubR1, Ndc80, Cenp-E and Cenp-F. This leads to an upregulation of Aurora B. Upregulation of these genes result in an overactive mitotic checkpoint and mitotic checkpoint defects in the form of chromosome missegregation, lagging chromosomes and multinucleation. These defects cause aneuploidy which results in chromosome instability.

Another aspect that needs to be studied further is the alternative splicing of these genes in TRAP150-depleted samples. It is not clear if the end product is a functional protein or if having more transcript produces excess protein product. If the incorrect forms of the proteins are being upregulated then they probably would not be able to perform their functions.

In addition to validating the upregulation of various transcripts, I also verified whether corresponding proteins are also upregulated. Aurora B protein levels increase after TRAP150 depletion (17% and 50% upregulated using siRNA oligos 1 and 4 respectively) as well as after Btf depletion (5% and 29% upregulated when using siRNA oligos 1 and 2 respectively) (Figure 5.11). However, Mad2 protein levels only increased after TRAP150 depletion (10% and 33% upregulated when using siRNA oligos 1 and 4 respectively) and when using Btf siRNA oligo 2 (17% upregulated). A downregulation was seen when using Btf siRNA oligo 1 (12% downregulated) Figure 5.11). This difference seen between siRNA oligos 1 and 2 can be due to the degree of Btf depletion caused by the siRNA oligos. My data shows that Aurora B as well as Mad2 protein levels

increase after TRAP150 and Btf depletion. Another way that an increase in protein level can be detected is through immunofluorescence experiments. Labeling of these proteins in TRAP150 depleted cells and then performing immunofluorescence can be a valuable way to detect this change via microscopy (Figure 5.14, 5.15, 5.16 and 5.17). Aurora B and CENP-E were detected at higher levels in kinetochores of misaligned chromosomes in TRAP150-depleted cells than in controls (Figure 4.14 and 4.15). However, no significant change was detected in the protein levels of CENP-F and Mad2 after TRAP150 depletion. Even though these transcripts are upregulated, this does not necessarily result in a concomitant increase in functional protein at the global level or at specific cellular structures.

Mitotic regulation is a complex and intricate processes that makes use of various mechanisms and proteins of the cell. Loss of mitotic regulation leads to aneuploidy and chromosome instability (Sorrentino et al., 2005). Many of these well known proteins are cyclins, kinetochore proteins as well as kinases and phosphatases. In addition, other proteins such as nuclear proteins also play a role in mitotic progression. These interactions are not as well known. My study was able to describe the roles of two nuclear proteins, Son and TRAP150, in mitosis. I was also able to characterize the aberrant phenotypes that are caused by depletion of these proteins from HeLa cells. Studying these novel roles further can help answer the multiple unknown questions about mitotic regulation and can in the long run aid in our understanding of cancerous tissue.

Bibliography

[1] Adams, R.R, H. Maiato, W.C. Earnshaw and M. Carmena. 2001. Essential role of Drosophila inner centromere protein (INCENP) and Aurora B in histone H3 Phosphorylation, metaphase chromosome alignment, kinetochore disjunction and chromosome segregation. J. Cell Biol, 153:865-879.

[2] Ahn, E. Y., R.C. DeKelver, M.C. Lo, T.A. Nguyen, S. Matsuura, A. Boyapati, S. Pandit, X.D. Fu and D.E. Zhang. 2001.Son controls cell-cycle progression by coordinated regulation of RNA splicing. Mol. Cell, 42: 185-198.

[3] Amaral, P.P., M.E. Dinger, T.R. Mercer and J.S. Mattick. 2008. The eukaryotic genome as an RNA machine. Science, 319: 1787-1789.

[4] Andersen, S.S. 1999. Balanced regulation of microtubule dynamics during the cell cycle: a contemporary view. BioEssays, 21: 53-60.

[5] Andersen, S.S. et al. 2003. Proteomic characterization of the human centrosome by protein correlation profiling. Nature, 426: 570-574.

[6]Andrews, P.D., Y. Ovechkina, N. Morrice, M. Wagenbach, K. Duncan, L. Word eman and J.R. Swedlow. 2004. Aurora B regulates MCAK at the mitotic centromere. Dev. Cell, 6:253–268.

[7] Bentley,D. 2005. Rules of engagement: co-transcriptional recruitment of pre-mRNA processing factors. Curr. Opin. Cell Biol, 17: 251-256.

[8] Bessonov, S., M. Anokhing, C.L. Will, H. Urlaub and R. Luhrmann. 2008. Isolation of an active step 1 spliceosome and composition of its RNP core. Nature, 452: 846-850.

[9] Bharadwaj, R., W. Qi and H. Yu. 2004. Identification of two novel components of the human centrosome Ndc80 kinetochore complex. J. Biol. Chem, 279: 13076-13085.

[10] Black, D.L. 2003. Mechanisms of alternative pre-messenger RNA splicing. Annu. Rev. Biochem, 72:291-336.

[11] Blaustein, M., F. Pelisch, T. Tanos, M.J. Munoz, D. Wengier, L. Quadrana, J.R. Sanford, J.P. Muschietti, A.R. Kornblihtt, and J.F. Caceres et al. 2005. Concerted regulation of nuclear and cytoplasmic activities of SR proteins by AKT. Nat. Struct. Mol. Biol, 12: 1037-1044.

[12] Blencowe, B.J. 2006. Alternative splicing: new insights from global analyses. Cell, 126: 37-47.

[13] Blencowe, B.J. 2000. Exonic splicing enhancers: mechanism of action, diversity and role in human genetic diseases. Trends Biochem. Sci., 25:106-110.

[14] Bloom, J. and F.R. Cross. 2007. Multiple levels of cyclin specificity in cell cycle control. Nature Rev. Mol. Cell Biol, 8: 149.

[15] Bourgeois, C.F., F. Lejeune and J. Stevenin. 2004. Broad specificity of SR (serine/arginine) proteins in the regulation of alternative splicing of pre-messenger RNA. Prog. Nucleic Acid Res. Mol. Biol, 78: 37-88.

[16] Brinley, B.R. and E. Stubblefield. 1996. The fine structure of the kinetochore of a mammalian cell in vitro. Chromosoma, 19: 28-43.

[17] Buratti, E., A.F., Muro, M. Giombi, D. Gherbassi, A. Laconcig and F.E. Baralle. 2004. RNA folding affects the recruitment of SR proteins by mouse and human polypurinic enhancer elements in the fibronectin EDA exon. Mol. Cell Biol., 24: 1387-1400.

[18] Caceres, J.F., T. Misteli, G.R. Screaton, D.L. Spector and A. Krainer. 1997. Role of the modular domains of SR proteins in subnuclear localization and alternative splicing specificity. J. Cell Biol., 138: 225-238.

[19] Caceres, J.F., G.R. Screaton and A.R. Krainer. 1998. A specific subset of SR proteins shuttles continuously between the nucleus and the cytoplasm. Genes Dev., 12: 55-56.

[20] Calarco, J.A., S. Superina, D. O'Hanlon, M. Gabut, B. Raj, Q. Pan, U. Skalska, L. Clarke, D. Gelinas and D. Van der Kooy et al. 2009. Regulation of vertebrate nervous system alternative splicing and development by an SR related protein. Cell, 138: 898-910.

[21] Chan, G.K. and T.J. Yen. 2003. The mitotic checkpoint: a signaling pathway that allows a single unattached kinetochore to inhibit mitotic exit. Prog. Cell Cycle Res, 5: 431-439.

[22] Chan, G.K. et al. 1999. Human BubR1 is a mitotic checkpoint kinase that monitors CENP-E functions at kinetochores and binds the cyclosome/APC. J. Cell Biol, 146: 941-954.

[23] Cheeseman, I.M., J.S. Chappie, E.M. Wilson-Kubalek and A. Desai. 2006. The conserved KMN network constitutes the core microtubule-binding site of the kinetochore. Cell, 127: 983-997.

[24] Cheeseman, I.M., T. Hori, T. Fukagawa and A. Desai. 2008. KNL1 and the CENP-H/I/K complex coordinately direct kinetochore assembly in vertebrates. Mol. Biol. Cell, 19: 587-594.

[25] Chia, N. Y., Y.S. Chan, B. Feng, X. Lu, Y. L. Orlov, D. Moreau, P.Kumar, L. Yang, J. Jiang, M.S. Lau et al. 2010. A genome-wide RNAi screen reveals determinants of human embryonic stem cell identity. Nature, 468: 316-320.

[26] Choo, A. 1997. The centromere. Oxford University Press, New York.

[27] Ciferri, C., S. Pasqualato, E. Screpanti, G. Varetti, S. Santaguida, G. Dosreis, A. Maiolica, J. Polka, J. DeLuca, P. Dewulf. 2008. Implications for kinetochore-microtubule attachment from the structure of an engineered Ndc80 complex. Cell, 133:427-439.

[28] Cimini, D., B. Moree, J.C. Canman and E.D. Salmon. 2003. Merotelic kinetochore orientation occurs frequently during early mitosis in mammalian tissue cells and error correction is achieved by two different mechanisms. *J. Cell Sci.,* 116: 4213-4225.

[29] Cimini, D. 2008. Merotelic kinetochore orientation, aneuploidy, and cancer. Biochim. Biophys. Acta., 1786: 32-40.

[30] Coller, H.A. 2007. What's taking so long? S-phase entry from quiescence versus proliferation. Nature Rev. Mol. Cell Biol., 8: 667.

[31] Colwill, K., T., B. Pawson. J. Andrews, J.L. Prasad, J.C. Manley, J.C. Belland and P.I. Duncan. 1996. The Clk/Sty protein kinase phosphorylates SR splicing factors and regulates their intranuclear distribution. EMBO J., 15: 265-275.

[32] Cooke et al. 1997. Localization of CENP-E in the fibrous corona and outer plate of mammalian kinetochores from prometaphase through anaphase. Chromosoma, 106: 446-455.

[33] Spector, D.L. 2006. SnapShot: cellular bodies Cell, 127:1071

[34] Darzynkiewicz, Z., Crissman, and J.W. Jacobberger. 2004. Cytometry of the Cell Cycle: Cycling through history. Cytometry 58A: 21.

[35] Das, R., J. Yu, Z. Zhang, M.P. Gygi, A.R. Krainer, S.P. Gygi and R. Reed, R. 2007. SR proteins function in coupling RNAP II transcription to pre-mRNA splicing. Mol. Cell, 26: 867-881.

[36] De La Guardia, C., C.A. Casiano, J. Trinidad-Pinedo, and A. Baez. 2001. Cenp-F Gene Amplification and Overexpression in Head and Neck Squamous Cell Carcinomas. Head & Neck, 23.2: 104-12.

[37] DeLuca, J.G. et al. 2005. Hec1 and nuf2 are components of the kinetochore outer plate essential for organizing microtubule attachment sites. Mol. Biol. Cell, 16: 519-531.

[38] DeLuca, J.G. et al. 2006. Kinetochore microtubule dynamics and attachment stability are regulated by Hec1. Cell, 127: 969-982.

[39] DeLuca, J.G. et al. 2003. Nuf2 and Hec1 are required for retention of the checkpoint proteins Mad1 and Mad2 to kinetochores. Curr. Biol., 13: 2103-2109.

[40] DeLuca, J.G., B. Moree, J.M. Hickey, J.V. KilMartin and E.D. Salmon, E.D. 2002. hNuf2 inhibition blocks stable kinetochore-microtubule attachment and induces mitotic cell death in HeLa cells. J. Cell Biol., 159: 549-555.

[41] Desai, A., S. Rybina, T. Muller-Reichert, A. Sheuchenko, A. Hyman and K. Oegema. 2003. KNL-1 directs assembly of the microtubule-binding interface of the kinetochore in C.elegans. Genes Dev., 17: 2421-2435.

[42] Diaz-Rodriguez, E., R. Sotillo, J.M. Schvartzman, and R. Benezra. 2008. Hec1 Overexpression Hyperactivates the Mitotic Checkpoint and Induces Tumor Formation in Vivo. Proc. Nat. Acad. Sci. USA, 105: 16719-6724.

[43] Dobles, M., V. Liberal, M.L. Scott, R. Benezra and P.K. Sorger. 2000. Chromosome missegregation and apoptosis in mice lacking the mitotic checkpoint protein Mad2. Cell, 101:635-645.

[44] Dong, Y., K.J. Vandenbeldt, X. Meng, A. Khodjakov and B.F. McEwen. 2007. The outer plate in vertebrate kinetochores is a flexible network with multiple microtubule interactions. Nat. Cell Biol., 9: 516-522.

[45] Duncan, P.I., B.W. Howell, R.M. Marius, S. Drmanic, E.M. Douville, E. and J.C. Bell. 1995. Alternative splicing of STY, a nuclear dual specificity kinase. J. Biol. Chem., 270: 21524-21531.

[46] Earnshaw, W.C. and N. Rothfield. 1985. Identification of a family of human centromere proteins using autoimmune sera from patients with sceroderma. Chromosoma, 91: 313-321.

[47] Egloff, S. and S. Murphy. 2008. Cracking the RNA polymerase II CTD code. Trends Genet., 24: 280-288.

[48] Ekholm, S. V. and S.I. Reed. 2000. Regulation of G(1) cyclin-dependent kinases in the mammalian cell cycle. Curr. Opin. Cell Biol., 12:676-684.

[49] Ferreira, J.A., M. Carmo-Fonseca and A.I. Lamond. 1994. Differential interaction of splicing snRNPs with coiled bodies and interchromatin granules during mitosis and assembly of daughter nuclei. J. Cell Biol., 126: 11-23.

[50] Ferreira, J.A., M. Carmo-Fonseca and A.I. Lamond. 1994. Differential interaction of splicing snRNPs with coiled bodies and interchromatin granules during mitosis and assembly of daughter cell nuclei. J. Cell Biol, 126: 11-23.

[51] Foltz, D.R., L.E. Jansen, B.E. Black, A.O. Bailey, J.R. Yates and D.W. Cleveland. 2006. The human CENP-A centromeric nucleosome-associated complex. Nat. Cell Biol., 8: 458-469.

[52] Fondell, J.D., H. Ge and R.G. Roeder. 1996. Ligand induction of a transcriptionally active thyroid hormone receptor coactivator complex. Proc. Natl. Acad. Sci. USA , 93: 8329-8333.

[53] Fu, X.D. 2004. Towards a splicing code. Cell 119, 736-738.

[54] Fu, X.D. and T. Maniatis. 1992. The 35 kDa mammalian splicing factor SC35 mediates specific interactions between U1 and U2 small nuclear ribonucleoprotein particles at the 3’ splice site. Proc. Natl. Acad. Sci. USA, 89: 1725.

[55] Fukagawa, T., Y. Mikami, A. Nishihashi, V. Regnier, T. Haraguchi, Y. Hiraoka, N. Sugata, K. Todokoro, W. Brown and T. Ikemura. 2001. CENP-H, a constitutive centromere component, is required for centromere targeting of CENP-C in vertebrate cells. EMBO J., 20: 4603-4617.

[56] Goshima, G., T. Kiyomitsu, K. Yoda and M. Yanagida. 2003. Human centromere chromatin protein hMis12 essential for equal segregation is independent of CENP-A loading pathway. J. Cell Biol., 160: 25-39.

[57]Grabsch, H., S. Takeno, W.J. Parsons, N. Pomjanski, A. Boecking, H.E. Gab bert,W. Mueller. 2003. Overexpression of the mitotic checkpoint genes BUB1, BUBR1, and BUB3 in gastric cancer—association with tumour cell proliferation. J. Pathol., 200:16–22.

[58] Graveley, B.R. 2000. Sorting out the complexity of SR protein functions. RNA, 6: 1197-1211.

[59] Graveley, B.R., K.J. Hertel and T. Maniatis. 1998. A systematic analysis of the factors that determine the strength of pre-mRNA splicing enhancers. EMBO J., 17:6747-6756.

[60] Gurley, L.R. et al. 1978. Histone phosphorylation and chromatin.

[61] Haering, C.H., and K. Nasmyth. 2003. Building and breaking bridges between sister chromatids. BioEssays, 25:1178.

[62] Hardwick, K.G. and J.V. Shah. 2010. Spindle checkpoint silencing: ensuring rapid and concerted anaphase onset. Biol. Rep., 2:55.

[63] Hartwell, L.H. and T.A. Weinert. 1989. Checkpoints: controls that ensure the order of cell cycle events. Science, 246: 629-634.

[64] Hedley, M.L., H. Amrein, and T. Maniatis. An amino acid sequence motif sufficient for subnuclear localization of an arginine/serine rich splicing factor. Proc. Natl. Acad. Sci. USA, 92: 11524-11528.

[65] Hertel, K.J. 2008. Combinatorial control of exon recognition. J. Biol. Chem., 283:1211-1215.

[66] Hirose, Y. and J.L. Manley. 2000. RNA Polymerase II and the integration of nuclear events. Genes Dev., 14: 1415-1429.

[67] Holland, A.J. and D.W. Cleveland. 2009. Boveri revisited: chromosomal instability, aneuploidy and tumorigenesis. Nat. Rev. Mol. Cell Biol., 10: 478-487.

[68] Hori, T., T. Haraguchi, Y. Hiraoka, H. Kimura and T. Fukagawa. 2003. Dynamic behavior of Nuf2-Hec1 complex that localizes to the centrosome and centromere and is essential for mitotic progression in vertebrate cells. J. Cell Sci., 116: 3347-3362.

[69] Howell, B.J. et al. 2001. Cytoplasmic dynein/ dynactin drives kinetochore protein transport to the spindle poles and has a role in mitotic spindle checkpoint inactivation. J. Cell Biol., 155: 1159-1172.

[70] Howman, E.V., K.J. Fowler, K.J., A.J. Newson, S. Redward, A.C. Macdonald, P. Kalitsis and K.H. Choo. 2000. Early disruption of centromeric chromatin organization in centromere protein A (CENP-A) null mice. Proc. Natl. Acad. Sci. USA, 97: 1148-1153.

[71] Huang, Y. and J.A. Steitz. 2005. SRprises along a messenger's journey. Mol. Cell., 17: 613-615.

[72] Huen, M. S., S. M. Sy, K.M. Leung, Y.P. Ching, G.L. Tipoe, C. Man, S. Dong and J. Chen. 2010. SON is a spliceosome-associated factor required for mitotic progression. Cell Cycle, 9: 2679-2685.

[73] Inoue, S. and E.D. Salmon. 1995. Force generation by microtubule assembly/disassembly in mitosis and related movements. Mol. Biol. Cell, 6: 1619-1640.

[74] Jablonski, S.A., G.K. Chan, C.A. Cooke, W.C. Earnshaw and T.J. Yen. 1998. The hBub1 and hBubR1 kinases sequentially assemble onto kinetochores during prophase with hBubR1 concentrating at the kinetochore plates in mitosis. Chromosoma, 107: 386-396.

[75] Jallepalli, P.V. and C. Lengauer. 2001. Chromosome segregation and cancer: cutting through the mystery. Nat. Rev. Cancer, 1:109-117.

[76] Janicki S.M., T. Tsukamoto, S.E. Salghetti, W.P. Tansey, R. Sachidanandam, K.V. Prasanth, T. Ried, Y. Shav-Tal, E. Bertrand, R.H. Singer, D.L. Spector. 2004. From silencing to gene expression: real-time analysis in single cells. Cell, 116: 683–69.

[77] Johnson, V.L., M.I. Scott, S.V. Holt, D. Hussein, S.S. Taylor, S.S. 2004. Bub1 is required for kinetochore localization of BubR1, CENP-E, CENP-F and Mad2 and chromosome congression. J. Cell Sci., 117:1577-1589.

[78] Kaitna, S., M. Mendoza, V. Jantsch-Plunger, M. Glotzer. 2000. INCENP and an aurora-like kinase form a complex essential for chromosome segregation and efficient completion of cytokinesis. Curr. Biol., 10: 1172-1181.

[79] Kemmler, S. et al. 2009. Mimicking Ndc80 phosphorylation triggers spindle assembly checkpoint signaling. EMBO J., 28: 1099-1110.

[80] Kijatima, T.S., S. Hauf, M. Ohsugi, T. Yamamoto, Y. Wafanabe. 2005. Human Bub1 defines the persistent cohesion site along the mitotic chromosome by affecting Shugoshin localization. Curr. Biol.,15:353-359.

[81] Kimura, K., M. Hirano, R. Kobayashi and T. Hirano. 1998. Phosphorylation and activation of 13S condensin by Cdc2 in vitro. Science, 282: 487-490.

[82] King, J.M. and R.B. Nicklas. 2000. Tension on chromosomes increases the number of kinetochore microtubules but only within limits. J. Cell Sci., 113: 3815-3823.

[83] King, E.M., S.J. van der Sar, K.G. Hardwick. 2007. Mad3 KEN boxes mediate both Cdc20 and Mad3 turnover, and are critical for the spindle checkpoint. PLoS ONE.

[84] Kirschner, M.W. and T. Mitchison. 1986. Beyond self-assembly; from microtubule to morphogenesis. Cell, 45: 329-342.

[85] Kline-Smith, S. L., A. Khodjakov, P. Hergert and C.E. Walczak, C. E. 2004.

Depletion of centromeric MCAK leads to chromosome congression and segregation defects due to improper kinetochore attachments. Mol. Biol. Cell, *15*: 1146–1159.

[86] Knowlton, A.L., W. Lan and P.T. Stukenberg. 2006. Aurora B is enriched at merotelic attachment sites, where it regulates MCAK. Curr. Biol., 16:1705–1710

[87] Kops, G.J. B.A. Weaver and D.W. Cleveland. 2005. On the road to cancer: aneuploidy and the mitotic checkpoint. Nat. Rev. Cancer, 5: 773-785.

[88] Kotwaliwale, C. and S. Biggins. 2006. Microtubule capture: a concerted effort. Cell, 127: 1105-1108.

[89] Krawczak, M., J. Reiss and D.N. Cooper. 1992. The mutational spectrum of single base-pair substitutions in mRNA splice junctions of human genes: causes and consequences. Hum. Genet., 90: 41-54.

[90] Lamond, A.I., and D.L. Spector. 2003. Nuclear Speckles: A Model for Nuclear Organelles. *Nature*, 4: 605-12.

[91] Lampson, M.A., K. Renduchitala, A. Khodjakov, T.M. Kapoor. 2004. Correcting improper chromosome- spindle attachments during cell division. Nat. Cell Biol, 6: 232-237.

[92] Lee, K.M., I.W. Hsu, and W.Y. Tarn. 2010. TRAP 150 Activates Pre-mRNA Splicing and Promotes Nuclear MRNA Degradation. *Nucleic Acids Research*, 38.10: 3340-350.

[93] Lesser, G.P., S. Fakan and T.E. Martin. 1989. Ultrastructural distribution of ribonucleoprotein complexes during mitosis. snRNP antigens are contained in mitotic granule clusters. Eur. J Cell Biol, 50: 376-389.

[94] Lewis, J.D., and D. Tollervey. 2000. Like attracts like: getting RNA processing together in the nucleus. Science, 288: 1385-1389.

[95] Li, H. and P.M. Bingham. 1991. Arginine/serine rich domains of the su(wa) and tra RNA processing regulators target proteins to a subnuclear compartment implicated in splicing. Cell, 67: 335-342.

[96] Liu, S.T., J.B. Rattner, S.A. Jablonski and T.J. Yen. 2006. Mapping the assembly pathways that specify formation of the trilaminar kinetochore plates in human cells. J. Cell Biol., 175: 41-53.

[97] Long, J.C. and J.F. Caceres, J.F. 2009. The SR protein family of splicing factors: master regulators of gene expression. Biochem J., 417: 15-27.

[98] Lowe, M. et al. 1998. Cdc2 Kinase directly phosphorylates the cis-Golgi matrix protein GM130 and is required for Golgi fragmentation in mitosis. Cell 94: 783- 793.

[99] Maiato, H., P.J. Hergert, S. Moutinho-Pereira, Y. Dong, K.J. Vandenbeldt, C.L. Rieder and B.F. McEwen. 2006. The ultrastructure of the kinetochore and the kinetochore fiber in Drosophila somatic cells. Chromosoma, 115: 469-480.

[100] Maiato, Helder, Jennifer DeLuca, E.D Salmon, and William C. Earnshaw. 2004.The Dynamic Kinetochore-microtubule Interface. J. Cell Sci., 117: 5461-477.

[101] Martin-Lluesma, S., V.M. Stucke and E.A. Nigg. 2002. Role of Hec1 in spindle checkpoint signaling and kinetochore recruitment of Mad1/Mad2. Science, 297: 2267-2270.

[102] Matera, A.G, M. Izaguire-Sierra, K. Praveen and T.K. Rajendra. 2009. Nuclear bodies: random aggregates of sticky proteins or crucibles of macromolecular assembly? Dev. Cell, 17: 639–64.

[103] Matlin, A.J. and M.J. Moore. 2007. Spliceosome assembly and composition. Adv. Exp. Med. Biol., 623: 14-35.

[104] Mattick, J.S. 2009. The genetic signatures of noncoding RNAs. PLoS Genet. 5, e1000459.10.1371/journal.pgen.1000459.

[105] Mazia, D. 1987. The chromosome cycle and the centrosome cycle in the mitotic cycle. Int. Rev. Cytol., 100: 49-92.

[106] McCleland, M.L., R.D. Gardner, M.J. Kallio, J.R. Daum, G.J. Gorbsky, D.J. Burke and P.T. Stukenberg. 2003. The highly conserved Ndc80 complex is required for kinetochore assembly, chromosome congression and spindle checkpoint activity. Genes Dev., 17: 101-114.

[107] McCleland, M.L., M.J. Kallio, M.J, G.A. Barrett-Wilt, C.A. Kestner, J. Shabanowitz, D.F. Hunt, G.J. Gorbsky and P.T. Stukenberg. 2004. The

vertebrate Ndc80 complex contains Spc24 and Spc25 homologs, which are required to establish and maintain kinetochore-microtubule attachment. Curr. Biol., 14: 131-137.

[108] McCleland,M.L., R.D.Gardner, and M.J. Kallio. 2003. The Highly Conserved Ndc80 Complex Is Required for Kinetochore Assembly, Chromosome Congression, and Spindle Checkpoint Activity. Genes Dev. , 17: 101-14.

[109] McEwen, B.F., A.B. Heagle, G.O. Cassels, K.F. Buttle and C.L. Rieder. 1997. Kinetochore fiber maturation in PtK1 cells and its implications for the mechanisms of chromosome congression and anaphase onset. J. Cell Biol., 137: 1567-1580.

[110] McIntosh, J.R., E.L. Grishchuck, M.K. Morphew, A.K. Efremov, K. Zhudenkov, V.A. Volkov, I.M. Cheeseman, A. Desai, D.N. Mastronarde and F.I. Ataullakhanov. 2008. Fibrils connect microtubule tips with kinetochores: a mechanism to couple tubulin dynamics to chromosome motion. Cell, 135: 322-333.

[111] Melcak, I. et al. 2000. Nuclear pre-mRNA compartmentalization: trafficking of released transcripts to splicing factor reservoirs. Mol. Biol. Cell, 11: 497-510.

[112] Meraldi, P. and P.K. Sorger. 2005. A dual role for Bub1 in the spindle checkpoint and chromosome congression. EMBO J., 24: 1621-1633.

[113] Mollinari, C., C. Reynaud, S. Martineau-Thuillier, S. Monier, S. Kieffer, J. Garin, P.R. Andreassen, A. Boulet, B. Goud, J.P. Kleman, R.L. Margolis. 2003.

The mammalian passenger protein TD-60 is an RCC1 family member with an essential role in prometaphase to metaphase progression. Dev. Cell, 5: 295-307.

[114] Muro, A.F., M. Caputi, R. Pariyarath, F. Pagani, E. Buratti and F.E. Baralle. 1999. Regulation of fibronectin EDA exon alternative splicing: possible role of RNA secondary structure for enhancer display. Mol. Cell Biol., 19:2657-2671.

[115] Murray, A.W. and J.W. Szostak. 1985. Chromosome segregation in mitosis and meiosis. Annu. Rev. Cell Biol., 1: 289-315.

[116] Musacchio, A. and E.D. Salmon. 2007. The spindle assembly checkpoint in space and time. Nat. Rev. Mol. Cell Biol., 8: 379-393.

[117] Musacchio, A. and E.D. Salmon. 2007. The spindle assembly checkpoint in space and time. Nat. Rev. Mol. Cell Biol., 8:379-393.

[118] Narlikar, G.J., H.Y. Fan and R.E. Kingston. 2002. Cooperation between complexes that regulate chromatin structure and transcription. Cell, 108: 475-487.

[119] Nicklas, R.B and P. Arana. 1999. Evolution and the meaning of metaphase. J. Cell Sci., 1202 (Pt4): 681-690.

[120] Nicklas, R.B. and S.C. Ward. 1994. Elements of error correction in mitosis: microtubule capture, release and tension. J. Cell Biol., 126: 1241-1253.

[121] Nigg, E.A. 2006. Origins and consequences of centrosome aberrations in human cancers. Int. J. Cancer, 119: 2717-2723.

[122] Nigg, E.A. 1995. Cyclin-dependent protein kinases: key regulators of the eukaryotic cell cycle. BioEssays., 17: 471-480.

[123] Nigg, E.A. 2001. Mitotic kinases as regulators of cell division and its checkpoints. Nature Rev. Mol. Cell Biol., 2: 21.

[124] Noton, E. and J.F. Diffley. 2000. CDK inactivation is the only essential function of the APC/C and the mitotic exit network proteins for origin resetting during mitosis. Mol. Cell, 5: 85-95.

[125] Oegema, K., A. Desai, S. Rybina, M. Kirkham and A.A. Hyman, A.A. 2001. Functional analysis of kinetochore assembly in Caenorhabditis elegans. J. Cell Biol., 153: 1209-1226.

[126] Ota, T., S. Suto, H. Katayama, Z.B. Han, F. Suzuki, M. Maeda, M. Tanino, Y. Terada, and M. Tatsuka. 2002. Increased Mitotic Phosphorylation of Histone H3 Attributable to AIM-1/Aurora-B Overexpression Contributes to Chromosome Number Instability. Cancer Res., 62: 5168-177.

[127] Patel, N.A., S. Kaneko, H.S. Apostolatos, S.S. Bae, J.E. Watson, K. Davidowitz, D.S. Chapell, M.J. Birnbaum, J.Q. Cheng and D.R. Cooper, D.R. 2005. Molecular and genetic studies imply AKT-mediated signaling promotes protein kinase Cβ II alternative splicing via phosphorylation of serine/arginine rich splicing factor SRp40. J. Biol. Chem., 280: 14302-14309.

[128] Pfarr, C.M. et al. 1990. Cytoplasmic dynein is localized to kinetochores during mitosis. Nature, 345: 263-265.

[129] Phair, R.D. and T. Misteli, T. 2000. High mobility of proteins in the mammalian cell nucleus. Nature, 404: 604-609.

[130] Phatphani, H.P., and A.L. Greenleaf. 2006. Phosphorylation and functions of the RNA polymerase II CTD. Genes Dev., 20: 2922-2936.

[131] Pinsky, B.A. et al. 2006. The Ipl1-Aurora protein kinase activities the spindle checkpoint by creating unattached kinetochores. Nat. Cell Biol., 8: 78-83.

[132] Pinto, M., J. Vieira, F. R. Ribeiro, M. J. Soares, R. Henrique, J. Oliveira, C. Jeronimo, and M. R. Teixeira. 2008. Overexpression of the Mitotic Checkpoint Genes BUB1 and BUBR1 Is Associated with Genomic Complexity in Clear Cell Kidney Carcinomas. Cellular Oncol., 30: 389-95.

[133] Prasad, J., K. Colwill, T. Pawson, and J.L. Manley, J.L. 1999. The protein kinase Clk/Sty directly modulates SR protein activity: both hyper- and hypophosphorylation inhibit splicing. Mol. Cell. Biol., 19: 6991-7000.

[134] Prasanth, K.V., P. Sacco-Bubulya, S.G. Prasanth and D.L. Spector. 2003. Sequential entry of components of gene expression machinery into daughter nuclei. Mol. Biol. Cell, 14: 1043-1057.

[135] Putkey, F.R., T. Cramer, M.K. Morphew, A.D. Silk, R.S. Johnson, J.R. McIntosh and D.W. Cleveland. 2002. Unstable kinetochore microtubule capture and chromosomal instability following deletion of CENP-E. Dev. Cell, 3: 351-365.

[136] Rappsilber, J., U. Ryder, A.I. Lamond, and M. Mann. 2002. Large scale proteomic analysis of the human spliceosome. Genome Res., 12:1231-1245.

[137] Reuter, R., B. Appel, J. Rinke and R. Luhrmann. 1985. Localization and structure of snRNPs during mitosis. Immunofluorescent and biochemical studies. Exp. Cell Res., 159: 63-79.

[139] Ricke, R. M., K. B. Jeganathan, and J. M. Van Deursen. 2011. Bub1 Overexpression Induces Aneuploidy and Tumor Formation through Aurora B Kinase Hyperactivation. J. Cell Biol., 193.6: 1049-064.

[140] Rieder, C.L. 1982. The formation, structure and composition of the mammalian kinetochore and kinetochore fiber. Int. Rev. Cytol., 79: 1-58.

[141] Rieder, C.L. and E.D. Salmon.1998. The vertebrate cell kinetochore and its role during mitosis. Trends Cell Biol., 8: 310–318.

[142] Roscigno, R.F. and M.A. Garcia-Blanco. 1995. SR proteins escort the U4/U6.U5 tri-snRNP to the spliceosome. RNA, 1: 692-706.

[143] Rossi, F., E. Labourier, T. Forne, G. Divita, J. Derancourt, J.F. Riou, E. Antoine, G. Cathala, C. Bronel and J. Tazi. 1996. Specific phosphorylation of SR proteins by mammalian DNA topoisomerase I. Nature, 381: 80-82.

[144] Sacco-Bubulya, P., and D.L. Spector. 2002. Disassembly of interchromatin granule clusters alters the coordination of transcription and pre-mRNA splicing. J. Cell Biol., 156: 425-436.

[145] Saitoh, N., C.S. Spahr, S.D. Patterson, P. Bubulya, A.F. Neuwald and D.L. Spector, D.L. 2004. Proteomic analysis of interchromatin granule clusters. Mol. Biol. Cell, 15: 3876-3890.

[146] Sauer, G et al. 2005. Proteome analysis of the human mitotic spindle. Mol. Cell Proteomics, 4: 35-43.

[147] Schvartzman, J.M., R. Sotillo and R.Benezra. 2010. Mitotic chromosomal instability and cancer: mouse modeling of the human disease. Nat. Rev. Cancer, 10:102-115.

[148] Shah, J.V. and D.W. Cleveland. 2000. Waiting for anaphase: Mad2 and the spindle assembly checkpoint. Cell, 103: 997-1000.

[149] Sharma, A., H. Takata, K.I. Shibahara, A. Bubulya, and P.A. Bubulya. 2010. Son Is Essential for Nuclear Speckle Organization and Cell Cycle Progression." Mol. Biol. of the Cell, 21: 650-63

[150] Sharma, A. , M. Markey, K. Torres-Munoz, S. Varia, M. Kadakia, A. Bubulya, and P. Bubulya. 2011. Son Maintains Accurate Splicing for a Subset of Human Pre-mRNAs. J. Cell Sci., 124.24: 4286-298.

[151] Shepard, P. J. and K.J. Hertel. 2009. The SR protein family. Genome Biol., 10: 242

[152] Skeen, V.P. and E.D. Salmon. 1993. Directional instability of kinetochore motility during chromosome congression and segregation in mitotic newt lung cells: a push-pull mechanism. J. Cell Biol., 122: 859-875.

[153] Skibbens, R.V., V.P. Skeen and E.D. Salmon. 1993. Directional instability of kinetochore motility during chromosome congression and segregation of mitotic newt lung cell: a push–pull mechanism. J Cell Biol., 122:859–876.

[154] Sorrentino, R. *et al*. 2005. Aurora B overexpression associates with the thyroid carcinoma undifferentiated phenotype and is required for thyroidcarcinoma cell proliferation. J. Clin. Endocrinol. Metab., 90: 928–935.

[155] Spector, D.L. and H.C. Smith. 1986. Redistribution of u-snRNPs during mitosis. Exp. Cell Res., 163: 87-94.

[156] Spector, D.L., X.D. Fu and T. Maniatis. 1991. Associations between distinct pre-mRNA splicing components and the cell nucleus. EMBO J., 10: 3467-3481.

[157] Spector, D.L., W.H. Schrier and H. Busch. 1983. Immunoelectron microscopic localization of snRNPs. Bio. Cell, 49: 1-10.

[158] Spector, D. L., and A. I. Lamond. 2010. Nuclear Speckles. CSH Perspectives in Biology, 1-12.

[159] Speliotes, E.K., A. Uten,D. Vaux and H.R. Horvitz. 2000. The surviving-like C.elegans BIR-1 protein acts with the aurora like kinase AIR-2 to affect chromosomes and the spindle midzone. Mol. Cell, 6:211-223.

[160] Staknis, D. and R., Reed.1994. SR. proteins promote the first specific recognition of pre-mRNA and are present together with the U1 small nuclear

ribonucleoprotein particle in a general splicing enhancer complex. Mol. Cell Biol., 14: 7670.

[161] Stamm, S. 2008. Regulation of alternative splicing by reversible protein phosphorylation. J. Biol. Chem., 283: 1223-1227.

[162] Stever, E.R., L. Wordeman, T.A. Schroer and M.P. Sheetz. 1990. Localization of cytoplasmic dynein to mitotic spindles and kinetochores. Nature, 345: 266-268.

[163] Sun, C.T., W.Y. Lo, I.H. Wang, Y.H. Lo, S.R. Shiou, C.K. Lai and L.P. Ting. 2001. Transcription repression of human hepatitis B virus genes by NREBP/Son. J. Biol. Chem., 276: 24059-24067.

[164] Tarn, W.Y. and J.A. Steitz.1995. Modulation of 5' splice site choice in pre-messenger RNA by two distinct steps. Proc. Natl. Acad. Sci., USA 92: 2504.

[165] Taylor, S.S., and F. McKeon. 1997. Kinetochore localization of murine Bub1 is required for normal mitotic timing and checkpoint response to spindle damage. Cell, 89:727–735.

[166] Thiry, M. 1995. The interchromatin granules. Histol. Histopathol., 10: 1035-1045.

[167] Thiry, M. 1995. Behavior of interchromatin granules during the cell cycle. Eur. J. Cell Biol., 68: 14-24.

[168] Van Hooser, A.A., I.I. Ouspenski, H.C. Gregson, D.A. Starr, T.J. Yen, M.L. Goldberg, K. Yokomori, W.C. Earnshaw, K.F. Sullivan and B.R. Brinkley, B.R.

2001. Specification of kinetochore-forming chromatin by the histone H3 variant CENP-A. J. Cell Sci., 114: 3529-3542.

[169] Vandenbeldt, K.J., R.M. Barnard, P.J. Hergert, X. Meng, H. Maiato and B.F. McEwen. 2006. Kinetochores use a novel mechanism for coordinating the dynamics of individual microtubules. Curr. Biol., 16: 1217-1223.

[170] Verheijen, R., H. Kuijpers, P. Voojis, W. Van Venrooij and F. Ramarkers. 1986. Distribution of the 70K U1RNA-associated protein during interphase and mitosis. Correlation with other U RNP particles and proteins of the nuclear matrix. J. Cell Sci., 86: 173-190.

[171] Wei, R.R., J. Al-Bassam and S.C. Harrison. 2007. The Ndc80/Hec1 complex is a contact point for kinetochore-microtubule attachment. Nature Struct. Mol. Biol., 14:54-59.

[172] Winey, M. 1999. Cell Cycle: driving the centrosome cycle. Curr. Biol., 9:R449-R452.

[173] Wittman, T., A. Hyman, A. Desai, 2001. The Spindle: a dynamic assembly of microtubules and motors. Nat. Cell Biol., 3:E28-E34.

[174] Wood, KW, R. Sakowicz, L.S. Goldstein, D.W. Cleveland 1997. "CENP-E is a plus end-directed kinetochore motor required for metaphase chromosome alignment". Cell 91, 3:357- 66.

[175] Wordeman, L. and T.J. Mitchison 1995. Identification and partial characterization of mitotic centromere-associated kinesin, a kinesin-related protein that associates with centromeres during mitosis. J. Cell Biol., 128:95-104.

[176] Wu, J.Y. and T.Maniatis.1993. Specific interactions between proteins implicated in splice site selection and regulated alternative splicing. Cell, 75:1061.

[177] Wynn, S.L. et al. 2000. Organization and conservation of the GART/Son/DONSON locus in mouse and human genomes. Genomics, 68:57-62.

[178] Yeakly, J.M., H. Tronchere, J. Olsen, J.A. Dyck, H.Y. Wang and X.D. Fu. 1999. Phosphorylation regulates in vivo interaction and molecular targeting of serine/arginine-rich pre-mRNA splicing factors. J. Cell Biol., 145:447-455.

[179] Yen, T. J., D. A. Compton, D. Wise, R. P. Zinkowski, B. R. Brinkley, W. C. Earnshaw and D. W.Cleveland. 1991. CENP-E, a human centromere associated protein required for progression from metaphase to anaphase. *EMBO J*., 10:1245-1254.

[180] Yen, T.J., G. Li, B.T. Schaar, I. Szilak and D.W. Cleveland. 1992. CENP-E is a putative kinetochore motor that accumulates just before mitosis. Nature, 359:536-539.

[181] Yu, H. 2002. Regulation of APC-Cdc20 by the spindle checkpoint. Curr. Opin. Cell Biol., 14:706-714.

[182] Yu, W., J.M. Solowska, L. Qiang, A. Karabay, D. Baird and P.W. Baas 2005. Regulation of microtubule severing by katanin subunits during neuronal development. J. Neurosci., 25:5573-5583.

[183] Yu, W., J. M. Solowska, L. Qiang, A. Karabay, D. Baird and P. W. Baas. 2005. Regulation of microtubule severing by katanin subunits during neuronal development. J. Neurosci., 25:5573-5583.

[184] Zachariae, W. and K. Nasmyth. 1999. Whose end is destruction: Cell division and the anaphase-promoting complex. Genes and Dev., 13:2039-2058.

[185] Zhang, Y., N. Li, C. Caron, G. Matthias, D. Hess, S. Khochbin and P. Matthias. 2003. HDAC6 interacts with and deacetylates tubulin and microtubules in vivo. EMBO J., 22:1168-1179.

[186] Zhao, Z., H. Xu and W. Gong. 2010. Histone deacetylase 6 (HDAC6) is an independent deacetylase for alpha tubulin. Protein Pept. Lett., 17:555-558.

[187] Zhou, J. et al. 2002. Attachment and tension in the spindle assembly checkpoint. J. Cell Sci, 115:3547-3555.

[188] Zhou, Z., L.J. Licklider, S.P. Gygi and R. Reed. 2002. Comprehensive proteomic analysis of the human spliceosome. Nature, 419:182-185.

Appendix 1:

Top 10 downregulated genes affected by TRAP150 Depletion

Definition	Symbol	Relative Fold Change
Beta-galactoside alpha-2,6-sialyltransferase 1	ST6GAL1	-10.46839479
Protein EVI2B Precursor	EVI2B	-9.529371799
Cytoplasmic FMR1-interacting protein 2	CYFIP2	-9.075634443
Probable G-protein coupled receptor 87	GPR87	-7.919768903
Interleukin-6 Precursor (IL-6)	IL6	-7.566821958
Cadherin-5 Precursor	CDH5	-6.660613186
Plasminogen activator inhibitor 1 Precursor	SERPINE1	-6.589847138
Transmembrane protein 45B	TMEM45B	-6.576941262
ETS homologous factor	EHF	-5.792819986

Appendix 2

Top 10 upregulated genes affected by TRAP150 Depletion

Definition	Symbol	Relative Fold Change
Histone chaperone ASF1B	ASF1B	9.385094358
Rac GTPase-activating protein 1	RACGAP1P	9.141858572
Leptin receptor gene-related protein	LEPROT	7.698327248
Phospholipid scramblase 4	PLSCR4	7.405258
FK506-binding protein 7 Precursor	FKBP7	6.800342926
Methyltransferase-like protein 7A Precursor	METTL7A	6.559537817
Zinc finger protein 92	ZNF92	5.980172085
Serine/threonine-protein kinase PLK1	PLK1	5.957780616
Rac GTPase-activating protein 1	AC108078.3-1	5.334934067
DEP domain-containing protein 1A	DEPDC1	5.243911484